THE SCATTERING OF 1.0- AND 2.4-MeV POLARIZED NEUTRONS FROM HELIUM

by

James Richard Sawers, Jr.
Department of Physics
Duke University

Date: _____

Approved:

_____
Richard L. Walter, Supervisor

_____

_____

_____

A dissertation submitted in partial fulfillment of the requirements for the degree of Doctor of Philosophy in the Department of Physics in the Graduate School of Arts and Sciences of Duke University

1966

ABSTRACT

(Physics)

THE SCATTERING OF 1.0- AND 2.4-MeV POLARIZED NEUTRONS FROM HELIUM

by

James Richard Sawers, Jr.
Department of Physics
Duke University

Date: _____

Approved:

_____
Richard L. Walter, Supervisor

_____

_____

_____

An abstract of a dissertation submitted in partial fulfillment of the requirements for the degree of Doctor of Philosophy in the Department of Physics in the Graduate School of Arts and Sciences of Duke University

1966

SCATTERING 1.0- and 2.4-MeV POLARIZED NEUTRONS FROM HELIUM

by

James Richard Sawers

Precision angular distributions of the asymmetry in the scattering of 1.0 and 2.4 MeV polarized neutrons from helium were determined. The reactions $Li^7(p,n)Be^7$ and $C^{12}(d,n)N^{13}$ served as neutron sources and target thicknesses of 46 and 175 keV respectively were used. Analyzing angles ranged from 30° to 140° in 10° increments. A spin precession solenoid was employed and the helium was contained in a high pressure scintillation cell. Neutrons scattered through the desired scattering angle were detected with plastic scintillators. Recorded backgrounds were minimized by accepting only helium recoil counts, which satisfied specific energy requirements and which were coincident with the neutrons detected in the plastic scintillators. A Monte Carlo program employing the formalism of Wolfenstein, was written for calculating the effects on the observed asymmetry of multiple scattering in the helium cell. Results from this code also allowed the data to be corrected for the effects of the finite geometry of the helium cell and the neutron detectors. It is demonstrated that polarization data alone are sufficient to accurately determine the scattering phase shifts at 2.44 MeV. Here the phase shift values were found to be -37.2 ± 2.4, 21.2 ± 0.5 and $121.6 \pm 0.5^\circ$ for the δ_0^+, δ_1^-, and δ_1^+ phase shifts respectively. Hard sphere calculations employing the s-wave

phase shift give a hard sphere radius of 2.42 ± 0.13 fm which is consistent with the values recently obtained by others from both n-α and p-α scattering data. D-waves were not found to be necessary.

Below the $P_{3/2}$ resonance at 1.3 MeV, the phase shifts were not as sensitive to the measured relative asymmetries. It appears that additional cross-section data will be required to accurately determine the phase shifts in this energy region. Since it was observed that at 1.0 MeV equally good fits to the present data could be obtained with values of δ_0^+ differing by as much as 15°, the hard sphere formalism, in conjunction with the scattering radius obtained at 2.4 MeV, was used to fix the s-wave phase shift at -24.5° ± 1.5°. The fit to the data then required that δ_1^+ = 4.4 ± 1.0 and δ_1^- 61.2 ± 4.5. Examination of the presently determined phase shifts shows that s-wave phase shifts to be smaller than the commonly accepted ones of Dodder, Gammel, and Seagrave (DGS). At both energies the δ_1^+ was in excellent agreement with DGS although δ_1^- appeared 1.6° below DGS at 1.0 MeV and 2.8° high at 2.44 MeV. In addition the earlier asymmetry data of May, Walter, and Barschall for n-He scattering at 2.0 MeV were corrected for the effects of multiple scattering and finite size and then were analyzed for phase shifts determinations. For the May data, the angle at which the polarization crossed through zero was observed to be shifted toward back angles relative to the DGS prediction. This shift was also observed in the present experiment at 2.44 MeV.

By searching the δ's and P_1 it was found that one can limit the value of P_1 to -0.458 ± 0.006 for the reaction $C^{12}(d,n)N^{13}$ for an incident deuteron energy of 2.82 MeV when the neutrons are observed at 25° (lab). A similar determination of the incident polarization in the reaction $Li^7(p,n)Be^7$ can be obtained when the s-wave phase shift is restricted to the hard sphere value. For an incident proton energy of 2.92 MeV and at a laboratory angle of 50° the neutron polarization was observed to be 0.304 ± 0.008.

ACKNOWLEDGMENTS

To Dr. R. L. Walter, who suggested this project, for his continued interest in and support of the present investigation, I wish to extend my gratitude. Special thanks are due to Mr. G. L. Morgan for his assistance in taking the data and for the use of several computer codes programmed by him. Dr. L. A. Schaller and Mr. R. S. Thomason are owed a debt of gratitude for their assistance in the data taking. In addition, I should like to thank Drs. Walter and Schaller and Mr. Morgan for many discussions concerning related experiments recently performed at Duke. I should like to express my appreciation to Dr. F. O. Purser for many fruitful conversations on a variety of topics related to this work. Also I wish to express my indebtedness to Mr. R. A. Schroeder for discussions on computer techniques and to the staff of the Duke University Computing Laboratory for its cooperation. I wish to thank Mr. S. E. Edwards for his help with the electronics and the entire Nuclear Physics group for assistance with the accelerator. I wish to thank Mrs. Joseph Bailey for preparing the drawings and Mrs. William Johnson for performing many tedious calculations.

This work was supported by the Atomic Energy Commission.

J. R. S.

CONTENTS

LIST OF FIGURES

LIST OF TABLES

THE SCATTERING OF 1.0- AND 2.4-MeV POLARIZED NEUTRONS FROM HELIUM

Chapter I

INTRODUCTION

Since the mid - 1950's the development of techniques for neutron polarization measurement has been rapid. The polarization of a neutron beam is measured by elastic scattering from light nuclei, where the resonance parameters are known, such as C^{12}, O^{16}, and He^4. The preferred analyzer has been He^4 since the analyzing power is large and does not change rapidly with energy. Additionally, helium cells permit coincidence requirements to be used to reduce background. The recent advent of extremely fast electronic systems, making close geometries feasible in scattering experiments and thereby increasing the counting rate, has been a prime contributor to this development. Also neutron spin precession has made the interchanging of the effective positions of the counters fast and accurate. With the major experimental difficulties overcome, a continually enlarging corpus of increasingly accurate polarization data is available. Since in a majority of the polarization determinations the analyzing scatterer has been helium, there has resulted a renewed interest in the n-α elastic scattering phase shifts, as the analyzing power of helium is calculated from these numbers. As there is some doubt concerning the reliability of presently available phase shifts, the present work was embarked upon in order that precise data might be obtained with which to test existing phase shift sets and perhaps from which new phase shifts might be determined.

Since the phase shifts determined experimentally have exhibited inconsistent values, the problem will be reviewed briefly. At the present time the most widely used phase shifts for the scattering of neutrons of several MeV by α-particles were calculated by Dodder and Gammel (1952) and later published by Seagrave (1953). These phase shifts (hereafter referred to as the DGS) were obtained principally from the analysis of experiments on the scattering of 5.8 and 9.5 MeV protons by alpha particles, using single level dispersion theory. The n-α phase shifts were deduced from the p-α phase shifts by assuming charge symmetry of nuclear forces and taking into account the difference in Coulomb energy. Adair's (1952) assumptions that the resonant energies for He^5 and Li^5 differ by about 1.0 MeV and that the reduced widths of the states formed by p-waves in He^5 and Li^5 are identical were used. The s-wave phase shifts were calculated using the same logarithmic derivative of the wave function at the nuclear surface for the n-α scattering as for the p-α scattering. This is equivalent to assuming that under the influence of the nuclear potential the s-wave wave functions are the same in both cases.

Until the present time, in view of the higher precision with which the p-α $d\sigma/d\Omega$ angular distributions could be measured in comparison with like measurements for the n-α case, it is to be expected that phase shifts derived from p-α scattering are more accurately known than those directly obtained from n-α experiments. In an attempt to verify the Dodder-Gammel analysis for n-α scattering, Seagrave obtained five angular distributions from 2.6 to 14.1 MeV. He was able to obtain good agreement every where except at 2.6 MeV where his results required a significantly smaller value of the $p_{1/2}$ phase shift. He employed s-, p-, and d-waves in obtaining his fit, although there remained considerable uncertainty concerning the d-wave phase shifts both because of uncertainties in the experimental data and because of the neglect of higher angular momenta partial waves. At any rate the effect due to d-waves was small and d-waves were not conclusively

necessary below 5 MeV.

Later Gammel and Thaler (1958) extended the p-α phase shift analysis to 40 MeV on the basis of additional data on the scattering and polarization. This analysis included f-waves which merit consideration above 10 MeV. These authors used an optical model to extrapolate the DGS phase shifts to higher energies. Perkins (1960) has since employed the results of this analysis to deduce the phase shifts for n-α scattering (GTP phase shifts). He assumed that the logarithmic derivatives of the wave functions at the radius of 2.9 fm for the p-α system described the n-α system at a center-of-mass energy reduced by 0.8 MeV. Due to the appearance of a $d_{3/2}$ state in He^5 at 22.2 MeV incident neutron energy and to the threshold for T-D breakup at 22.2 MeV, the problem of obtaining a fit to the experimental data with the GTP phase shifts seems difficult (Austin et al. (1962); May et al. (1963); Perkins and Glashausser (1964); Shamu and Jenkin (1964)). On the other hand, Hoop et al. (1965) have determined the angular distribution of 10- to 25- MeV neutrons scattered from α-particles and found their data consistent with the GTP predictions. Above 15 MeV an even more satisfactory fit is obtained using the phase shifts determined from the analysis of Weitkamp's (1963) 23-MeV p-α data.

One other problem in the literature is concerned with the value of the $p_{1/2}$ phase shift in the neighborhood of 2.5 MeV incident neutron energy. As was mentioned above, Seagrave obtained a smaller value of the $p_{1/2}$ phase shift than had been predicted by Dodder and Gammel (DGS phase shifts). A value of δ_1^- only slightly lower than DGS had been previously obtained by Adair in the 2-3 MeV region. Even more recently, Demanins et al. (1962) obtained two precision angular distributions of $d\sigma/d\Omega$ at 2.4 and 2.9 MeV and calculated values of δ_1^- still smaller than those of Seagrave. Clementel and Villi (1955) using graphical methods obtained n-α phase shifts directly from Adair's data. Their values are consistent with DGS. Striebel and Huber (1957) repeated an earlier ex-

periment by Huber and Baldinger (1952) extending Adair's work to higher energies. Using an ionization chamber to obtain eight angular distributions of $d\sigma/d\Omega$ between 2.6 and 4.1 MeV, they found agreement with Adair and DGS but failed to agree with the previous results of Huber and Baldinger.

In an attempt to get more experimental information in this energy region Levintov et al. (1957) measured angular distributions of the neutron polarization over a limited angular range and concluded that their results supported Seagrave's low values of the $p_{1/2}$ phase shift. However, in discussing the effective range theory of nucleon-alpha scattering Pisent and Villi (1959) pointed out that the Levintov work was not of sufficient accuracy to verify Seagrave's δ_1^-. Haeberli (1963) also pointed out that the Russian group had made a sign error which might explain their conclusion. In addition, the polarization work of May et al. (1963) strongly favored the DGS phase shifts at 2.0 MeV over the lower values of δ_1^-.

The article by Austin et al. (1962) in reviewing the n-α situation concludes that the majority of data below 10 MeV may be fitted satisfactorily with the DGS phase shifts in spite of the fact that some discrepancies do exist. This has been the prevalent feeling in the neutron polarization community until lately.

Quite recently Roper (1965) calculated a new set of phase shifts, the only n-α phase shifts designed for use below 1.0 MeV. His results are not entirely encouraging (nor physically reasonable) in that the phase shifts do not lie on smooth curves, making interpolation impossible. Roper (1965) felt that this arose from a lack of consistent and accurate experimental data in the low energy region. An experiment by Jewell et al. (1966) determined the asymmetry in n-α scattering for 262-keV neutrons. The agreement with Roper's prediction was satisfactory but the experiment was not sufficiently comprehensive to permit a conclusive statement concerning the phase shifts. Another preliminary set of phase shifts, quite similar to the DGS below 6 MeV, has been arrived at by Hoop and Barschall (1965).

The present experiment was undertaken for the purpose of determining the accuracy with which the DGS phase shifts and the other sets of phase shifts are capable of predicting the polarization in n-α scattering. If this ability is poor then it was hoped that the present data could be used as the basis for a new set of phase shifts. Furthermore, it was expected that the value of the δ_1^- in the 2.5 MeV region might be stabilized.

A considerable amount of the analysis of this data was carried out on an IBM 7072 computer and to avoid unnecessary length in this report the computer codes are only briefly discussed. However complete listings are available to interested parties.

Chapter II

THEORY

Since neutrons are particles which have a non-zero spin and since this spin is restricted to spin states +1/2 and -1/2, it is conceivable that a beam of neutrons might have more neutrons with spin oriented in a given direction than in the opposing direction. This can actually occur, in which case we say that the beam is polarized. The degree of polarization, i.e. the preference for a certain spin state may be defined as

$$P = \frac{N_+ - N_-}{N_+ + N_-} \tag{1}$$

where N_+ and N_- are the numbers of neutrons in spin state +1/2 and -1/2 respectively. By convention (Basel, 1960) the orientation of the +1/2 spin state is chosen as parallel to the direction of $\vec{k}_{inc} \times \vec{k}_{out}$ for a given nuclear reaction, where $\vec{k}_{inc}$ and $\vec{k}_{out}$ are the incident and outgoing neutron momenta respectively.

Now since conventional neutron detectors measure only the number of neutrons striking them irrespective of their spin orientation, more sophisticated techniques must be used if spin orientation is the prime consideration in the desired measurement. For neutrons of several MeV, nuclear elastic scattering is commonly used as the polarization

analyzer. Use is made of the fact that under certain conditions neutrons with a given spin orientation will preferentially scatter in a given direction while those of the opposite spin orientation preferentially scatter in the opposite direction. Thus, the scattered flux, assuming a non-zero incident polarization, will be greater on one side than the flux scattered through a like angle on the opposite side of the incident beam axis.

The ratio of right-to-left scattered flux clearly depends on two quantities: the degree of polarization in the incident beam; and on the ability of the scattering process to analyze the spin orientation of the beam. These two quantities cannot be separated experimentally. Consequently, people have used as an analyzing scatterer a nucleus for which the analyzing power can be calculated. This type of experiment has been completed utilizing several light nuclei where the resonance parameters are known from the observation of total and differential cross sections, such as He^4, C^{12}, and O^{16}. The results for He^4 are felt to be the most reliable at the present time.

The idea of detecting the presence of polarization in a beam of neutrons by resonance scattering was originally proposed by Schwinger (1946). He pointed out that the scattering of neutrons by He^4 showed evidence for a large spin-orbit splitting in the p-state, and that for neutron energies near 1 MeV n-He^4 scattering should be a good polarization analyzer. Actually we now know this to be true over a much wider energy range. The level diagram for He^5 is shown in Figure 1. There are two relatively broad states: a $P_{3/2}$ state at just above 1 MeV, $\Gamma = 0.55$ MeV and a $P_{1/2}$ state at 4.6 MeV, $\Gamma = 3.0$ MeV. It is interference between these two states that gives rise to the polarization in neutron scattering. The relatively large widths and wide spacing of these levels permit high values of the analyzing power over a broad energy range.

It has turned out to be quite difficult to obtain highly reliable absolute values of neutron polarization because of the indirect manner in

which the analyzing power of the scatterer has had to be deduced. This has remained a central problem in all polarization experiments employing elastic scattering as the analyzing process. However, in principle the analyzing power can be obtained from a double scattering experiment employing two successive scatterings from the same nucleus. For reasons of intensity and background this is not feasible at present. Another and more elegant approach to the problem was suggested by Barschall (1956) who observed that the polarization of neutrons produced in a reaction can, under certain stringent requirements, be measured directly if the inverse reaction rather than a scattering is used for the analysis. Still another possibility is to use scattering processes where the analyzing power can be accurately calculated without precise knowledge of the nuclear properties. The method proposed by Schwinger (1948) employes small angle deflections using the interaction of the neutron magnetic moment with the Coulomb field of the nucleus, which can be calculated quite accurately from classical arguments. However background and angle measurements problems as well as difficulties associated with the finite detector size render this method very difficult as the scattering angles employed must be of the order of one degree.

It is now convenient in our discussion of polarization theory to consider the more general case which allows the possibility of a reaction taking place within the second scatterer rather than having simple elastic scattering. The discussion will follow the schematic diagram in Figure 2. The $\vec{k}$'s are the momenta with the 1's indicating the first scatter and the 2's referring to the second. Also "inc" and "out" refer to the incident and outgoing directions respectively. The $\vec{n}$'s are the unit vectors perpendicular to the first and second scattering planes, i.e. $\vec{n}_1 \parallel \vec{k}^1_{inc} \times \vec{k}^1_{out}$ and $\vec{n}_2 \parallel \vec{k}^2_{inc} \times \vec{k}^2_{out}$. The outgoing momentum from the first reaction is equal to the incident momentum in the second, i.e., $\vec{k}^1_{out} = \vec{k}^2_{inc}$. The azimuthal

Fig. 1. Level Diagram for He^5

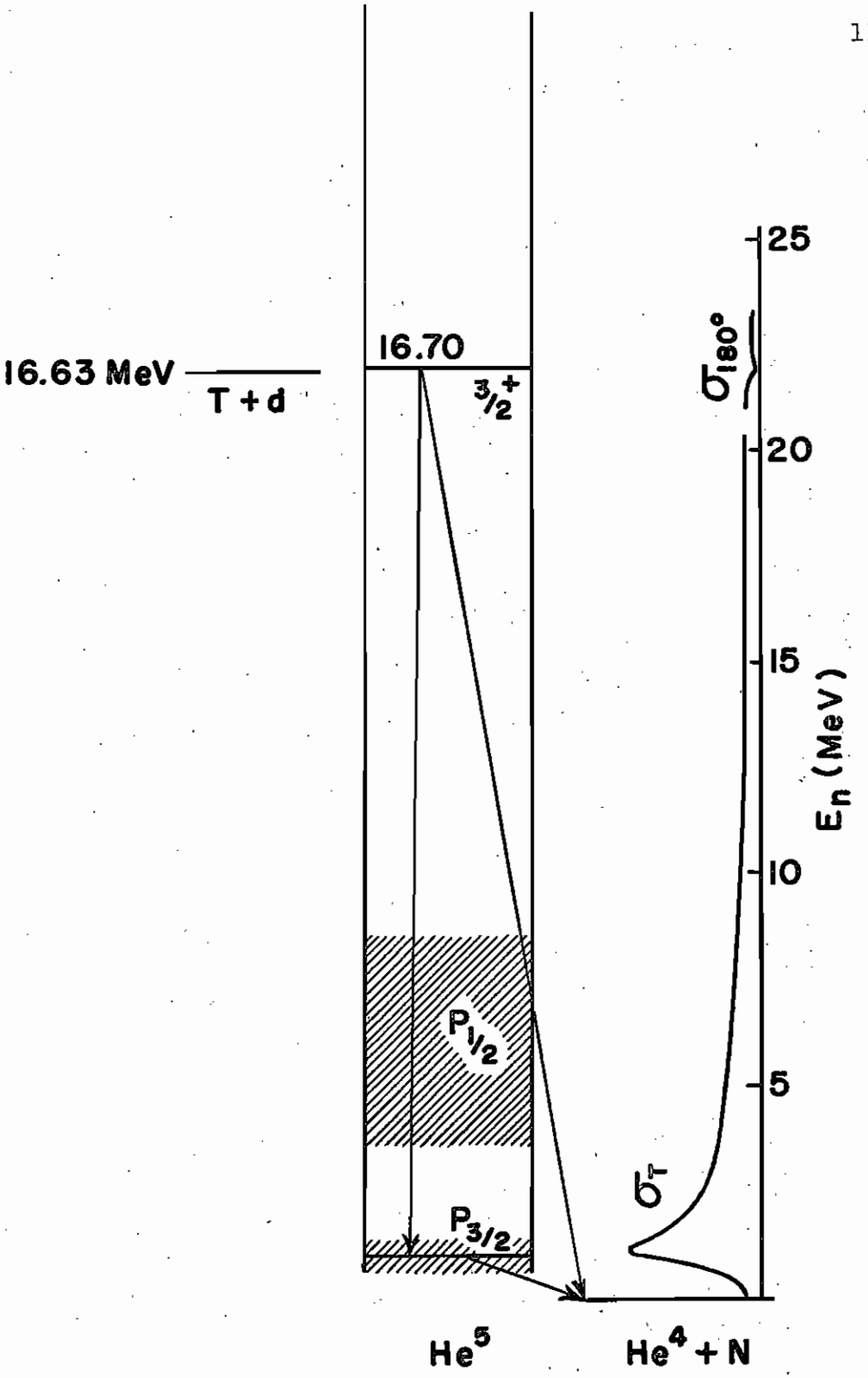
16.63 MeV
T + d
16.70
3/2+
P1/2
P3/2
He5
He4 + N
σ180°
σT
25
20
15
10
5
En (MeV)

angle $\emptyset$ is the angle between n_1 and n_2 :

$$\cos \emptyset = \vec{n}_1 \cdot \vec{n}_2 . \tag{2}$$

From the general theory (Welton, 1963) it is known that if the neutron beam from the first target is polarized, the differential cross section in the second reaction depends not only on the scattering angle θ_2 but also on the azimuthal angle $\emptyset$. The azimuthal variation of $d\sigma/d\Omega$ is in cos $\emptyset$ and is of amplitude proportional to the polarization P_1 of the incident beam

$$\frac{d\sigma(\theta_2, \emptyset)}{d\Omega} = \frac{d\sigma(\theta_2)}{d\Omega} \left[1 + \vec{P}_1 \cdot \vec{A}_2(\theta_2) \right] \tag{3}$$

where $\vec{A}_2(\theta_2) = \vec{n}_2 A_2(\theta_2)$ and $\frac{d\sigma(\theta_2)}{d\Omega}$ is the differential cross section for an unpolarized incident beam. $A_2(\theta_2)$ is the amplitude of the azimuthal variation for a completely polarized incident beam and is called the asymmetry in the reaction. Frequently the term analyzing power is used as A_2 determines how effective a detector of the incident polarization the second reaction is. It has been shown that (Blin-Stoyle, 1952) A_2 may be interpreted as the polarization in the inverse reaction (i.e., A_2 is the polarization resulting when an incident unpolarized beam, $-\vec{k}^2_{out}$ scatters in the direction $-\vec{k}^2_{inc}$).

Of present interest is the particular instance where the second reaction is an elastic scattering process for in this case there is no distinction between a reaction and its inverse. Consequently, the neutron polarization P_2 which results when an initially unpolarized beam is scattered elastically is equal to the amplitude of azimuthal variation A_2 observed with a completely polarized beam assuming energy, angle, and target are the same (Wolfenstein, 1956). Thus we may rewrite eq. (3)

as:

$$\frac{d\sigma(\theta_2, \phi)}{d\Omega} = \frac{d\sigma(\theta_2)}{d\Omega} \left[1 + P_1 P_2 \cos \phi\right] . \quad (4)$$

Although the neutron detectors are not shown in Figure 2, they are generally placed at angles corresponding to plus and minus θ_2 in order to measure the fluxes $I(\theta_2, 0)$ and $I(\theta_2, \pi)$ corresponding to azimuthal angles 0 and π respectively. These positions are commonly called right and left.* We shall take the right to be associated with $\phi = 0$, i.e. corresponding to two successive scatters to the right. The ratio of intensities

$$r = \frac{I(\theta_2, 0)}{I(\theta_2, \pi)} \quad (5)$$

we shall call the right-left ratio. From eqs. (4) and (5) we may write:

$$r = \frac{1 + P_1 P_2}{1 - P_1 P_2} \quad (6)$$

Solving for $P_1 P_2$, we have

$$P_1 P_2 = \frac{r - 1}{r + 1} \quad (7)$$

Now the measurement of either P_1 or P_2 is straight forward if the other quantity is known. The usual procedure is to measure $P_1 P_2$ and to calculate P_2 thereby obtaining P_1. However, the object of the present experiment is to measure P_2 which precludes the exact knowledge of P_1 since P_1 previously had been measured assuming calculations of P_2 had been correct. In the present experiment P was kept constant and an angular distribution of $P_1 P_2 (\theta_2)$ was determined with P_1 as multipli-

---

* In our case right and left correspond to up and down as discussed in Chapter III, Sec. C.

Fig. 2. Geometry for Double Scattering Polarization Experiments

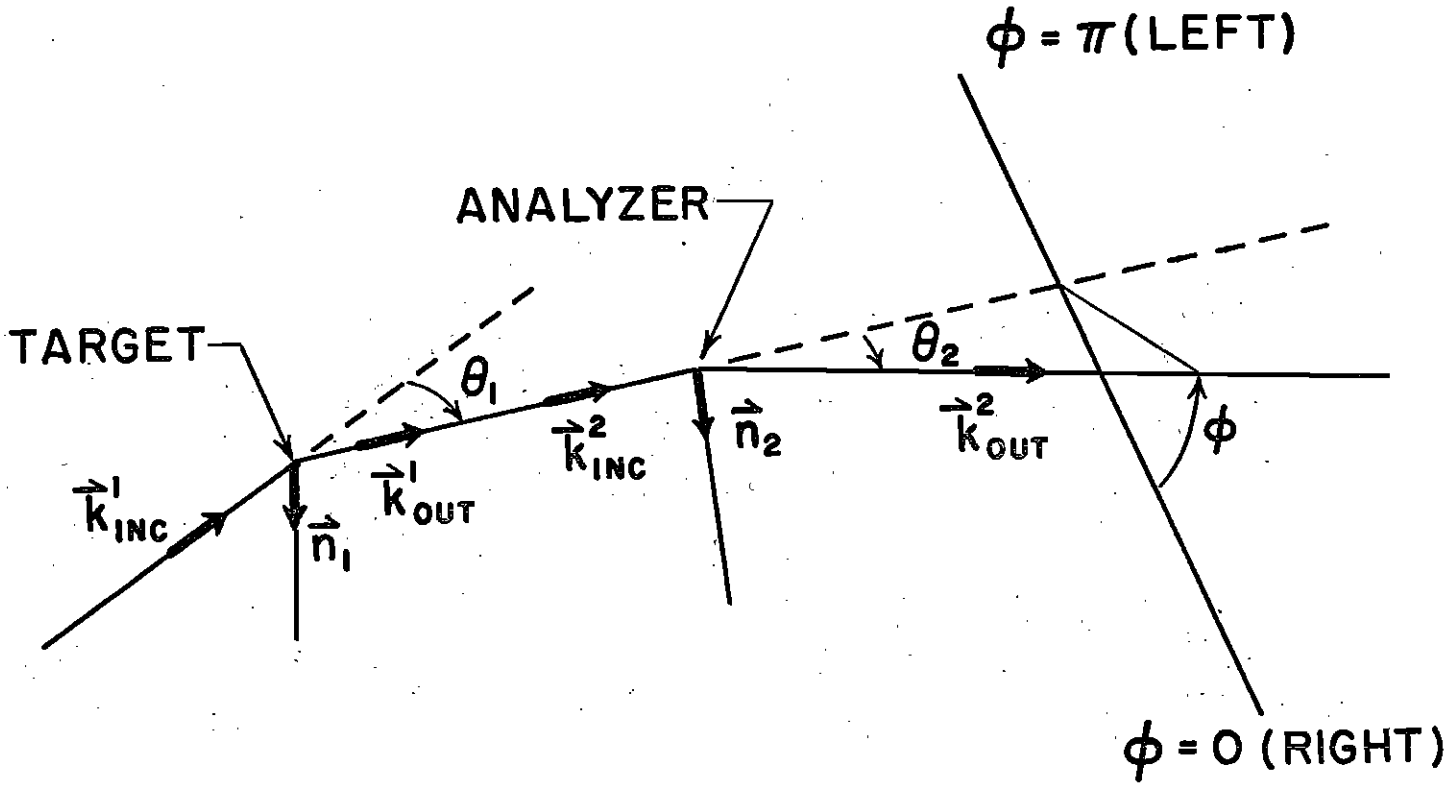
$\phi = \pi$ (LEFT)
ANALYZER
TARGET
θ_1
θ_2
$\vec{k}^1_{INC}$
$\vec{n}_1$
$\vec{k}^1_{OUT}$
$\vec{k}^2_{INC}$
$\vec{n}_2$
$\vec{k}^2_{OUT}$
ϕ
$\phi = 0$ (RIGHT)

cative factor which solely determined the amplitude of the angular distribution. By assuming the angular momenta involved in the second reaction are limited to only small values and using the following formulae, we may calculate the shape of the $P_2(\theta_2)$ angular distribution as a function of the scattering phase shifts alone. The expression for the cross section and polarization as a function of the scattering phase shifts were first given by Lepore (1950) and are:

$$\sigma(\theta) = |g|^2 + |h|^2 \tag{8}$$

$$P(\theta) = - \frac{2\,\mathrm{Im}(g^* h)}{|g|^2 + |h|^2} \tag{9}$$

where

$$g(\theta) = \lambda\!\!\!^{-} \sum_{\ell} P_{\ell}(\cos\theta)\ (\ell + 1) \sin \delta_{\ell}^{+}\, e^{i\delta_{\ell}^{+}} + \ell \sin \delta_{\ell}^{-}\, e^{i\delta_{\ell}^{-}} \tag{10}$$

$$h(\theta) = \lambda\!\!\!^{-} \sum_{\ell} P_{\ell}^{(1)}(\cos\theta) \sin(\delta_{\ell}^{+} - \delta_{\ell}^{-})\, e^{i(\delta_{\ell}^{+} + \delta_{\ell}^{-})} \tag{11}$$

with $P_{\ell}(\cos\theta)$ and $P_{\ell}^{(1)}(\cos\theta)$ representing the Legendre polynomials and the first order associated Legendre polynomial respectively, $\lambda\!\!\!^{-}$ is the reciprocal of the wave number and ℓ the orbital angular momentum quantum number. Thus, at low energies the shape and amplitude of the $P_1 P_2(\theta_2)$ angular distribution are determined solely by a few scattering phase shifts plus P_1, a small number of variables. Therefore, a large number of sufficiently accurate and consistent points on the angular distribution of $P_1 P_2(\theta_2)$ should allow a determination of the scattering phase shifts for the neutron energy at which the distribution was obtained and thus permit an accurate calculation of $P_2(\theta_2)$. The mathematical procedure used in determining the scattering phase shifts is described in Chapter VI.

An additional section relating to theoretical topics appears in Chapter V, where the triple scattering formalism is discussed in detail.

Chapter III

EXPERIMENTAL APPARATUS AND TECHNIQUE

A. General

The discussion of the experimental apparatus and technique is rather lengthy and complex. A brief general summary of the method will first be given, then each component of the system will be discussed in detail. The experimental arrangement is illustrated in Figure 3. Polarized neutrons which emerged at a reaction angle θ_1 had their spins precessed 90° by a magnetic field produced by a solenoid. After passing through the solenoid the neutrons were incident on a high pressure helium scintillation cell. Those neutrons which scattered through the desired analyzing angle θ_2 were detected by a pair of plastic scintillators. Coincidence and pulse height requirements had to be met before a count was considered in computing the asymmetry in the counting rates of the plastic detectors.

B. Accelerator and Target Region

Polarized neutrons were produced using either the reaction Li^7 (p, n) Be^7 or C^{12} (d, n) N^{13}. The protons or deuterons were accelerated

Fig. 3. Experimental Arrangement

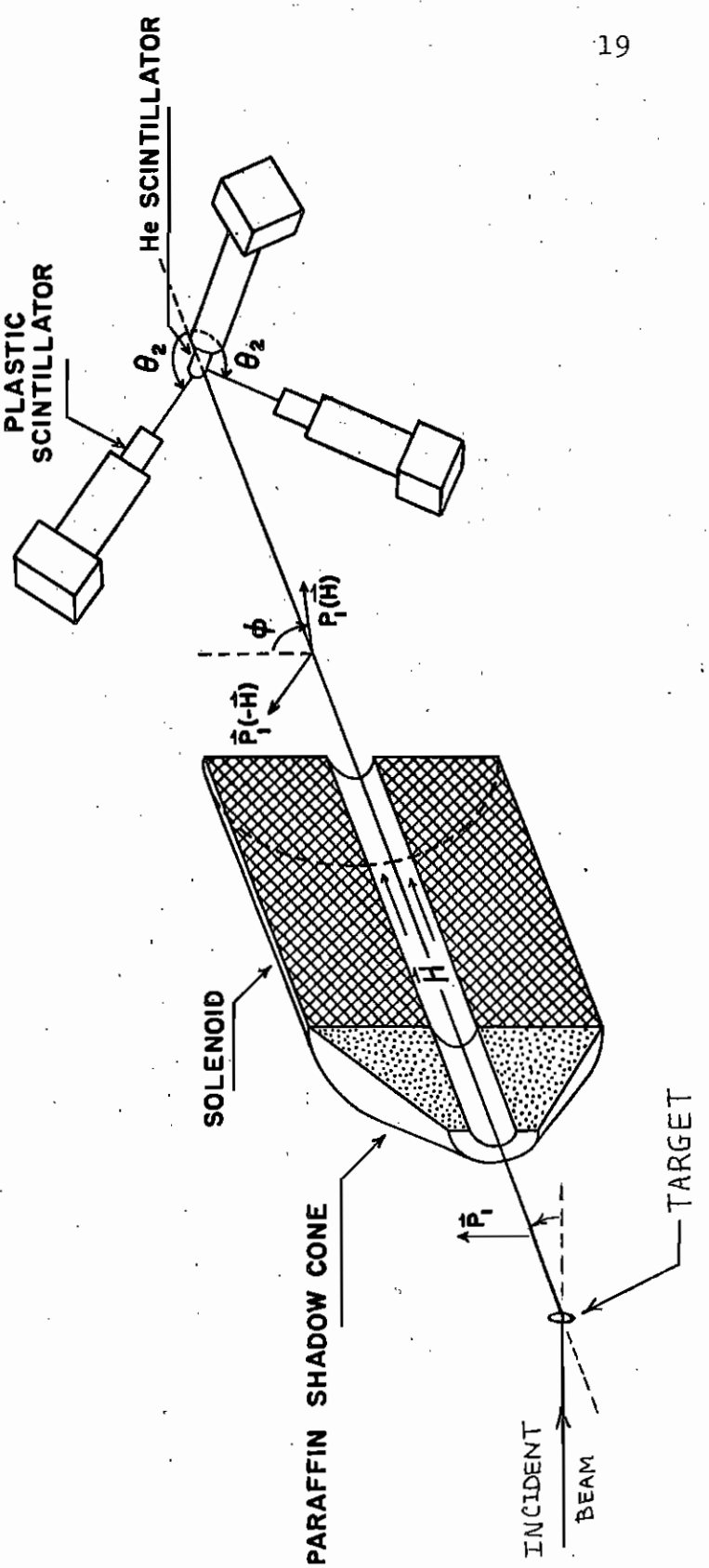
He SCINTILLATOR
PLASTIC SCINTILLATOR
θ_2
θ_2
ϕ
$\vec{P}_1(H)$
$\vec{P}_1(-\vec{H})$
H
SOLENOID
PARAFFIN SHADOW CONE
$\vec{P}_1$
TARGET
INCIDENT BEAM

by the Duke University 4-MeV Van de Graaff accelerator and were magnetically analyzed. The resulting monoenergetic beam was incident on the desired target. Machine energies were measured using a precision digital voltmeter to read the signal from a generating voltmeter, the technique having been described by Hollandsworth et al. (1964). Erroneous voltage readings can result from electronic drift. However, since the Van de Graaff voltage calibration was checked many times during the course of the experiment, it was estimated that the energy was constant to within $\pm$ 8 keV. By making several asymmetry determinations for each angle, effects of possible energy error would tend to cancel. Therefore it is estimated that the mean energy of the angular distributions were known to $\pm$ 7 keV. Energy calibration was obtained by observing the Li^7 (p, n) Be^7 zero degree threshold as determined with a "long counter" similar to that described by Hanson and McKibben (1947).

As is shown in the schematic diagram of the target region, (See Figure 4), a set of three beam collimators was used to assure that the beam approached the target along a well-defined axis. Prior to the first collimator there were four quadrupole focusing magnets and three deflecting magnets to allow control of the beam position and to permit focusing on the target. The last collimator was 0.64 cm in diameter and cantilevered to within 9 cm of the target. This collimator was electrically insulated from the beam pipe and from the target itself. The collimator and the target currents fed separate current indicating devices. Target current was about 6.5 μA for both the lithium and carbon targets. The beam was intentionally defocussed so that "hot spots" were avoided by keeping the collimator current at 0.5 μA. In this manner one could be reasonably confident that the beam profile remained constant and that its position on the target did not vary appreciably. An air-water spray was used to cool the targets. Care was taken so that the cooling system could not leak charge from the target to the collimator or to ground. The target itself was either evaporated Li

Fig. 4. Beam Tube, Vacuum System and Rotating Target

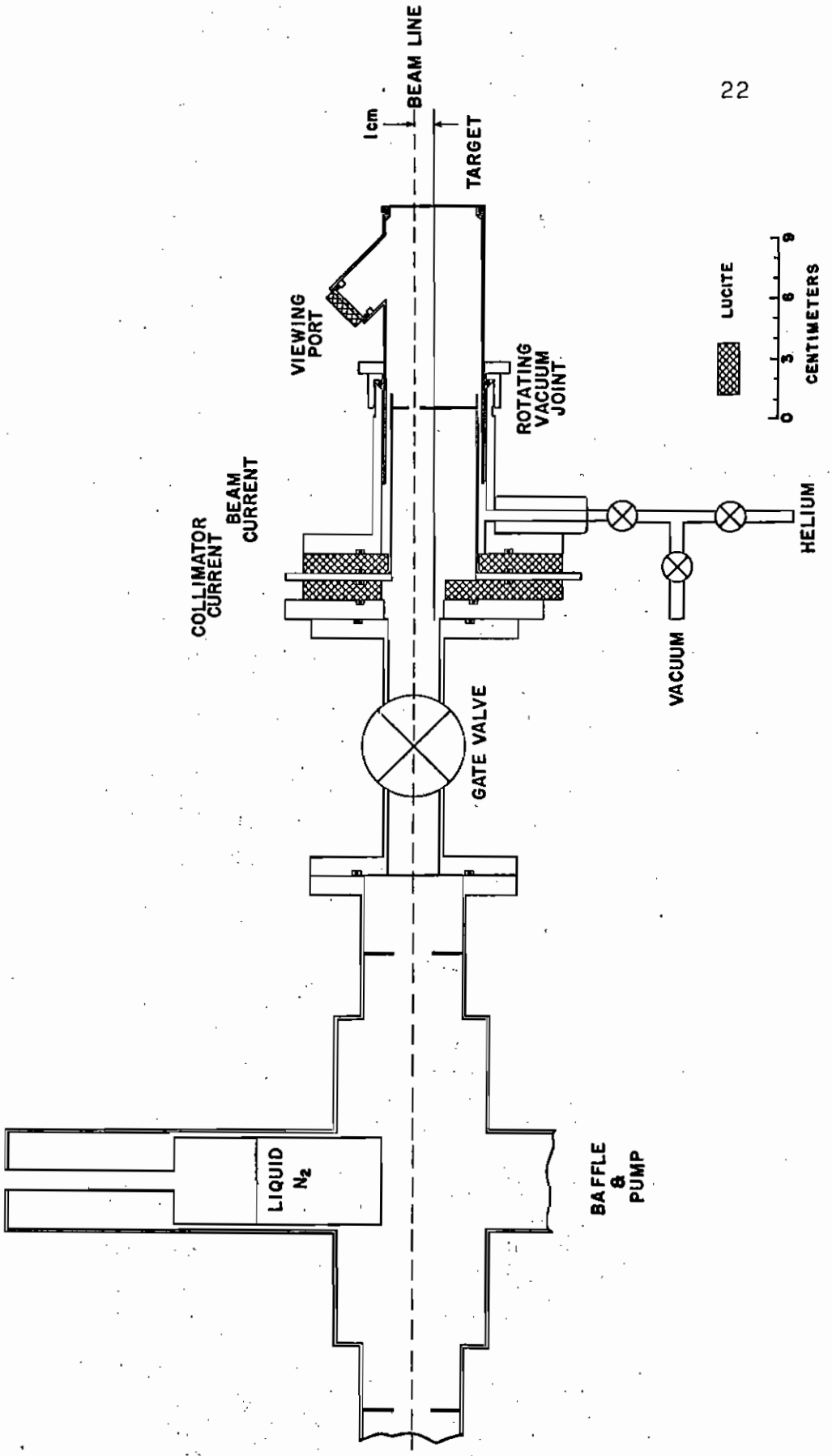
1cm
BEAM LINE
TARGET
VIEWING PORT
ROTATING VACUUM JOINT
LUCITE
0
3
6
9
CENTIMETERS
COLLIMATOR CURRENT
BEAM CURRENT
HELIUM
VACUUM
GATE VALVE
LIQUID N_2
BAFFLE & PUMP

metal or deposited C on a 5 cm circular blank of Ta mounted 1 cm off beam axis and in such a manner that it could be easily rotated about its own center as shown in Figure 4. By this means various portions of the target could be exposed to the beam. A viewing port was provided so that visual inspection of the target condition was possible.

To prevent carbon buildup on the carbon targets and more importantly to prevent contamination of the highly active lithium metal targets, an efficient pump and trapping system were installed in the immediate vicinity of the target. The pump was a 7 1/s silicon oil pump with a mechanical fore pump. The trap was stainless steel capable of holding liquid nitrogen for about six hours. The water-cooled baffle and the enlargement of the beam tube where the trap and pump inlet were installed were made of nickel-plated brass. For the most part neoprene O-rings were used to seal the vacuum system though in some cases indium O-rings were used.

At Duke it was convenient to produce the Li metal targets in an evaporator separate from the accelerator vacuum system and then to install them on the beam tube. The targets were transported in sealed containers filled with helium. During the installation process, a helium "house" enveloped the beam tube and the target carriage vessel (see Appendix I). Provisions were made for letting the last 15 cm of beam tube up to atmospheric pressure with helium without disturbing the diffusion pump. Thus, the lithium metal targets could be installed with little or no exposure to the deteriorating effects of the atmosphere.

In order to minimize the effects of room scattered neutrons the largest experimental area available in this laboratory was chosen for the present measurement. To reduce background effects in neutron experiments, this area had been constructed with a false floor about 1 m above the true floor. A naval gunmount, which supported the polarimeter and by rotation allowed selection of the angle θ_1, stood on a concrete pedestal in the center of the pit.

C. Solenoid

Neutron detector efficiencies are difficult to accurately determine absolutely. Therefore, it becomes necessary to interchange the detector on one side of the neutron beam with the detector on the opposite side when measuring an asymmetry (see Chapter VII, Sec. D). This is true whether one or two detectors are used in the asymmetry measurement as the dominant factor is the requirement that a single detector be accurately interchanged with its mirror position regardless of the position of the second detector should there be one. By using the interchange technique, precise knowledge of the detector efficiency becomes superfluous. However, great care must be taken during the interchange process in order to insure that the radial distance from the analyzing scatterer to the detector remains constant since this distance has a pronounced effect on the solid angle. Also, care in obtaining the mirror angle is required if the laboratory differential cross section is varying with angle. Even a small error in either of these two alignments is capable of introducing large false asymmetries. An elegant method of eliminating these false asymmetries was first proposed and employed by Hillman et al. (1956). His method, which was also employed in the present experiment, utilized the Larmour precession of the polarization vector P_1 through 90° about the beam axis in a solenoidal magnetic field inserted between the neutron producing target and the analyzing scatterer. The analyzing plane determined by the beam axis and the helium cell-plastic detector line is now vertical and is perpendicular to the plane of the neutron producing reaction. The scattered neutron intensity is then measured. By reversing the field of the solenoid the polarization vector can be rotated through -90° (i.e. 180° with respect to the initial orientation obtained with the solenoid current in the original "forward" direction). The neutron intensity is again measured. The two intensities thus obtained are completely equivalent to the normal right and left intensities. Furthermore,

this process is advantageous in that it can be done accurately, remotely, and rapidly thereby allowing many sets of data to be taken. By alternating "forward-reverse" (FR) and "reverse-forward" (RF) sets, false asymmetries caused by long term electronic drift are minimized.

The solenoid used was a modified "Plasmaflux" design* with a 5.1 cm diameter center hole and constructed in three identical sections. With the existing power supply-- a 35-kilowatt, 325-ampere motor-generator set-- the maximum central field strength is 7.8 Kilogauss. Figure 5 indicates the physical conformation of the solenoid and a typical field configuration.

There are three ways in which the solenoid can conceivably have an effect on the data. All are attributable to the fringing field. The most probable of these would be for the fringing field to have an effect on the gain of the photomultiplier tubes used to detect scintillations. The effect was measured for several of the analyzing arrangements used and was found to be negligible. These tests are discussed in detail in Chapter VII, Sec. D. Let it suffice to say that any such gain effect had been prevented by surrounding the solenoid with Armco iron 3.18 cm thick on the ends and 0.95 cm thick on the sides and top. The bottom was left open to provide access for cooling water and current connections. This shielding reduced the fringing field in the region of the photomultipliers to about one gauss. In addition the photomultipliers were surrounded by three layers of mu-metal and by an Armco cylinder with 1 cm walls plus the standard mu-metal electrostatic shield. Since the magnetic field would have a more pronounced effect in the region of the photocathode, the Armco cylinder was

---

* Obtained from Magnion, Inc., Cambridge, Mass.

Fig. 5. Solenoid Coils, Magnetic Shield and Typical Field Configuration

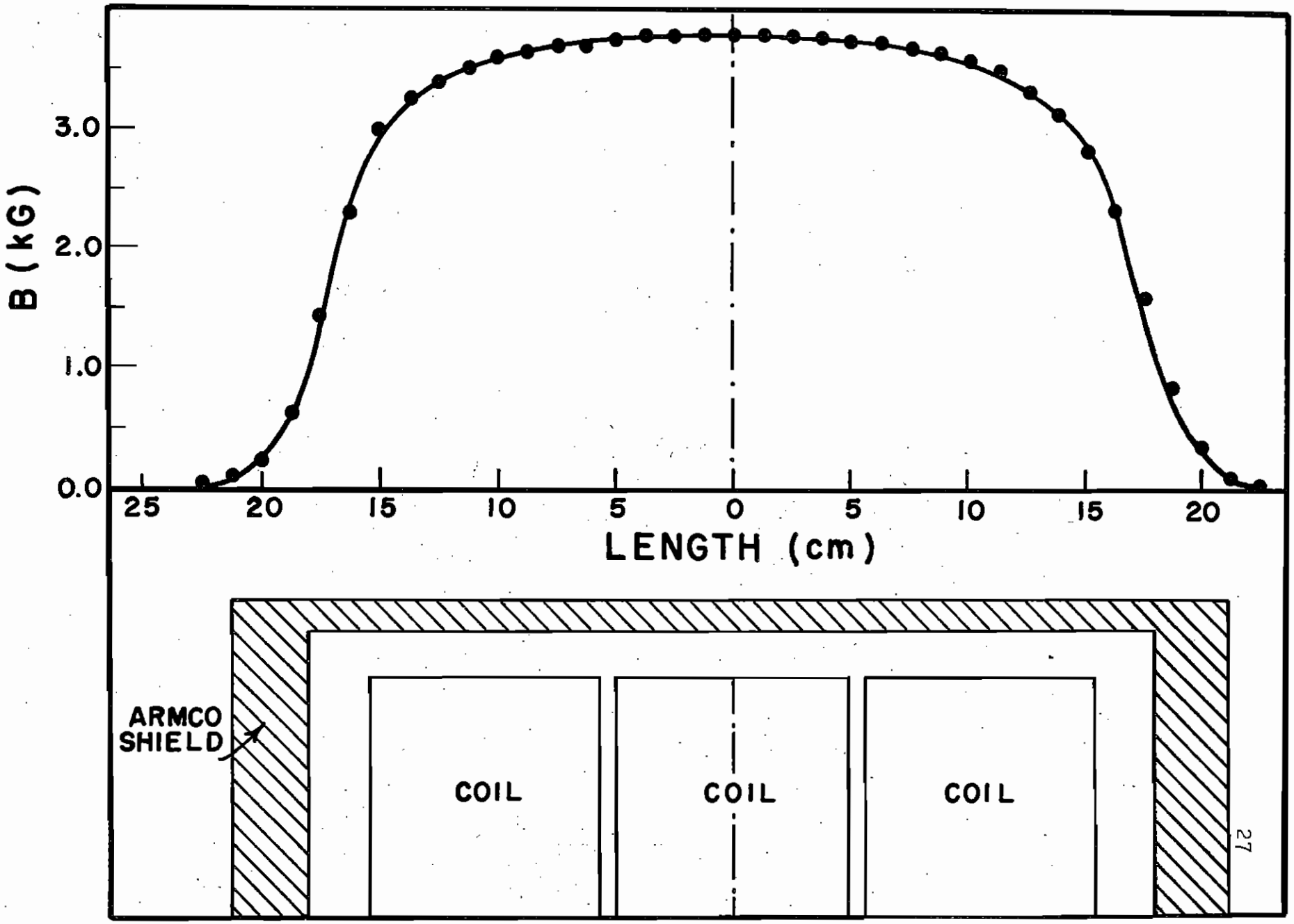
B (kG)
3.0
2.0
1.0
0.0
25
20
15
10
5
0
5
10
15
20
LENGTH (cm)
ARMCO SHIELD
COIL
COIL
COIL

extended 5 cm beyond the photocathode. A 5 cm light pipe was used to allow this shielding of the photocathode without placing the Armco in front of the scintillator itself. As an extra precaution an additional two layers of mu-metal extending 10 cm beyond the photocathode were added to the plastic detector photomultipliers.

Another possible fringe field effect would be that caused by the fringe field bending the incident beam in the region of the target and causing the beam to strike different areas of the target which might not have the same thickness. Using a Hall effect probe the field was measured in the region of the target and found to be less than one gauss. It was felt that this small a field could not have an appreciable effect on the beam over the short distance in which it could act. However, this one gauss fringe field would be enough to markedly affect the paths of back-streaming electrons inside the vacuum system caused by the charged particle beam striking the target. If we assume that the electron could follow one of two different paths depending on the solenoid current direction, then the amount of target current integrated by the beam integrator would be dependent on the solenoid current. That is, the integrated beam composed of two distinct parts: one, the incident charged particle beam and the other a varying backstream of electrons. This could cause one to erroneously count longer with a certain direction of solenoid current. Therefore, to prevent this eventuality, bias voltages were applied to both the target and beam collimator. At most the electron backstream effect could be only second order as is discussed in the section on false asymmetries.

Finally it is known that some depolarization of a neutron beam will occur as it passes through a solenoidal magnetic field due to the effect of the radial component of the field (Atkinson and Sherwood, 1965). But since the amount of depolarization would be a constant fraction of the polarization, this effect would simply decrease the effective value of P_1, which serves only to determine the magnitude of the $P_1P_2(\theta_2)$ angular distribution,

and therefore would have no effect on the phase shift calculation. Consequently, the depolarization due to this effect is only of secondary importance to the prime consideration in this work. However, a by-product of this present experiment is an accurate determination of P_1 whose true value is dependent on the amount of depolarization. The magnetic depolarization is discussed in Chapter VIII in connection with the value of P_1.

D. Polarimeter

A typical arrangement of the polarimeter has been shown in Figure 3. The plastic detectors were shielded from the neutron producing target by approximately 70 cm of paraffin, iron, copper, water and polyethylene. The charged particle beam struck the target and through use of a tapered polyethylene collimator inserted through the center of the paraffin shadow cone and the solenoid, a narrow neutron beam of half angle 1.3° was selected at an angle θ_1. The direction of its polarization vector was either parallel or anti-parallel to the normal to the reaction plane, i.e. it was vertical. Depending on the direction of the solenoid current the solenoid was capable of precessing the polarization vector through an angle $\emptyset$ to the right or to the left of the vertical. In this particular case the angle $\emptyset$ was chosen to be plus or minus $\pi/2$. Thus, the analyzing plane is vertical. Within this vertical analyzing plane the plastic scintillators could be placed at any angle from 0° to 150° in 10° increments. In the present experiment data were taken between 30° and 140°. Since at extreme forward angles the energy left in the helium cell was not sufficient to produce a pulse which could clearly be distinguished from phototube noise, the determination of the asymmetry for angles less than 30° was impossible.

Physical layout considerations precluded the inclusion of angles larger than 140°. The measurement of the analyzing angle is discussed fully in Chapter VII. For the reaction angle θ_1, an accurate determination is not actually necessary, since our only requirement on $P_1(\theta_1)$ is that it remain constant. The gunmount was anchored to the floor with this restriction in mind. The angle θ_1 was chosen to be 50° for 1.0 MeV and 25° for the 2.4 MeV measurement.

E. Helium Cell

The helium scientillation cell shown in Figure 6 employed in the present experiment was similar to the one described by Shamu (1962). The scintillation mechanisms of the noble gases have been discussed at length by Boersma (1963) and Koch (1960). The present cell was turned from a solid block of type 304 stainless steel and in the region of the sensitive volume had a wall thickness of 0.22 cm. The interior of the cell was polished and coated with a thin evaporated layer of aluminum over which a layer of MgO was deposited. The design purposed of this interior was to allow maximum light reflection. A detailed description of the coating technique is available in Appendix II. The viewing end of the helium cell was closed with a 1.9 cm tempered glass disc and an 0.95 cm backup plate of Lucite. A Teflon O-ring was used to seal the helium volume. A thin layer of diphenyl stilbene was evaporated onto the MgO coating and onto the glass window to serve as a wavelength shifter. This was necessary since the photomultiplier-light pipe combination provided poor sensitivity in the ultra-violet region of the spectrum where the most intense light from the helium cell was produced. After evacuation, the cell was filled with 1725 lbs/in^2 of research grade helium and 75 lbs/in^2 of xenon which served

Fig. 6. Helium Scintillation Cell

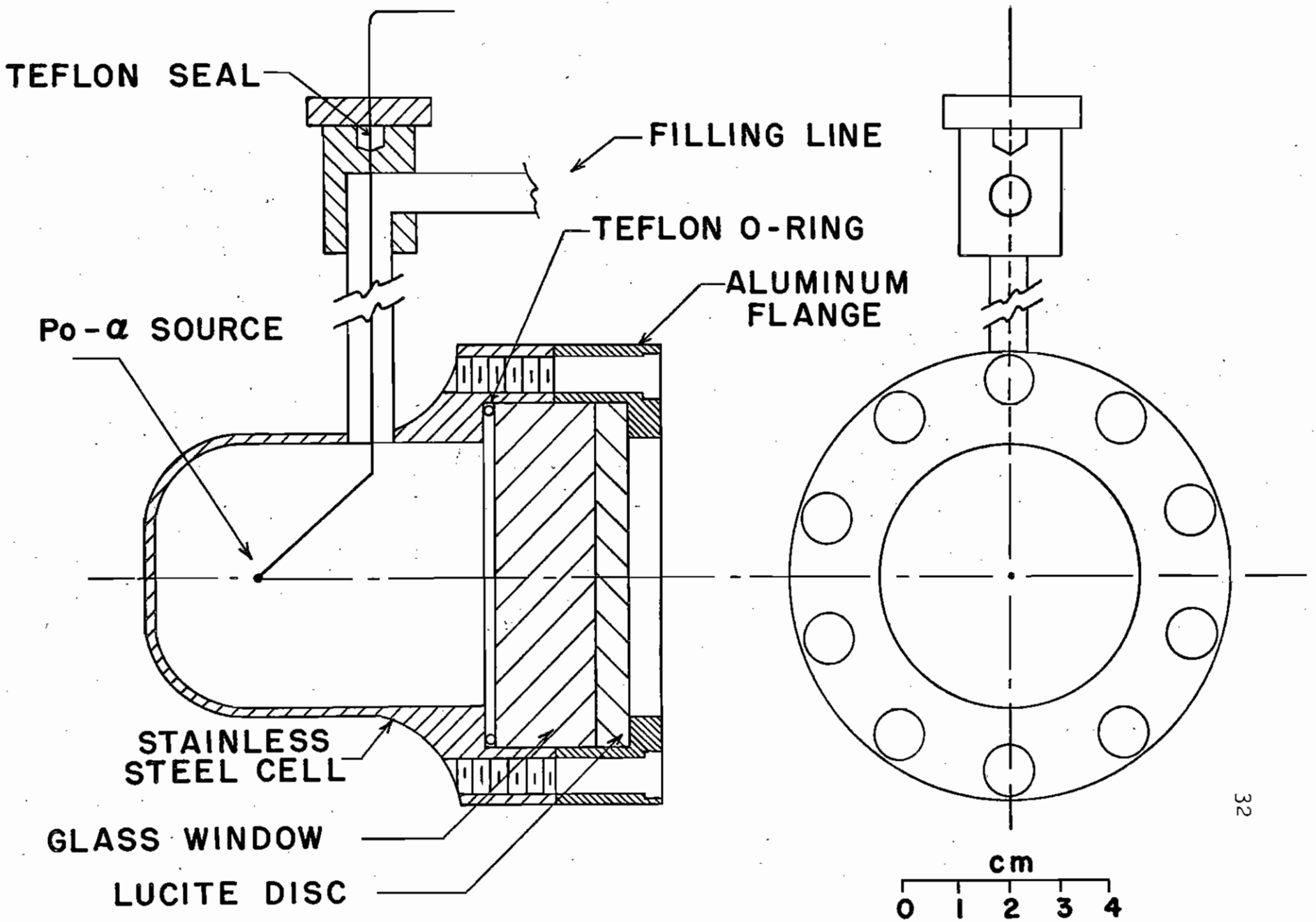
TEFLON SEAL
FILLING LINE
TEFLON O-RING
ALUMINUM FLANGE
Po-α SOURCE
STAINLESS STEEL CELL
GLASS WINDOW
LUCITE DISC
cm
0 1 2 3 4

to increase the light output. The amount of injected xenon was reduced from the value typically used to reduce the γ-ray sensitivity of the helium cell. However, the amount used was sufficient to provide satisfactory output pulses. A Lucite light pipe conducted the light flash into a RCA 6810-A photomultiplier magnetically shielded as described above.

In polarization measurements, high background fluxes are typically present in the vicinity of the plastic detectors. Helium scintillation cells are particularly well suited for determinations of this sort as the scintillations from the cell can be used to trigger a coincidence circuit. The helium cell output pulse height, which is a measure of the recoil energy of the struck α-particle, is linear in the cosine of the center-of-mass scattering angle (Shamu, 1962; Morgan, 1965). Thus by employing pulse height requirements only those neutrons which leave the required amount of energy in the helium cell for a given scattering angle are considered in calculating the asymmetry. The number of background counts may be reduced considerably in this manner.

The energy resolution of the present helium cell was about 9% for pulses from a weak Po-α source within the cell. Using the energy dependence of the resolution determined by Morgan (1965), the resolution of the present cell was about 28% and 19% for 1.0- and 2.4-MeV neutrons respectively.

F. Detectors

The plastic detectors employed in this experiment were two 5.1 x 2.5 x 5.1 cm^3 NE-102 plastic phosphors* placed 19 cm from the

---

* Available from Nuclear Enterprises, Ltd., Winnepeg, Canada.

center of the helium cell. In a plastic phosphor the neutrons are detectable because of the ionizing properties of the recoiling nuclei--primarily protons. NE-102 was selected because of its short decay time, ease of handling, and relatively low cost. The scintillators were wrapped with aluminum foil on five sides to prevent loss of light. To avoid excessive γ-ray sensitivity, a 0.5 cm thick layer of lead also covered five sides of the scintillator. Possible false asymmetries due to inscattering from the lead are discussed in Chapter VII, Sec. D. A 5 cm Lucite light pipe abutted the open face of the scantillator and conducted the light flash into a magnetically shielded photomultiplier tube. The light pipe allowed the magnetic shielding which surrounded the photomultiplier to extend 5 cm beyond the photo cathode. For the 1.0 MeV measurement, the detector discriminators were set so that only those pulses corresponding to maximum recoils initiated by neutrons of energy greater than approximately 200 keV were observed. The discriminator level at 2.4 MeV corresponded to about 240 keV.

G. Electronics

A block diagram of the electronic system is shown in Figure 7. The fast signal was taken from the anode of the RCA 6810-A and fed to a White emitter follower with a 50 ohm output impedance. An additional emitter follower isolating the tenth dynode signal was available to provide a slow pulse from the helium scintillator. The RCA 6810-A was selected because of its large output pulse which is necessary for precise timing in fast coincidence work. Accurate time determination may be made by allowing a discriminator to trigger relatively low on the leading edge of the output pulse. In order to use this technique, the peak height of the anode pulses

Fig. 7. Block Diagram of Electronics

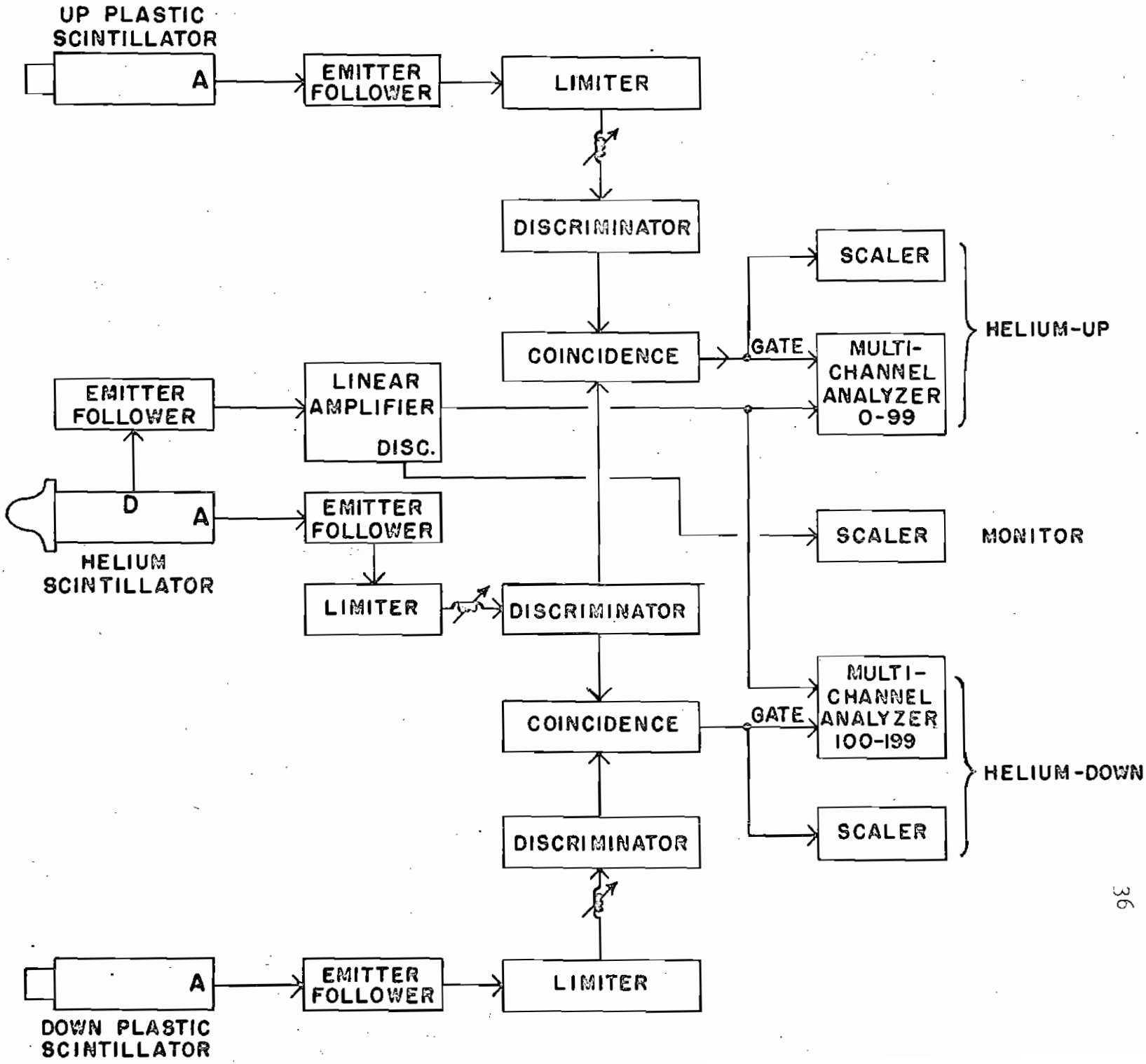
UP PLASTIC SCINTILLATOR
A
EMITTER FOLLOWER
LIMITER
DISCRIMINATOR
SCALER
COINCIDENCE
GATE
MULTI-CHANNEL ANALYZER 0-99
HELIUM-UP
EMITTER FOLLOWER
LINEAR AMPLIFIER
DISC.
D
A
EMITTER FOLLOWER
HELIUM SCINTILLATOR
SCALER
MONITOR
LIMITER
DISCRIMINATOR
MULTI-CHANNEL ANALYZER 100-199
COINCIDENCE
GATE
HELIUM-DOWN
DISCRIMINATOR
SCALER
A
EMITTER FOLLOWER
LIMITER
DOWN PLASTIC SCINTILLATOR

was considerably greater than the coincidence circuitry was capable of handling. Therefore a solid state pulse height limiter was used to limit the height to about 200 millivolts while maintaining the rapid rise time. After suitable delay, the pulses from each of the limiters were used to drive one half of a Chronetics Model 101 "Dual Discriminator"* which has a trigger level of 100 millivolts. These discriminators, when used with 5 ns external clipping stubs and at a Repetition Rate of 20 mc, yield output pulses of about 5 ns full width at half maximum. The total time resolution of the system was about 20 ns. The physical size of the detectors and the helium cell place a lower bound on the ultimate time resolution possible. The mean path of a neutron between its collision with an α-particle and its point of detection is 19 cm, however good coincidences can result from paths differing from the mean by as much as 5 cm in each direction. This effect alone resulted in a variation of about 10 ns between the detection times of good counts for back angles at 1.0 MeV.

Pulses from the helium cell discriminator and one of the plastic discriminators were fed to one half of a Chronetics Model 107 "Dual And" unit. Coincidence pulses from the "Dual And" unit were used to gate a 100-channel bloc in the Technical Measurement Corporation Model 404 Multichannel Analyzer.† Concurrently, pulses from the helium cell discriminator and the other plastic scintillator circuitry were fed to the other half of the "Dual And" unit and were used to gate the second 100-channel bloc in the analyzer. The multichannel analyzer observed the amplified slow helium cell output pulse. Thus, a coincidence peak was obtained in each 100-channel bloc in the analyzer corresponding to neutron scattering

---

* Available from Chronetics, Inc., Yonkers, New York.

† Available from Technical Measurement Corporation, North Haven, Connecticut.

through the desired analyzing angle. By integrating the peak area, one was able to obtain the number of neutrons which left the requisite amount of energy in the helium cell and at the same time were detected by a plastic scintillator. In order to monitor the operation of the coincidence electronics, scalers were used to count the "up-helium" and the "down-helium" coincidence pulses. A third scaler counted the discriminated output pulses of the slow helium amplifier which provided a monitor of the neutron flux.

For the extreme forward scattering angles, there was a large amount of relative broadening of the peak in the slow helium cell pulse due to the low light output resulting from small angle neutron scattering. Because of the large pulse height variations, the triggering time of the discriminators fluctuated; i.e. a time "jitter" existed. Therefore in order to include all good neutron scattering events, a longer clipping stub was employed so that the helium cell discriminator output pulse would be about 10 ns long.

At 1.0 MeV the delays in the up and down circuitry were set by observing the coincidence peak areas as a function of up-helium and down-helium delays. One could bring the coincidence circuit into timing for a given θ_2 by adjusting the helium delay. In order to optimize the timing of the coincidence system during a run and to check the above method, a Chronetics Model 105 "Time to Pulse Height Converter" was employed. The converter measured the time over-lap between the discriminator pulses from the helium cell circuitry and from one of the plastic scintillator circuits. By displaying this overlap on the multichannel analyzer and by changing the delays in such a manner to enhance the peaking of the highest voltage pulses which corresponded to maximum over-lap, one could optimize the timing of the coincidence unit. The delays obtained by this method agreed exactly with the results obtained using standard delay curve techniques. Figure 8 shows typical time-to-pulse height delay spectra for the higher energy where the γ-rays were more prominent and where the

Fig. 8. Typical 2.4 MeV Delay Curves

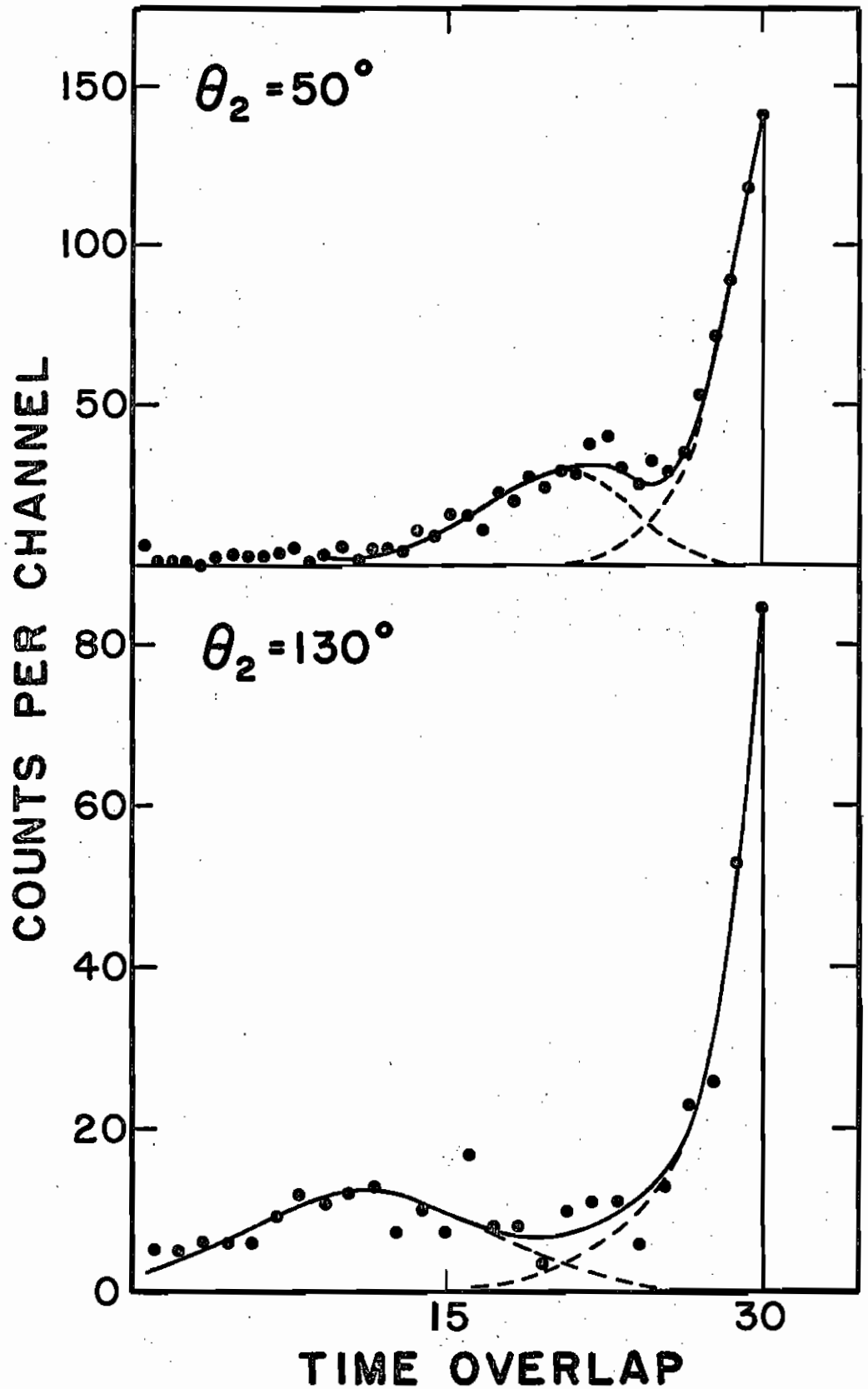
θ2 = 50°
θ2 = 130°
150
100
50
80
60
40
20
0
15
30
COUNTS PER CHANNEL
TIME OVERLAP

neutron flight time was less. Plotted are curves for analyzing angles of 50° and 130°. The high peak at the right is attributed to coincidence neutrons while the lower, broader left hand one is caused by γ-rays. As can be seen the γ-ray separation is not so pronounced at forward angles as the neutron flight time (9 ns) is so small that it can not be easily experimentally resolved from the γ-ray flight time. The neutron and γ-ray are separated by the expected amount at 50° however at 130° the separation is more pronounced than anticipated. This was attributed to differences in rise-times for neutrons and γ-ray pulses in the helium cell. The neutron-γ-ray separation was more pronounced at 1.0 MeV due to lower neutron velocities, i.e. greater flight time.

Chapter IV.

CHOICE OF TARGETS

There are several thing that must be considered in the choice of a neutron producing reaction for the source of polarized neutrons. Obviously the reaction must yield the polarized neutrons in as copious quantities as possible and must also have as high a polarization as possible. It is highly desirable that the target material be able to withstand beam currents of several microamperes so that counting time can be minimized. It was desired that the material be relatively cheap as several targets would probably have to be made. Furthermore the ease of fabrication and handling are to be considered.

These requirements leave us with two reactions which should be given major consideration: C^{12} (d,n) N^{13} and Li^{7} (p,n) Be^{7}. The carbon-12 reaction has several advantages. The Q-value of the ground state is low and there is freedom from excited state neutrons at the accelerator energy used. Furthermore, the targets are cheap and can withstand very high beam currents if properly cooled. On the other hand the appearance of room background due to deuterons striking carbon buildup on slits, etc. is a certain disadvantage. The polarization as a function of energy and angle is well known as is the differential cross section (Sawers et al., 1966) so that choice of the optimum energy and angle can be made with reasonable certainty. In addition, the polarization is high where the differential cross

section is large, an atypical situation. Shown in Figure 9 are the previous polarization measurements made at this laboratory for this reaction. The point marked present data was determined in this experiment and is discussed fully in Chapter VIII. In the region finally selected the polarization is about -0.46 and the laboratory differential cross section is about 32 mb/sr.

To reduce counting time, targets were chosen to be as thick as was consistent with an accurate measurement. The present choice of energy and angle gave a neutron energy of 2.44 MeV. At this energy the helium differential cross section and polarization are changing relatively slowly with energy and therefore permitted the use of a relatively thick target for the production of the neutrons. The carbon target used for this experiment was 175 keV thick for deuterons of 2.9 MeV incident energy. The thickness was measured by comparing the neutron yield from this target with the yield from a foil target of known thickness making proper allowances for background.* The thickness of the foil target was first determined by measuring the energy displacement of the Li^7 (p,n) Be^7 threshold with the foil in the beam path. The 175 keV target was made by depositing carbon from a colloidal solution of carbon in alcohol on a 10 mil thick tantalum cap. The tantalum cap fit over the beam pipe (Figure 4) which could be rotated about its axis thereby allowing selection of various spots on the single target used throughout the experiment. Shown on the left of Figure 10 is the target thickness as a function of the rotation angle. The dashed line represents 175 keV. The target can be seen to be uniform to within 10%.

---

* A great deal of experience has been gained at this laboratory in carbon foil production techniques (See Appendix I).

Fig. 9. Summary of Experimental Polarization Results for the Reaction $C^{12}(d,n)N^{13}$

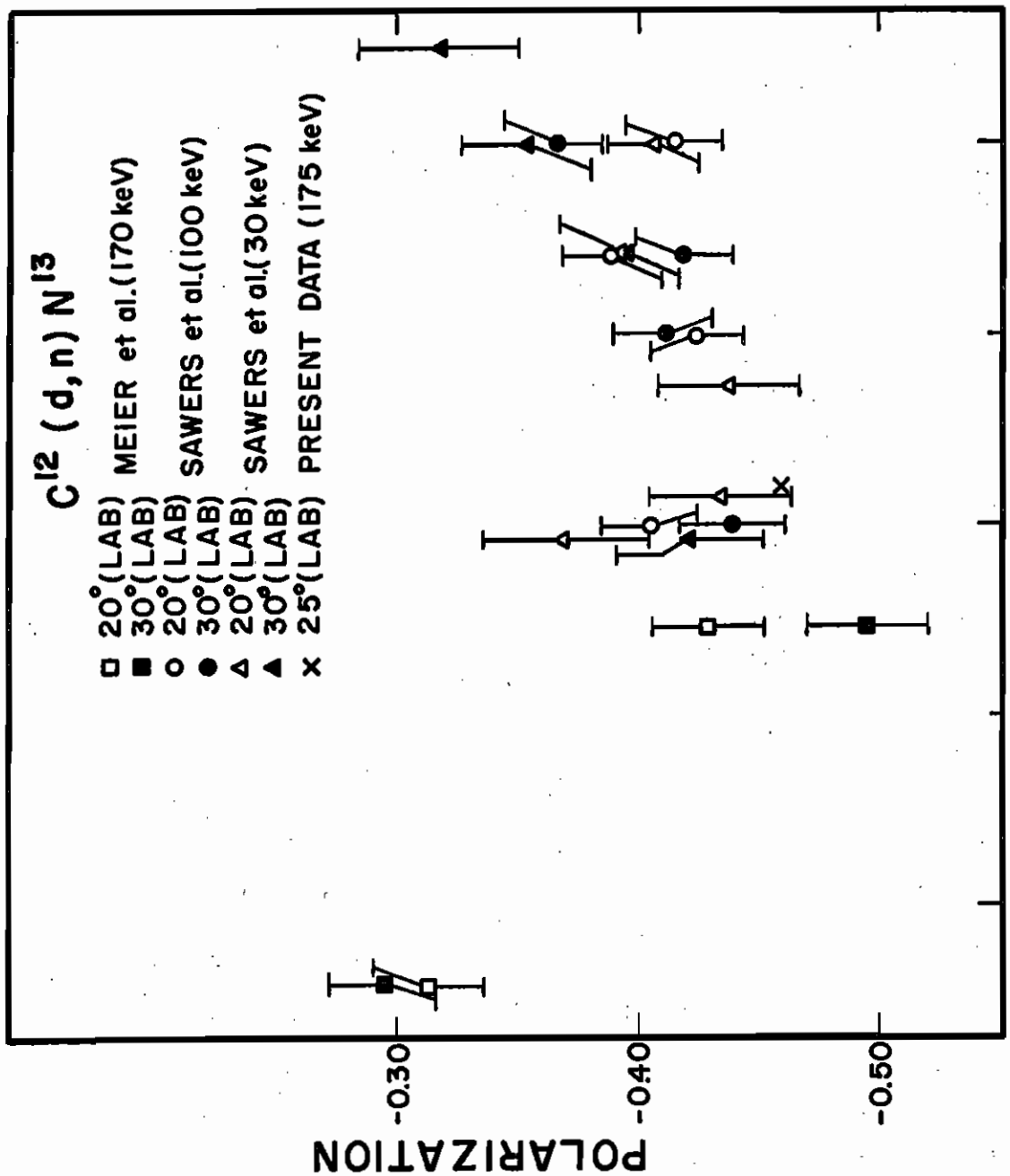
C^{12} (d, n) N^{13}
20°(LAB) MEIER et al.(170 keV)
30°(LAB)
20°(LAB) SAWERS et al.(100 keV)
30°(LAB)
20°(LAB) SAWERS et al.(30 keV)
30°(LAB)
25°(LAB) PRESENT DATA (175 keV)
POLARIZATION
-0.30
-0.40
-0.50
2.6
2.8
3.0
E_d (MeV)

Fig. 10. Carbon and Lithium Target Thickness vs. Rotation Angle

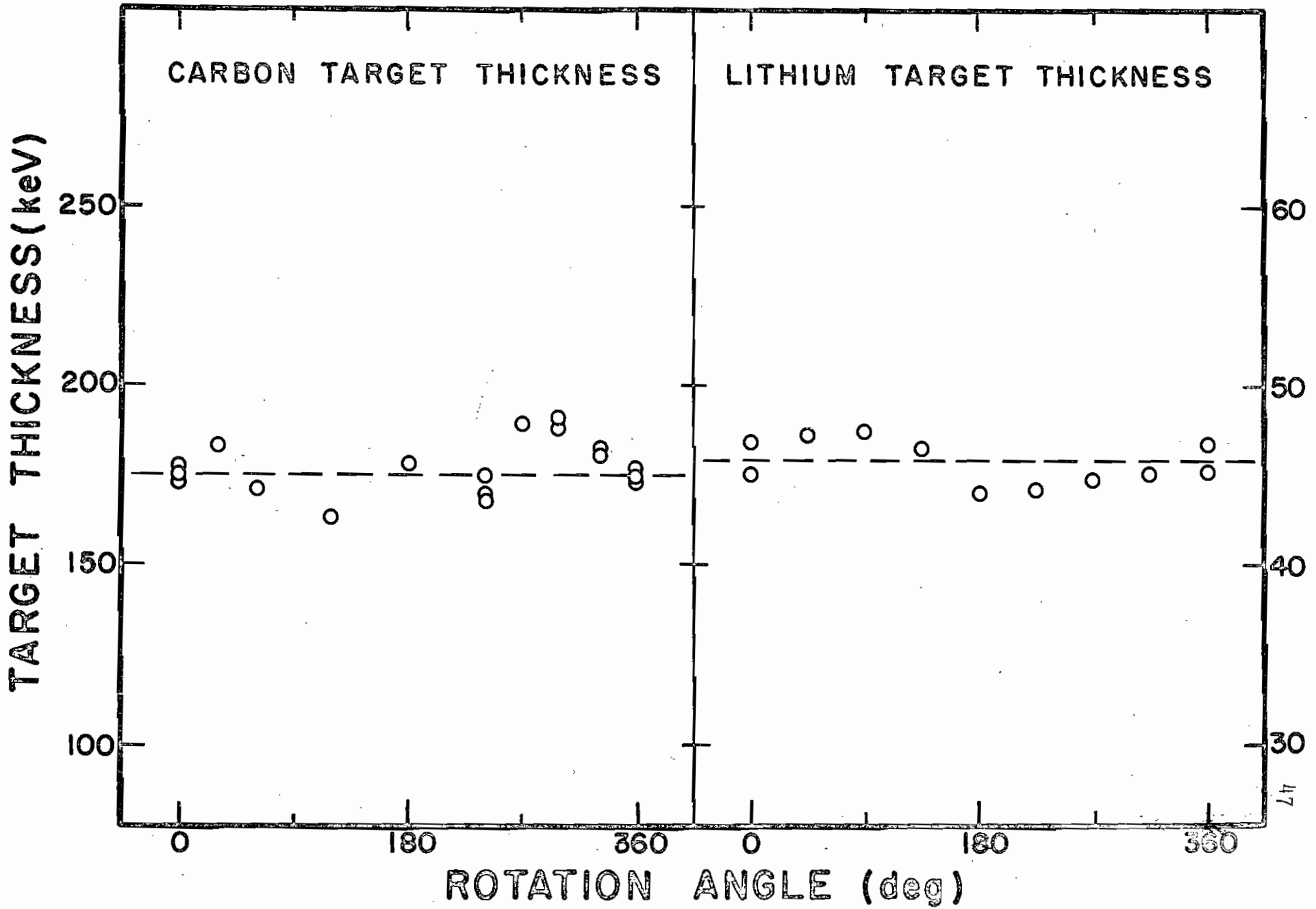
CARBON TARGET THICKNESS
LITHIUM TARGET THICKNESS
TARGET THICKNESS (keV)
250
200
150
100
60
50
40
30
0
180
360
0
180
360
ROTATION ANGLE (deg)

Fig. 11. Thin Target Asymmetry of $C^{12}(d, n)N^{13}$ Neutrons

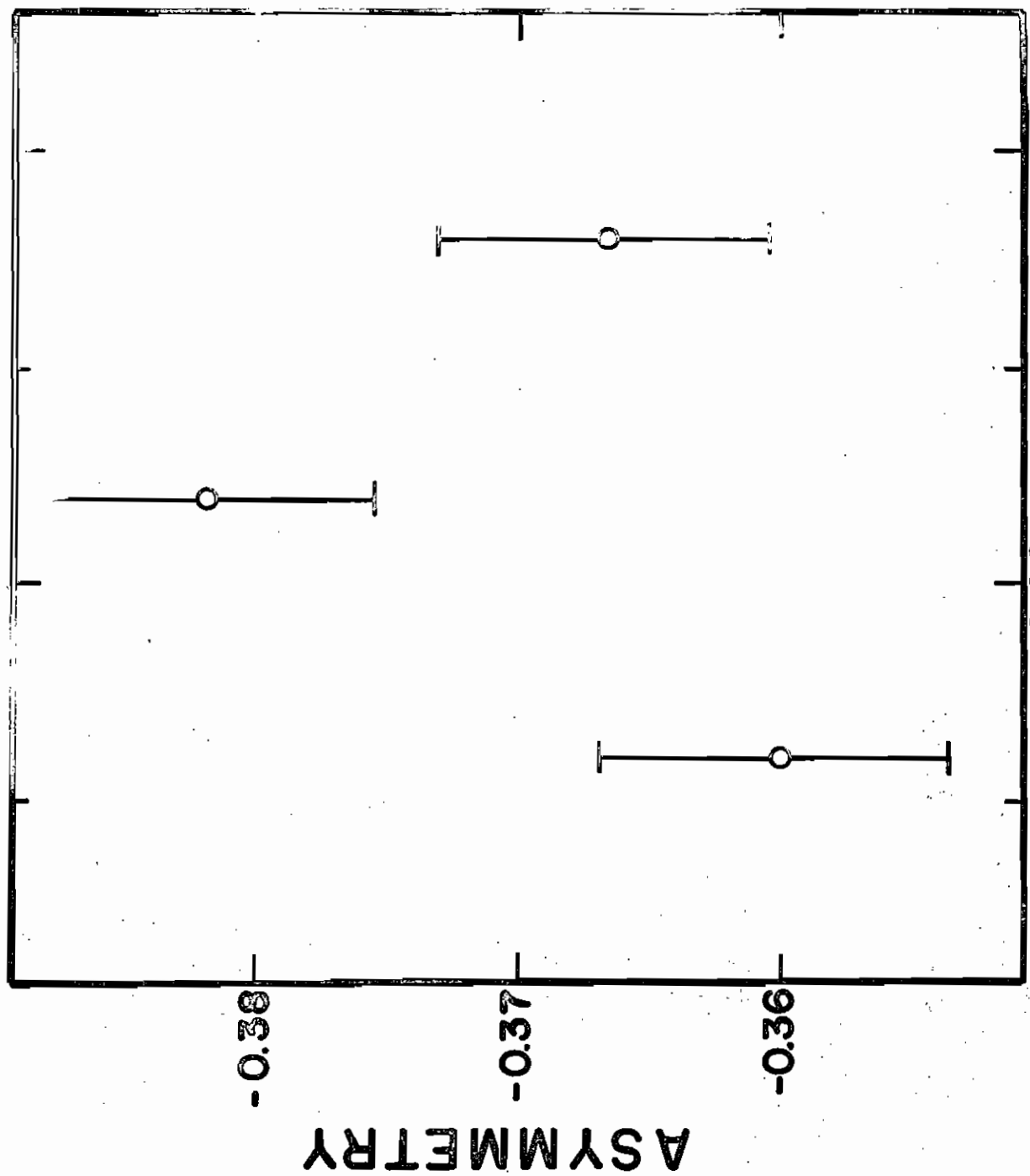
ASYMMETRY
-0.38
-0.37
-0.36
2.80
2.90
E_d (MeV)

The Van de Graaff voltage for the 2.4 MeV angular distribution was chosen so that i) the target thickness subtended the valley in the C^{12} (d, n) N^{13} yield near 2.85 MeV so that the production cross section would be relatively constant across the whole of the target thickness and ii) the polarization was optimum and nearly constant across the energy in question. This choice of energy and angle is reasonable as the polarization peaks at this energy for $\theta_1 = 25^{\circ}$ (lab) and fortunately the differential cross section peaks at this angle also.

As was mentioned above, the polarization was optimum and nearly constant for the present experiment. To determine the energy dependence more precisely, the asymmetry was measured with a 60-keV target at three energies across the energy spanned by the present target. The measured asymmetries are shown graphically in Figure 11. A slight peaking in the asymmetry was noted. Since the analyzing power and cross section of helium are nearly constant in this energy range, it was not felt that a correction for this small effect was necessary.

The reaction Li^7 (p, n) Be^7 is not as completely mapped as is the carbon reaction but in the region of 50° (lab) and $E_p = 3.0$ MeV the neutron polarization has been measured by several groups, most recently by Andress et al. (1965). The polarization near 50° (lab) is shown in Figure 12. The polarization could be expected to be in the neighborhood of 0.30. A laboratory production cross section essentially flat over the energies considered of about 35 mb/sr could be anticipated (Bevington et al. 1961). A marked disadvantage to using this reaction is that background will arise from the first excited state neutrons which are separated from the ground state neutrons by only 0.44 MeV. On the positive side, the 50° intensity ratio of excited state neutrons to ground state neutrons $I_1/I_0 = 0.1$ (Bevington et al., 1961). The helium cell pulse height for the excited state neutrons is lower than for the ground state. Since the analysis is carried out on the ground state coincidence peak, the nature of the excited

Fig. 12. Summary of Experimental Polarization Results for the Reaction $Li^7(p,n)Be^7$

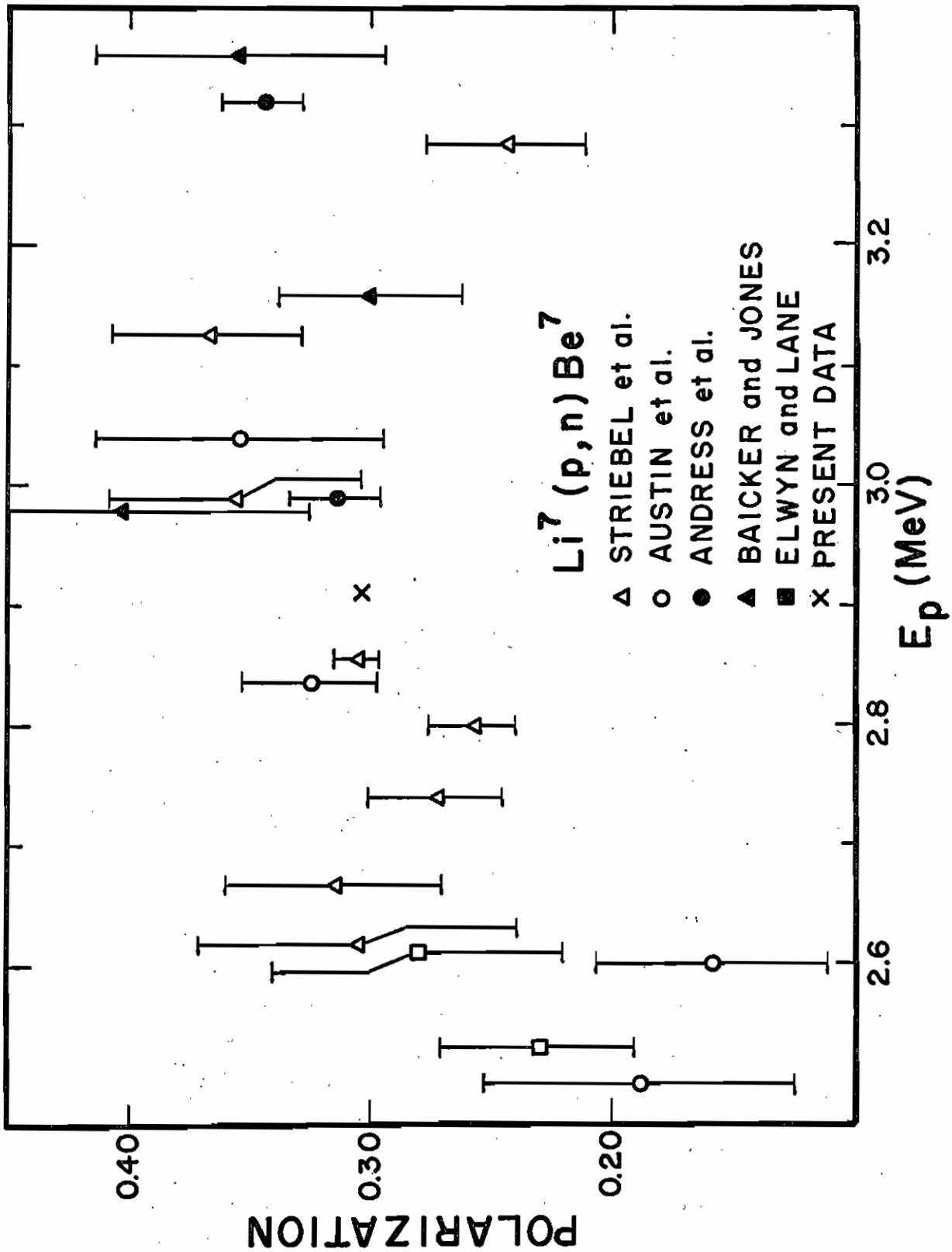
POLARIZATION
0.40
0.30
0.20
2.6
2.8
3.0
3.2
E_p (MeV)
$Li^7(p,n)Be^7$
△ STRIEBEL et al.
○ AUSTIN et al.
● ANDRESS et al.
▲ BAICKER and JONES
■ ELWYN and LANE
× PRESENT DATA

state contribution is that of a tail extending under the coincidence peak. Also the helium elastic scattering cross section for the excited state neutrons is considerable lower than for the ground state. In addition the plastic scintillator bias requirements tended to reduce this contribution even further as discussed later. Furthermore, recent work at this laboratory has shown that the polarization of the excited state neutrons is zero to within a statistical accuracy of 0.025 in the neighborhood of 3 MeV (Morgan et al., 1965). Therefore, the presence of this neutron group will at most contribute a non-subtracting unpolarized background.

It should also be mentioned that it is well known that the use of LiF targets, the most common of the lithium target materials, gives a large background of gamma-rays. With this in mind, and with the knowledge that metallic lithium targets yield three times more neutrons for a given proton thickness, it was decided to employ lithium metal targets. Precautions made necessary by the high chemical activity of lithium metal are described in Appendix I as are production techniques for these targets. The complex manufacturing techniques used were convenient as a vacuum evaporator was readily available. The alternative would have been to place a small lithium furnace in the neighborhood of the target. Since it was desired to have the final collimator as close to the target as possible, the use of a furnace was ruled out.

Since the helium differential cross section and polarization are strong functions of the energy below the 1.3 MeV resonance, the acceptable thickness of the target for the 1.0 MeV angular distribution was considerably less than for the 2.4 MeV distribution. Two different targets were used for the 1.0 MeV measurement and both were 46 keV thick to protons at lithium threshold as determined by the "rise-curve" method. The incident proton energy required to produce 1 MeV polarized neutrons at 50° (lab) is 2.92 MeV. At this energy the lithium metal targets were 33 keV thick to protons. After including the effect of the angular spread accepted

by the polarimeter the total neutron energy spread at the helium cell was 50 keV. Measurements were made and it was determined that the targets were uniform with respect to rotation to within 5% as is shown on the right of Figure 10. The small variations were averaged out by making asymmetry measurements at several orientations of the target for each θ_2. Therefore no special precautions were necessary to correct for the variation in target thickness, which in this energy region could cause some differences in the observed asymmetries as the cross section and the polarization are highly dependent on energy.

Chapter V.

MOCCASINS,

MONTE CARLO CALCULATION OF ASYMMETRY IN NEUTRON SCATTERING

A. Object of the Program

Earlier calculations at this laboratory (Andress et al. (1965) have indicated the need for considering multiple scattering within the helium cell when analyzing data from high accuracy experiments. In addition, the zone-type $\bar{P}_2$ calculations * by Purser (1965) previously used, have ignored ϕ dependence, where ϕ represents the projection of the scattering angle in the plane perpendicular to the mean scattering plane determined by the helium cell and the detector. While it was felt that the zone-type calculation was sufficiently accurate for measurements made near the peak in the polarization, it was suspected that for angles where either $d\sigma/d\Omega$ and/or P_2 were strong functions of θ_2 the results might tend to be erroneous. This was in fact found to be the case. Therefore, to determine the effect of $\overline{P_2}(\theta_2)$ and multiple scattering, a complete Monte Carlo program was written. MOCCASINS, the name assigned to this computer code, is designed to analyze single or double neutron scattering. A spherical volume of helium is assumed to be used in conjunction with one or more scintillators as a polari-

---

* $\bar{P}_2$ indicates the analyzing power averaged over the geometry of the polarimeter.

meter. In the single scattering mode MOCCASINS can be used to provide a Monte Carlo $\bar{P}_2$ calculation to any desired degree of statistical accuracy.

The object of the program is to calculate the probabilities and the associated polarizations for neutrons scattering from the helium into the plastic scintillators. In addition, the probability of leaving a given amount of recoil energy in the helium cell as a function of the recoil energy and detector position is available. This output, in the form of a histogram for each θ_2, allows matching of the calculated expected coincidence peak shape and magnitude. In order to accomplish this a simple program was written to smear the histogram with a Gaussian distribution whose standard deviation was selected to match the experimentally observed peak width.

The single scattering polarization $P_{ss}(\theta_{2j})$ is given by:

$$P_{ss}(\theta_{2j}) = \frac{\sum_{i=1}^{N} W_{ss_i}(\theta_{2j}) \cdot P_{ss_i}(\theta_{2j})}{\sum_{i=1}^{N} W_{ss_i}(\theta_{2j})} \qquad (1)$$

where the subscripted i enumerates the polarization $P_{ss_i}(\theta_{2j})$ and the composite probability $W_{ss_i}(\theta_{2j})$ associated with the individual neutron history i. The sum is over all neutron histories from i = 1 to N. Calculations of the polarization is straight forward and preceeds directly from the phase shift analysis. A completely analogous relation, eq. (2), holds for the multiple scattering case with the exception that the multiple scattering polarizations $P_{ms_i}(\theta_{2j}, N_{ms})$ must now be computed using the Wolfenstein triple scattering formalism described below:

$$P_{ms}(\theta_{2j}) = \frac{\sum_{i=1}^{N} \sum_{N_{ms}=1}^{N_{obs}} W_{ms_i}(\theta_{2j}, N_{ms}) \cdot P_{ms_i}(\theta_{2j}, N_{ms})}{\sum_{i=1}^{N} \sum_{N_{ms}=1}^{N_{obs}} W_{ms_i}(\theta_{2j}, N_{ms})} \quad . \qquad (2)$$

In addition, the composite probability $W_{ms_i}(\theta_{2j}, N_{ms})$ and the composite probability-polarization product must be summed over the multiple scattering sites for each initial site, i.e., for $N_{ms} = 1$ to N_{obs}. The composite probability for a complete history of either a singly or a multiply scattered neutron is evaluated using either eq. (3) or (4) given below, where the subscripts 1-3 refer to the sites of the first scatter, second scatter, and detection. These subscripts are also used to index the quantities associated with these scatters and the events prior to scattering.

$$W_{ss_i}(\theta_{2j}) = T_1 \cdot T_3 \cdot P_{event\ 1} \cdot P_{1\text{-det}} \cdot P_{coin} \cdot d\Omega_1 \cdot d\Omega_3 \ , \quad (3)$$

$$W_{ms_i}(\theta_{2j}, N_{ms}) = T_1 \cdot T_2 \cdot T_3 \cdot P_{event\ 1} \cdot P_{1\text{-}2} \cdot P_{2\text{-det}} \cdot P_{coin} \cdot d\Omega_1 \cdot d\Omega_2 \cdot d\Omega_3 \cdot (\text{FRACTION})^2 \cdot (N_{el}/N_{obs}) \quad (4)$$

where

T_1 = Transmission from the neutron source to site 1,

T_2 = Transmission from site 1 to site 2,

T_3 = Transmission from site of last scatter to point of detection,

$P_{event\ 1}$ = Probability of interaction occuring in volume element surrounding site 1,

$P_{event\ 2}$ = Probability of interaction occuring in volume element surrounding site 2,

$P_{1\text{-}2}$ = Probability that if a scatter occurs in the volume element surrounding site 1 that it will be in the direction from site 1 toward site 2,

$P_{1\text{-det}}$ = Probability that if a scatter occurs in the volume element surrounding site 1 that it will be in the direction from site 1 toward the detection point,

$P_{2\text{-det}}$ = Probability that if a scatter occurs in the volume element surrounding site 2 that it will be in the direction from site 2 toward detection point,

P_{coin} = Probability that if simultaneous scintillations occur in both the helium cell and in the plastic detector, that the pulse height in the helium cell will be of sufficient magnitude so that the pulse will occur in the coincidence peak,

$d\Omega_1$ = Solid angle subtended by volume element at site 1 as seen from the neutron source,

$d\Omega_2$ = Solid angle subtended by the volume element at site 2 as seen from site 1,

$d\Omega_3$ = Solid angle subtended by the detector as seen from site 1 in single scattering and from site 2 in multiple scattering,

FRACTION= Random fractional amount by which the separational distance between site 1 and site 2 has been reduced,

N_{el} = Number of volume elements of the chosen size that will fit in the helium sphere assuming no crevices,

N_{obs} = Number of volume elements considered, i.e. the number of second sites to first sites.

All of the numbers on the right of eqs. (3) and (4) except N_{el} and N_{obs} are dependent on θ_{2j} and i but for simplicity the dependence was not shown. In addition, FRACTION and all of the terms in eq. (4) subscripted with a 2 or a 3 are dependent on N_{ms}, the number indexing the second scattering sites with respect to the first scattering sites. The evaluation of T_1, T_2, T_3,

$P_{event\ 1}$, and $P_{event\ 2}$, with the exception of geometry is simply a transmission or an absorption calculation. $P_{1\text{-}2}$, $P_{1\text{-}det}$, and $P_{2\text{-}det}$ are evaluated using the ratio $(d\sigma/d\Omega)/\sigma_T$, where $d\sigma/d\Omega$ is evaluated at the desired angle. The determination of the solid angles $d\Omega_1$, $d\Omega_2$, and $d\Omega_3$ proceeds directly from the definition of a solid angle.

The calculation of P_{coin} if done rigorously is non-trivial as it requires numerical integration of a Gaussian; hence a speedier approximation must be used to prohibit use of extravagant amount of computer time. The normal Gaussian is replaced by a parabola which goes to zero at two standard deviations from the mean; the probability is considered zero elsewhere. This gives a reasonably good approximation to the Gaussian. In practice the peak of the parabola is taken to be the neutron energy as it strikes the plastic and the standard deviation is taken as the helium cell resolution. The helium cell-plastic scintillator geometry is used to calculate the maximum and minimum energies possible for good counts. The P_{coin} is simply the integral of the parabola over that portion of the acceptable energies that overlaps the parabola. Thus, by normalization requirements on the parabola's area we have

$$0 \leq P_{coin} \leq 1 \ .$$

A modified Russian roulette technique is employed to insure that the more interesting types of events (larger values of solid angle $d\Omega_2$) are examined more often. On the average site 2 will be far from site 1 in terms of the sampling volume element size. The possibility of close spacings of site 1 with respect to site 2 can give large values for the weight of the particular history where this occurs. To alleviate this problem, more positions with close spacings are chosen. Site 1 is randomly chosen and so is an initial site 2, then site 2 is moved to its final position a random amount closer to site 1. The random fractional amount by which

the initial site 1 to site 2 distance is reduced is called FRACTION. Since we are choosing more points closer in, we must reduce the weighting of these points proportionally. To avoid extremely large values of $d\Omega_2$, the minimum center-to-center distance from site 1 to site 2 is limited to three times the sampling volume radius.

In addition to Russian roulette, another technique is used to improve the statistics for multiple scattering. Neutron multiplication is allowed; that is, a multiplicity of second sites is chosen for each initial site and the neutron histories from each of these sites is then traced. The weight of each history is correspondingly reduced by one over the number of second sites to first sites, N_{obs}.

The only other number necessary for the calculation is the number of volume elements N_{el} that can be fit into the helium sphere. Since the second scattering has an equal probability of occuring in each of the elements, ignoring energy, angle and proximity effects, we must multiply the weight of a doubly scattered neutron by the total number of possible volumes in which an interaction might take place.

B. Triple Scattering Formalism

The only term in eq. (3) and (4) whose evaluation has not been explained is the polarization for multiply scattered neutrons $P_{ms_i}(\theta_{2j}, n_{ms})$. The Wolfenstein formalism can be specialized to this case; that is, the case of two scatters in the helium cell in addition to the production of a polarized beam. This is shown schematically in Figure 13. To describe the geometry of a triple scattering experiment, we must first define the normal unit vector $\vec{n}_i$,

$$\vec{n}_i = \frac{\vec{k}_i \times \vec{k}_{i+1}}{\vec{k}_i \times \vec{k}_{i+1}} \qquad (5)$$

Fig. 13. Geometry for Multiple Scattering within the Helium Scintillation Cell

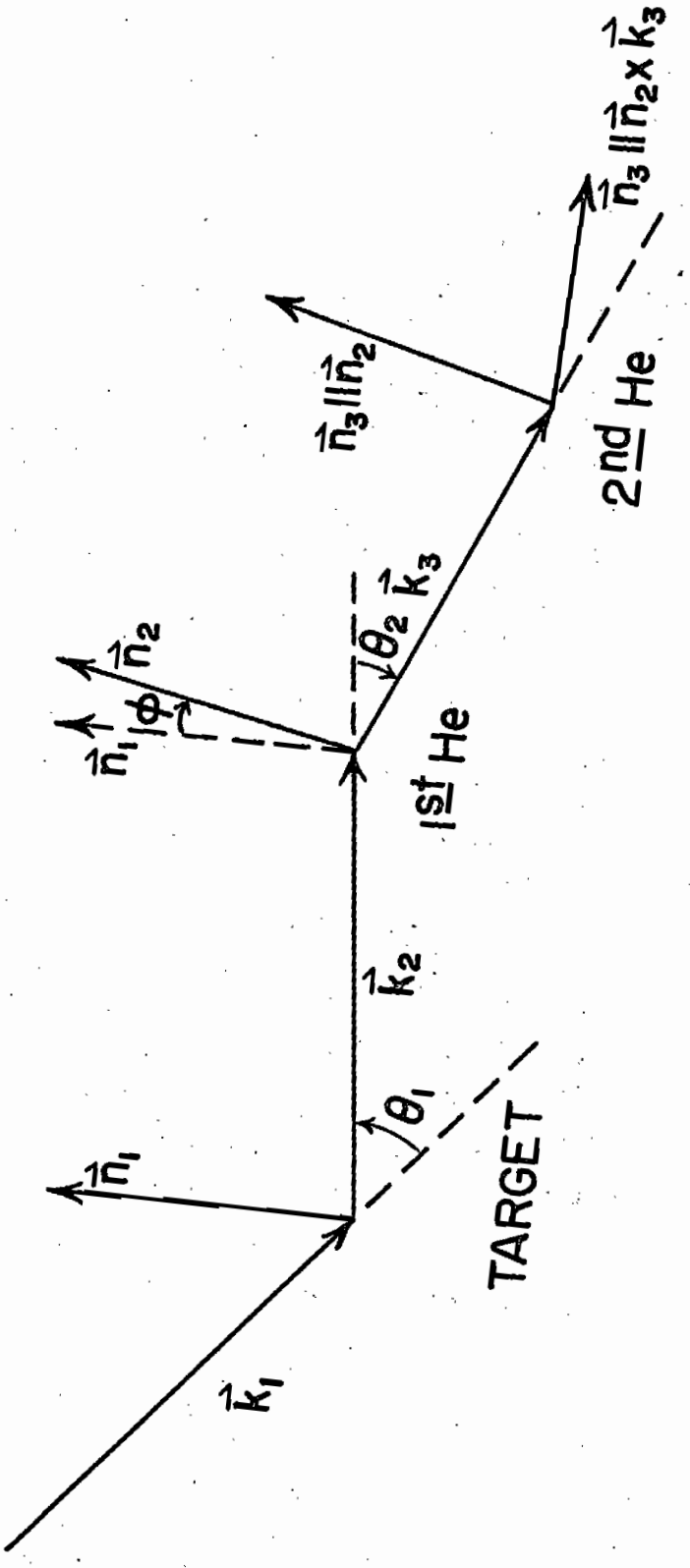
$\vec{n}_3 \| \vec{n}_2 \times \vec{k}_3$
$\vec{n}_3 \| \vec{n}_2$
2nd He
$\vec{k}_3$
θ_2
$\vec{n}_2$
$\vec{n}_1$
ϕ
1st He
$\vec{k}_2$
θ_1
$\vec{n}_1$
TARGET
$\vec{k}_1$

where $\vec{k}_i$ and $\vec{k}_{i+1}$ are the unit vectors in the incident and outgoing directions respectively and the subscript i is the number of the scattering event. The beam incident on the second scatter is polarized along $\vec{n}_1$. For a given scattering angle θ_2, the second scattering direction is completely defined by the azimuthal angle ϕ, defined by

$$\cos\phi = \vec{n}_1 \cdot \vec{n}_2 \quad \text{and} \quad \sin\phi = \vec{n}_1 \times \vec{n}_2 \cdot \vec{k}_2 . \tag{6}$$

In the third scattering a right-left asymmetry is measured relative to the direction $\vec{n}_3$; since polarization along the direction of motion can not be detected, two directions of $\vec{n}_3$ are sufficient. Therefore, we need only consider the cases where $\vec{n}_3 \parallel \vec{n}_2$ and where $\vec{n}_3 \parallel \vec{s}$ with

$$\vec{s} = \vec{n}_2 \times \vec{k}_3 . \tag{7}$$

Thus, the third scattering may be chosen to determine either $\langle\vec{\sigma}\rangle_2 \cdot \vec{n}_2$ or $\langle\vec{\sigma}\rangle_2 \cdot \vec{s}$, where $\langle\vec{\sigma}\rangle_2$ is the expectation value of the spin vector after the second scattering. These two numbers will be referred to as the triple scattering asymmetries ε_{3n} and ε_{3s}.

It may be shown (Wolfenstein and Ashkin 1952) that $I_2\langle\vec{\sigma}\rangle_2$ depends at most linearly on $\langle\vec{\sigma}\rangle_1$, where I_2 is the differential scattering corss section of the second scatter and $\langle\vec{\sigma}\rangle_1$ is the expectation value of the spin vector before the second scattering. Using this fact and noticing that $\langle\vec{\sigma}\rangle_2 \cdot n_2$ is scalar while $\langle\vec{\sigma}\rangle_2 \cdot s$ is pseudo-scalar, we determine the most general dependence of these quantities on $\vec{k}_2$ and $\vec{k}_3$ and $\langle\vec{\sigma}\rangle_1$:

$$I_2\langle\vec{\sigma}\rangle_2 \cdot \vec{n}_2 = I_o\,(P_2 + D\langle\vec{\sigma}\rangle_1 \cdot \vec{n}_2) \tag{8}$$

$$I_2\langle\vec{\sigma}\rangle_2 \cdot \vec{s} = I_o\,(A\langle\vec{\sigma}\rangle_1 \cdot \vec{k}_2 + R\langle\vec{\sigma}\rangle_1 \cdot (\vec{n}_2 \times \vec{k}_2)) \tag{9}$$

where P_2, D, A, and R are arbitrary functions of $\vec{k}_2 \cdot \vec{k}_3$, that is the scattering angle θ_2. We have factored out I_o the differential cross section

for the unpolarized beam which is a function of θ_2 alone. For later use we shall include the expression for the undetectable component of $\langle\vec{\sigma}\rangle_2$ with A' and R' arbitrary:

$$I_2\langle\vec{\sigma}\rangle_2 \cdot \vec{k}_3 = I_o \left[A'\langle\vec{\sigma}\rangle_1 \cdot \vec{k}_2 + R'\langle\vec{\sigma}\rangle_1 \cdot (\vec{n}_2 \times \vec{k}_2) \right] . \tag{10}$$

Substituting $P_1 n_1$ for $\langle\vec{\sigma}\rangle_1$ and recalling that

$$I_2 = I_o (1 + P_1 P_2 \cos \emptyset) \tag{11}$$

as was mentioned in the discussion on double scattering in Chapter II, we may write the triple scattering asymmetries

$$\varepsilon_{3n} = \frac{P_3 (P_2 + D P_1 \cos \emptyset)}{1 + P_1 P_2 \cos \emptyset} \tag{12}$$

$$\varepsilon_{3s} = \frac{P_3 P_1 R \sin \emptyset}{1 + P_1 P_2 \cos \emptyset} \tag{13}$$

where ε_{3n} is associated with the case where all scattering events are coplanar and ε_{3s} with the case where the first scattering plane is perpendicular to the second. The function A cannot be determined in a triple scattering experiment since $\langle\vec{\sigma}\rangle_1$ must be perpendicular to $\vec{k}_2$ after a single scattering. Therefore the term containing A drops from eq. (9) in arriving at eq. (13). There are then two new parameters D and R.

The parameter D may be considered as giving the extent to which the second scattering depolarizes an initially polarized beam. This may be seen by considering $\langle\vec{\sigma}\rangle_2$ for $P_1 = 1$ and $\cos \emptyset = \pm 1$; from eqs. (8) and (11) we find

$$\langle\vec{\sigma}\rangle_2 = \vec{n}_2 \frac{P_2 \pm D}{1 \pm P_2} \tag{14}$$

Therefore D = 1 is a necessary and sufficient condition for no depolarization The above equation together with the requirement that $\langle\vec{\sigma}\rangle_2 \leq 1$ yield the following limits on D:

$$-1 + 2 \left|P_2\right| \leq D \leq 1 \ . \tag{15}$$

If the target has spin zero and the incident beam is completely polarized, the beam after scattering can still be described by a wave function representing a pure state and the beam will still be completely polarized. Therefore, equation (15) requires D = 1 for spin zero nuclei.

For the case where the successive scattering planes are at right angles, letting $P_1 = 1$ and $\phi = 90^\circ$ for a spin zero nucleus we find from eqs. (8), (9), (10), and (11)

$$\langle\vec{\sigma}\rangle_2 = P_2 \vec{n}_2 + R\vec{s} + R' \vec{k}_3 \ . \tag{16}$$

It follows that

$$|R| \leq (1-P_2^{\,2})^{1/2} \ . \tag{17}$$

We may get a physical picture of the R-parameter for this case where we see that the original spin vector $\vec{n}_1$ is bent out of the scattering plane so that its component along $\vec{n}_2$ is P_2. This is shown schematically in Fig. 14.

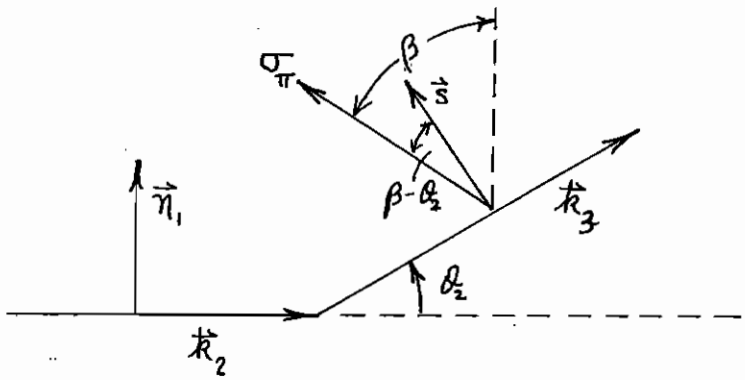

Fig. 14. Vectors Used in Defining the R-Parameter

Therefore, since $\langle \vec{\sigma} \rangle_2$ must equal unity, its projection in the plane has a magnitude $(1- P_2^{\,2})^{1/2}$. The projected vector σ_π may be rotated by an angle β about the $\vec{n}_2$ axis from the direction $\vec{n}_1$. It follows that

$$R = (1 - P_2^{\,2})^{1/2} \cos(\theta_2 - \beta) \tag{18}$$

where θ_2 is the laboratory scattering angle.

Wolfenstein has shown (1949, 1954) that the scattering amplitude may be written as an arbitrary matrix

$$M = g(\theta) - i\, \vec{\sigma} \cdot \vec{n}\, h(\theta) \tag{19}$$

where the g's and h's turn out to be the same as those given by eqs. ( ) and ( ) in Chapter II. In this notation the unpolarized differential cross section is given by

$$I_o = 1/2\, T_R (MM^+) = |g|^2 + |h|^2 \tag{20}$$

and the asymmetry in scattering a completely polarized beam is

$$P = \frac{T_R (M^+ \vec{\sigma} M)}{T_R (M^+ M)} = - \frac{2\, \mathrm{Im}(g^* h)}{|g|^2 + |h|^2} \quad . \tag{21}$$

By applying eq. (19) to an arbitrary spinor and using eqs. (20) and (21), Wolfenstein (1954) obtained the expressions

$$\sin\beta = - \frac{2\, \mathrm{Re}(g^* h)}{I_o (1- P^2)^{1/2}} \tag{22}$$

$$\cos\beta = \frac{(|g|^2 - |h|^2)}{I_o (1 - P^2)^{1/2}} \tag{23}$$

which allow complete determination of the R-Parameter. Once R and D have been determined, the triple scattering asymmetries ε_{3n} and ε_{3s},

observed for parallel and perpendicular scattering planes respectively, may be evaluated using eqs. (12) and (13). In general the triple scattering polarization $P_{ms_i}(\theta_{2j}, N_{ms})$ is the combination of $\mathcal{E}_{3n}$ and $\mathcal{E}_{3s}$ for the correct final analysis plane.

C. Description of the Method

To aid in the discussion of the program a flow diagram is shown in Figure 15. After reading the input data and proceeding through a few simple bookkeeping steps, the program either reads in a matrix of phase shifts as a function of energy and calculates the matrix POLPAC or simply reads a completed POLPAC deck from a previous MOCCASINS run. POLPAC consists of the laboratory scattering angle θ_{lab}, the incident laboratory neutron energy E_n, the differential cross section $d\sigma/d\Omega$, the polarization P, the Wolfenstein R-parameter R, the energy of the scattered neutron E, the total cross section σ_T, the mean free path of the neutron in helium λ_m, and the center of mass scattering angle θ_{cm}. The differential cross section, polarization, R-parameter, and the scattered neutron energy are listed as functions of both the E_n and θ_{lab} while the total cross section and the mean free path are functions of E_n only. The center-of-mass scattering angle is a function solely of θ_{lab}. Should a calculation of the POLPAC be desired the parameters are calculated directly from the phase shifts, the helium pressure, and the kinematics. Since the corrections made by MOCCASINS were estimated not to be larger than a few percent or so and since the DGS phase shifts available before the analysis of the present data were felt to be capable of describing the n-α scattering situation fairly well, the DGS values were used to calculate the POLPAC matrix. When any of the parameters contained in POLPAC is desired, a double linear interpolation with respect to θ_{lab} and E_n is used to extract

Fig. 15. Flow Diagram of MOCCASINS

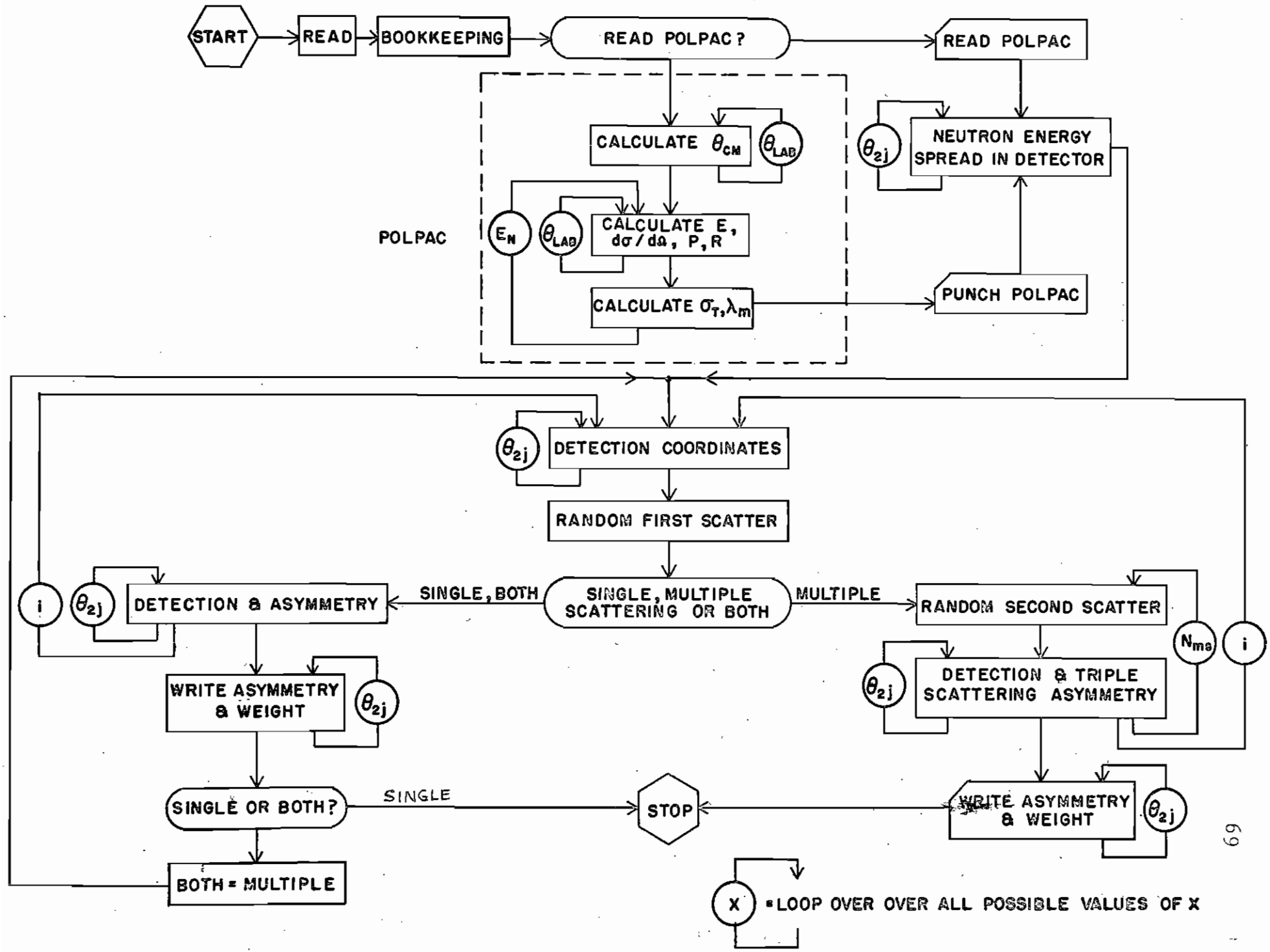
START
READ
BOOKKEEPING
READ POLPAC?
READ POLPAC
POLPAC
CALCULATE θ_{CM}
θ_{LAB}
E_N
CALCULATE E, $d\sigma/d\Omega$, P, R
CALCULATE σ_T, λ_m
PUNCH POLPAC
θ_{2j}
NEUTRON ENERGY SPREAD IN DETECTOR
DETECTION COORDINATES
RANDOM FIRST SCATTER
SINGLE, MULTIPLE SCATTERING OR BOTH
SINGLE, BOTH
DETECTION & ASYMMETRY
i
WRITE ASYMMETRY & WEIGHT
SINGLE OR BOTH?
SINGLE
STOP
BOTH = MULTIPLE
MULTIPLE
RANDOM SECOND SCATTER
DETECTION & TRIPLE SCATTERING ASYMMETRY
N_{ma}
WRITE ASYMMETRY & WEIGHT
X
= LOOP OVER OVER ALL POSSIBLE VALUES OF X

the required value. If the input data calls for a calculation of POLPAC, then the POLPAC matrix will be punched as a part of the output.

It is convenient at this point to define the analyzing angle θ_2 as the angle between the beam axis passing through the center of the helium cell and the line from the center of the helium cell to the center of the plastic scintillator. The θ_{2j} shown on the flow diagram indexes the angular position of the plastic scintillator. The maximum and minimum energies for good* neutrons in the plastic scintillator are then calculated for all values of θ_{2j} for use in computing P_{coin}.

The random position within the scintillator relative to the scintillator walls is then chosen. The coordinates of this position as a function of the detector position θ_{2j} are then calculated. This same relative random position is held for all positions of the plastic scintillators for a given value of i, the number indexing the singly scattered neutrons or, in the case of multiple scattering, the number indexing the first scattering.

The random first scattering position is chosen. Calculation of T_1, $P_{event\ 1}$, and $d\Omega_1$ is now straightforward. At this point two alternatives are available: either the desired calculation calls for multiple scattering only, multiple and single scattering or simply single scattering. In the two latter cases, the numbers associated with the detection process for single scattering, T_3, $P(\theta_{1\text{-det}})$, $d\Omega_3$, and P_{coin}, may be evaluated immediately for all values of θ_{2j}. The composite probability $W_{SS_i}(\theta_{2j})$ and the associated weighted polarization $W_{SS_i}(\theta_{2j}) \cdot P(\theta_{2j})$ are computed and stored as a running sum over i. In addition the probability $W_{SS_i}(\theta_{2j}, E_{det})$ of a neutron arriving at the plastic detector with a given amount of

---

* Good neutrons are those satisfying simultaneity and recoil energy requirements.

energy E_{det} is stored as a running sum over i and as a function of θ_{2j} and E_{det}. The program then loops back to choose new detection coordinates and continues until the desired number of single scattered neutrons have been analyzed. The output consisting of θ_{2j}, $W_{ss}(\theta_{2j})$, $P_{ss}(\theta_{2j})$ and $W_{ss}(\theta_{2j}, E_{det})$ is written and the program terminates if only single scattering is desired. Should both single and multiple scattering be desired, the program proceeds to the multiple scattering mode as it would have done initially had single scattering not been called. Random detection coordinates are chosen for each θ_{2j} as in the single scattering case. First and second scattering positions and the associated values of FRACTION are chosen using techniques described above for favoring certain sites. The calculation of T_1, $P_{event\ 1}$, and $d\Omega_1$ is identical with the single scattering case and the evaluation of $T_2(N_{ms})$, $P_{event\ 2}(N_{ms})$, and $d\Omega_2(N_{ms})$ is directly analogous using site 1 rather than the neutron producing target as the source. $P_{1\text{-}2}(N_{ms})$ is also evaluated.

Then the detection parameters $T_3(\theta_{2j}, N_{ms})$, $P_{2\text{-det}}(\theta_{2j}, N_{ms})$, $P_{coin}(\theta_{2j}, N_{ms})$ and $d\Omega_3(\theta_{2j}, N_{ms})$ and the triple scattering asymmetries are determined for each θ_{2j}. The composite probability $W_{ms_i}(\theta_{2j}, N_{ms}) \cdot P_{ms_i}(\theta_{2j}, N_{ms})$ are stored as a running sum over i and N_{ms}. Also a running sum over the same indices of the probability $W_{ms_i}(\theta_{2j}, N_{ms}, E_{det})$ as a function of the energy of the neutron as it strikes the detector is kept. The program now loops back for a new random second scattering position until the desired number of such positions N_{obs} have been analyzed. After each set of second scattering positions determined by N_{obs}, the program loops back on i for new detection coordinates and a new first scattering site until the desired number of incident neutrons have been analyzed. The output, consisting of θ_{2j}, $W_{ms}(\theta_{2j})$, $P_{ms}(\theta_{2j})$ and $W_{ms}(\theta_{2j}, E_{det})$, is written and the program terminates.

D. Approximations and Limitations

It is appropriate at this time to discuss the limitations of MOCCASINS and approximations that have been made in it. As was mentioned earlier the sensitive volume of the helium cell was assumed to be spherical. There are in fact small deviations from sphericity, however, these effects should tend to be a small part of the total correction. The plastic detectors are assumed to be trapezoidal solids rather than rectangular solids, but for the present detector dimensions involved and for the detector-helium cell separation used, no noticeable error should be introduced. Also the effect of the plastic scintillator efficiency has been ignored. This was done on the basis of a zone-type calculation by Purser (1965) which demonstrated that the effect of the bias level on the observed asymmetry was not noticeable until the bias reached about 80% of the incident neutron energy. The effect of xenon, whose cross section is comparable to helium, was ignored as it was present to only 4.4% and because the pulse height levels required for coincidence would preclude the observance of a recoil from anything as massive as xenon. The effect of the iron in the helium cell walls was also ignored as this would have required a considerable expansion of the program which was impossible with the present computer without writing a completely separate code. At any rate the effect of the iron was small; estimates of its contribution are discussed later.

Since the values of the POLPAC parameters are arrived at by matrix interpolation, care should be taken to insure that the matrix indices are sufficiently closely spaced so that linear interpolation with respect to angle and energy yield a good approximation to the correct value. Also the sampling volume element size in part determines the closeness of the spacing between the first and second scattering sites. Care should therefore be taken so that the radius of the sampling volume element is small enough to permit a representative distribution of the first scatter-

ing points with respect to the second scattering points. It has been previously mentioned that the calculation of P_{coin} is not exact. The effect of third and higher order scatters is ignored as simple cross section calculations limit the maximum contribution to less than 10^{-4} of the single scattering probability. Also ignored are wall effects, but in the present case the collimation together with the extremely short path of the recoiling alpha particle in the high pressure scintillation cell made this calculation unnecessary. Collisions with the wall could occur only against the extreme forward and extreme backward walls of the scintillator.

The results of the MOCCASINS calculation are tabulated with the final results in Chapter VII.

Chapter VI.

PHASE SHIFT FIT PROGRAM

The phase shift fit program allows both the total cross section and the polarization data to be fitted simultaneously. It is modeled after a computer code originally used at the University of Wisconsin. Such a program has been discussed by Suwa and Yokosawa (1963), Moss and Haeberli (1965), and Brown et al. (1966). The mathematical notation used in the program follows that of Foote et al. (1961). Because the program as devised at Wisconsin is considerably more general than required for the present analysis, only those features employed here will be discussed. The object of the analysis is to find the minimum of the Chi square given by:

$$X^2 = \sum_j \left\{ \frac{P_{exp}(\theta_j) - P_{calc}(\theta_j)}{\Delta P(\theta_j)} \right\}^2 + \left\{ \frac{\sigma^T_{exp} - \sigma^T_{calc}}{\Delta \sigma^T} \right\}^2 \qquad (1)$$

where $P_{exp}(\theta_j)$ is the experimental value of the polarization for the angle θ_j, and $\Delta P(\theta_j)$ represents the associated experimental uncertainty. Likewise σ^T_{exp} represents the total experimental cross section with uncertainty $\Delta \sigma^T$. The similar symbols marked "calc" are the corresponding calculated quantities. For each scattering angle $P_{calc}(\theta_j)$ is given as a function of the $\delta^{\pm}_{\ell}$. The superscripts are used in expressing the partial

waves of total angular momentum $\ell \pm 1/2$.

All waves up to and including f-waves can be taken into account and the higher waves are ignored, that is up to eight parameters, including P_1, may be used to obtain a fit. One may elect to restrict any phase shift to any desired value, thereby reducing the total number of free parameters. With a relatively large number of free parameters, an extensive random search requires a prohibitively large amount of computer time. Therefore the starting point for the search was taken to be the DGS phase shifts. That this approach will not lead to difficulties has been shown by Brown et al. (1966) who studied the charge symmetric p-α reaction and demonstrated that there is only a single valley in the X^2 surface consistent with their polarization data. Furthermore, in our energy range, the interaction could be adequately described with only s- and p-waves, thereby reducing the number of free parameters determining the fit.

Chapter VII.

DATA HANDLING

A. Data Acquisition

The 1.0 MeV data were acquired in three or more separate measurements each composed of about nine foreground and three chance background forward-reverse sets. In order to minimize the effects of long term electronic drift, alternate sets were taken as reverse-forward and each FR or RF set was limited to a total time of less than fifteen minutes. To prevent systematic errors resulting, for example, from variations in target thickness and long term electronic drift from creeping into the asymmetry measurements, the order in which the analyzing angle θ_2 was chosen was varied to insure that adjacent points were not measured simultaneously and that the order in which the points were taken was not repeated. Furthermore, since it was known that both the n-He cross section and the polarization were rapidly changing at this energy, $Li^7(p, n)\ Be^7$ threshold determinations were made periodically, so that the energy of the proton beam was not affected by long term drifts. Chance backgrounds were obtained by accumulating spectra with a 70 ns delay inserted in the output of the helium cell pulse height limiter. At the conclusion of the data run, the effect of room scattered neutrons which gave true coincidence events was measured by plugging the solenoid and observing

coincidence spectra under these conditions. The term "room background" as used in this report refers to the coincidence background obtained by plugging the solenoid. At this time, foreground measurements, with the solenoid unplugged, were also made so that the position of the peak relative to the room background would be known.

Data for the 2.4 MeV angular distribution were taken in a similar manner with the exception that the room background was taken concurrently with the data, that is, about nine foreground and three chance background and two room background FR (or RF) sets were made in each of the measurements of the asymmetry for a given angle. Also slightly fewer independent determinations were made at each angle, principally because the higher incident polarization reduced the need for a large number of counts. Table 1 gives the number of independent determinations and the number of good counts accumulated at each angle for both energies.

B. Data Analysis

The output of the multichannel analyzer was in the form of punched paper tape. While the experiment was still in progress, the tape was converted to typed spectra in order to determine a preliminary asymmetry and for obtaining a feel of general trends in the data. Later the paper tape was converted to punched cards which served as the input data for the asymmetry analysis program written by G. L. Morgan and modified by the author to handle the room background obtained with the solenoid plugged. The original program has been described by Purser (1966). The counts in a recoil spectrum were added channel by channel, subtracting chance backgrounds and room background at the higher energy, for the four permutations of solenoid current and detector position. The chance and room back-

Table 1. Number of Asymmetry Determinations and Accumulated Counts

	E_N = 1.01 MeV		E_N = 2.44 MeV	
θ_{lab}	Number of Determinations	Counts	Number of Determinations	Counts
30	4	82K	2	64 K
40	3	97	1	36
50	3	116	2	52
60	3	105	2	42
70	4	111	2	49
80	3	79	2	29
90	4	93	3	57
100	3	95	4	58
110	3	73	3	54
120	3	90	3	40
130	3	118	2	36
140	3	100	3	38

grounds were assumed to be unpolarized which is reasonable and within their statistics. Secondly, a channel-by-channel asymmetry was computed whose significance will be discussed in Chapter VIII.

The final experimental asymmetries were computed after manually selecting the channels to include in the peak. The four integrated peak areas, which had been computed individually for each determination of the asymmetry at a given angle, were respectively summed to obtain the total counts for the UP-FORWARD, DOWN-REVERSE, DOWN-FORWARD, UP-REVERSE coincidences at that angle. Representing these numbers by UF, DR, DF, and UR, the following formulae were employed to determine the experimental asymmetry:

$$r = \sqrt{\frac{UF}{DF} \cdot \frac{DR}{UR}} \; ; \quad \varepsilon = \frac{1 - r}{1 + r} \qquad (1)$$

To obtain optimum accuracy in the asymmetry values, only the central portion of the coincidence peak was integrated. This approach was necessitated by the appearance, especially at the higher energy, of a non-subtracting background. It was to minimize the effect of this background that the use of only the central portion of the peak was initiated. Integration was terminated when the number of counts per channel fell below approximately one half peak height at 2.4 MeV and about one third peak height at 1.0 MeV. It was felt that integration could be extended further down the peak shoulders at the lower energy since the non-subtracting background was not so prominent at 1.0 MeV.

At both energies corrections were made to the experimental asymmetry $\varepsilon(\theta_2)$ for the effects of the non-subtracting background, multiple scattering and $\overline{P}_2$*. The non-subtracting background is described below.

---

* $\overline{P}_2$ is the analyzing power obtained by averaging P_2 over the geometry of the helium cell and plastic scintillators.

The multiple scattering and the $\overline{P}_2$ corrections were made through the use of the computer code MOCCASINS written especially for this purpose and described in Chapter V. This computer code was used to analyze 1500 single scattering events and 1000 multiple scattering events at both energies. The accuracy of these results was sufficiently high that no appreciable statistical uncertainty was introduced into the experimental asymmetry.

In addition, small changes were necessary at 1.0 MeV due to the rapid changes in P_2 and the helium $d\sigma/d\Omega$ with energy. The change was calculated from the ratio:

$$\Delta P_2(\Delta E) = \frac{\iint P_2(E,\theta_2) \cdot \frac{d\sigma(E,\theta_2)}{d\Omega} \, d\theta_2 \, dE}{\int \frac{d\sigma(E_1\theta_2)}{d\Omega} d\theta_2 \, dE} \qquad (2)$$

where the integration is over the subtended angle and the spread in neutron beam energy. The resulting change in the asymmetry was less than 0.0022 at all points and generally was on the order of 0.0010. For measurements where the energy was found to have drifted by more than 10 keV, the determinations were thrown out and not considered in arriving at the final experimental asymmetry.

The non-subtracting background was assumed to be non-polarized on the basis that it showed values of the asymmetry not inconsistent with zero in the region below the peak and on the assumption that, in part, it arose from γ-rays and inelastic scattering from the iron in the helium cell walls. Part of this background also arose from the iron elastic scattering process. These elastically scattered neutrons had a polarization close to P_1* and were degraded very little in energy. Kinematical calculations

---

* The analyzing power of Fe for forward angle scattering is less than 0.08 (Purser, 1966).

have shown that one half of the elastically scattered neutrons appeared under the coincidence peak with the remainder appearing about equally divided above and below the peak. Therefore the elastically scattered neutrons behaved very much like the desired neutrons. To the small extent to which they entered, they could have only negligible effect on the asymmetry. In addition to its design purpose of calculating $\overline{P}_2$ and multiple scattering corrections, the MOCCASINS code was employed for calculation of the Fe scattering effect. The output yielded the energy dependence and polarization of the neutrons based on the assumption that all the neutrons arose from a source on the incident neutron beam axis just beyond the front wall of the helium cell. The total contribution in the selected peak channels due to neutrons elastically scattered from Fe is estimated to be about 1.3%, while the contribution from the inelastically scattered neutrons is estimated to be about 0.1% of the peak area. To get an experimental check of these percentages, the effect of the Fe in the helium cell wall was enhanced by surrounding the helium cell with Fe 1 cm thick everywhere and 2 cm thick on the side toward the source. A coincidence spectrum was measured under these conditions. This spectrum was somewhat difficult to interpret but appeared to be consistent with the calculated, expected effect.

In addition, at 1.0 MeV, the "excited state neutrons" arising from the reaction $Li^7(p,n)Be^{7*}$ appear below the coincidence peak. As mentioned before, these neutrons may be treated as a non-polarized, non-subtracting background. The effect of excited state neutrons was most prominent for $\theta_2 = 80^\circ$ (lab) where the integrated peak in the helium recoil spectrum produced by the excited state neutrons. However, the actual contribution to the peak area used in the asymmetry calculation was small as the excited state coincidence pulses arose from recoils which left only 56% as much energy in the helium cell as a coincidence recoil from a ground state neutron.

Further light has been shed on the subject of the non-subtracting background by recent experiments here at Duke (Morgan and Schaller, 1966). Using a recently installed computer as a two dimensional analyzer, these experimentors obtained a plot of the coincidences as a function of both the helium recoil energy and the time of flight between the helium cell and the plastic detector. In this manner, the γ-ray contribution relative to the n-He recoil counts was measured. The same polarimeter and associated equipment as were used in the present experiment were employed in the recent work. The measurement was made using 1.0 MeV $Li^7(p,n)Be^7$ neutrons for $\theta_2 = 90^\circ$ (lab). Figure 16 shows the spectrum obtained. The helium recoil energy is plotted vertically and the flight time horizontally. The numbers indicate the recorded coincidences. The peak in the lower left-hand corner is due to γ-rays. Coincidence pulses arising from ground state neutrons appear in the large peak on the right while the lower peak immediately below it and not completely resolved from it is attributed to the excited state neutrons.

The dashed vertical lines indicate the coincidence requirements employed in the present experiment while the dashed horizontal lines indicate the chosen region of integration on the helium recoil coincidence peak. In the present experiment the helium cell to plastic detector center-to-center distance was 19 cm, but Morgan and Schaller used a separation of 13.7 cm. Since the shorter flight path caused the neutron-γ-ray separation to be reduced in the latter experiment, the γ-ray background included in the present analysis would be lower than that deduced from this plot.

In addition Morgan and Schaller employed a plastic detector bias about 30% lower than the bias level used in the present experiment. This lower bias level tended to enhance the appearance of the excited state neutrons relative to the ground state. The top of Figure 17 shows the projected

Fig. 16. Two Parameter Analysis of Coincidence Pulses

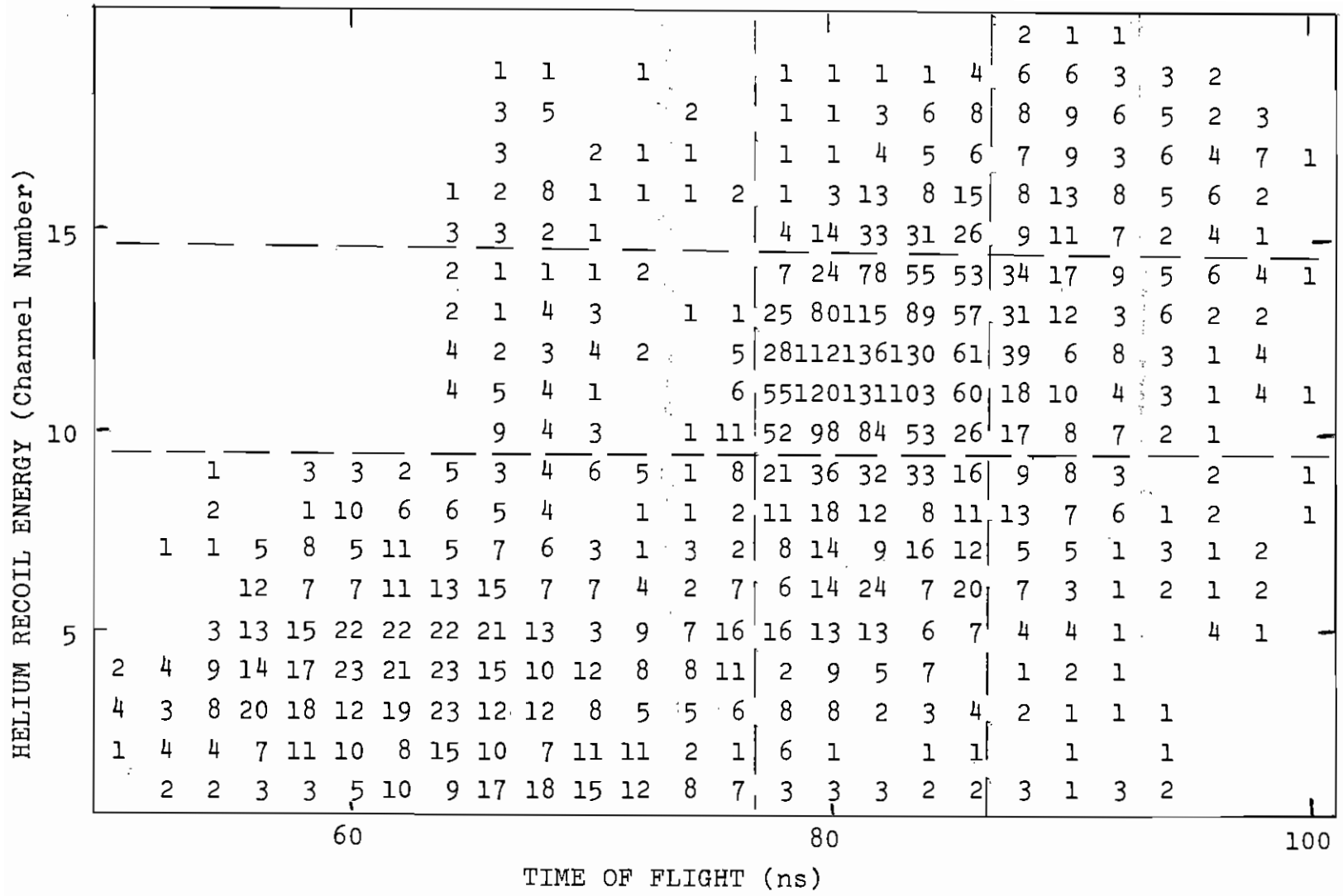
HELIUM RECOIL ENERGY (Channel Number)
15
10
5
60
80
100
TIME OF FLIGHT (ns)

Fig. 17. Projected Helium Recoil Spectrum and Neutron-Gamma Ray Separation

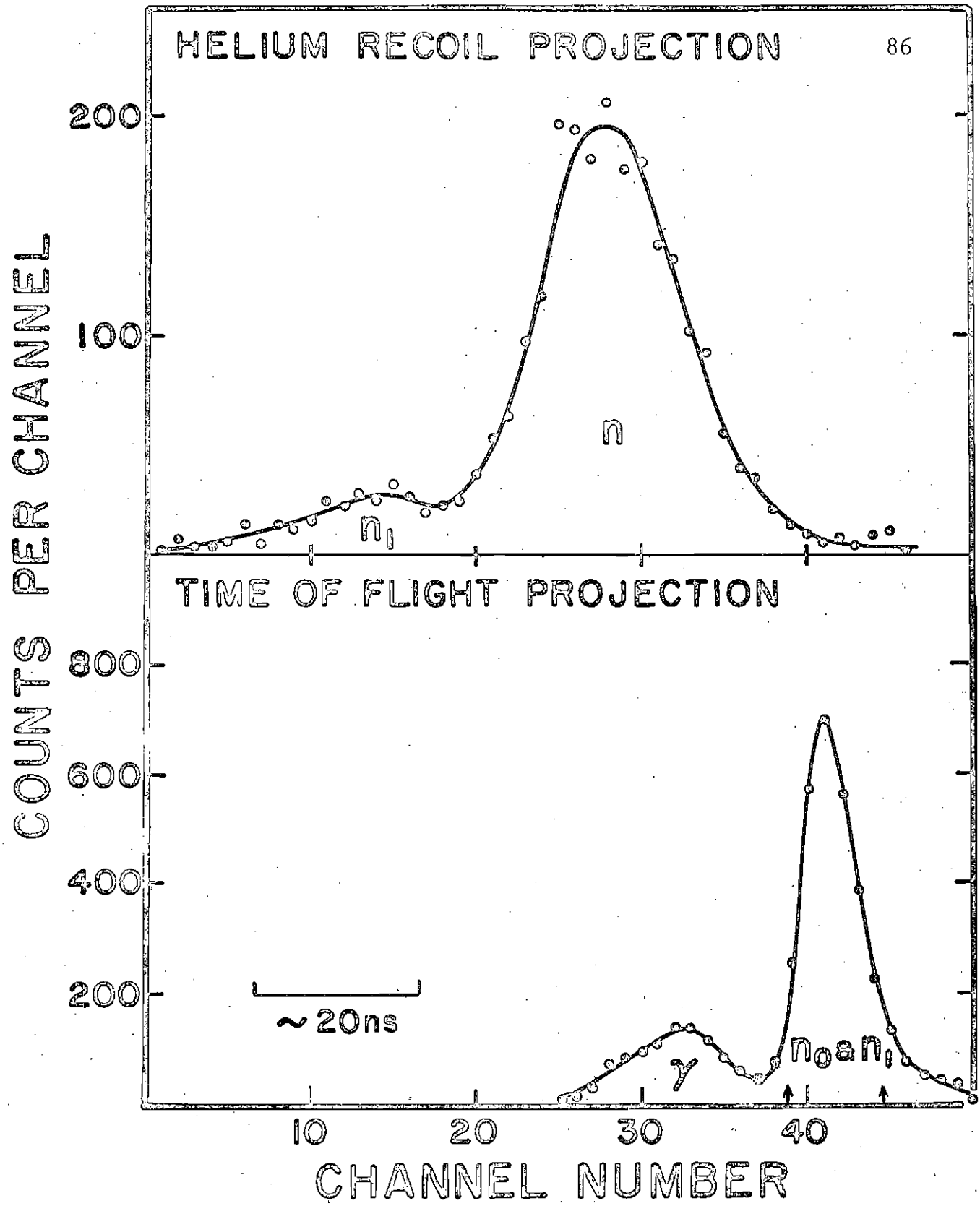
HELIUM RECOIL PROJECTION
200
100
n
n1
TIME OF FLIGHT PROJECTION
800
600
400
200
~ 20ns
γ
n0 & n1
COUNTS PER CHANNEL
10
20
30
40
CHANNEL NUMBER

helium recoil spectra obtained by summing the channels between the vertical lines. In comparison with the 80° coincidence spectrum shown in Figure 18, the excited state neutrons are more pronounced as was anticipated. The bottom of Figure 17 shows the neutron-γ-ray time separation. This spectrum was obtained by summing channels vertically over the entire two dimensional plot. As stated above, in the present experiment it is expected that the neutron-γ-ray separation would be even larger. The arrows indicate the time resolution of 10 ns which was employed in the present experiment. The accepted time bandwidth was about twice this size at 30° and 40° due to the longer clipping stubs employed at these angles. The experimental results of Morgan and Schaller show that very few γ-rays are under the coincidence peak in the present analysis.

Four typical coincidence spectra for each energy are shown in Figures 18 and 19. The assumed non-subtracting background contribution is shown by dashed lines; peak integration was carried out between the arrows shown. The expected channel-by-channel asymmetry is represented by the dot-dash curve. The experimental channel-by-channel asymmetry was computed from the data using eq. (1) but restricting the sums UF, DF, DR, and UR to only three channels. It was meaningful to use three channels so that statistical fluctuations in the asymmetry would be reduced. The vertical dashes are the resulting experimental channel-by-channel asymmetries, where the length of the dashes represents the statistical uncertainty. The dots represent the coincidence pulse height spectra. In order to see if these coincidence spectra had the expected shape, the MOCCASINS histogram output spectra were smeared with a Gaussian distribution representing the helium cell resolution function. The calculated histogram spectra from MOCCASINS included contributions from both multiple and single scattering. As a simplifying assumption in the final analysis, the non-subtracting background was taken to be linear. To demonstrate that

Fig. 18. Typical 1.0 MeV Coincidence Spectra and Channel-by-Channel Asymmetry

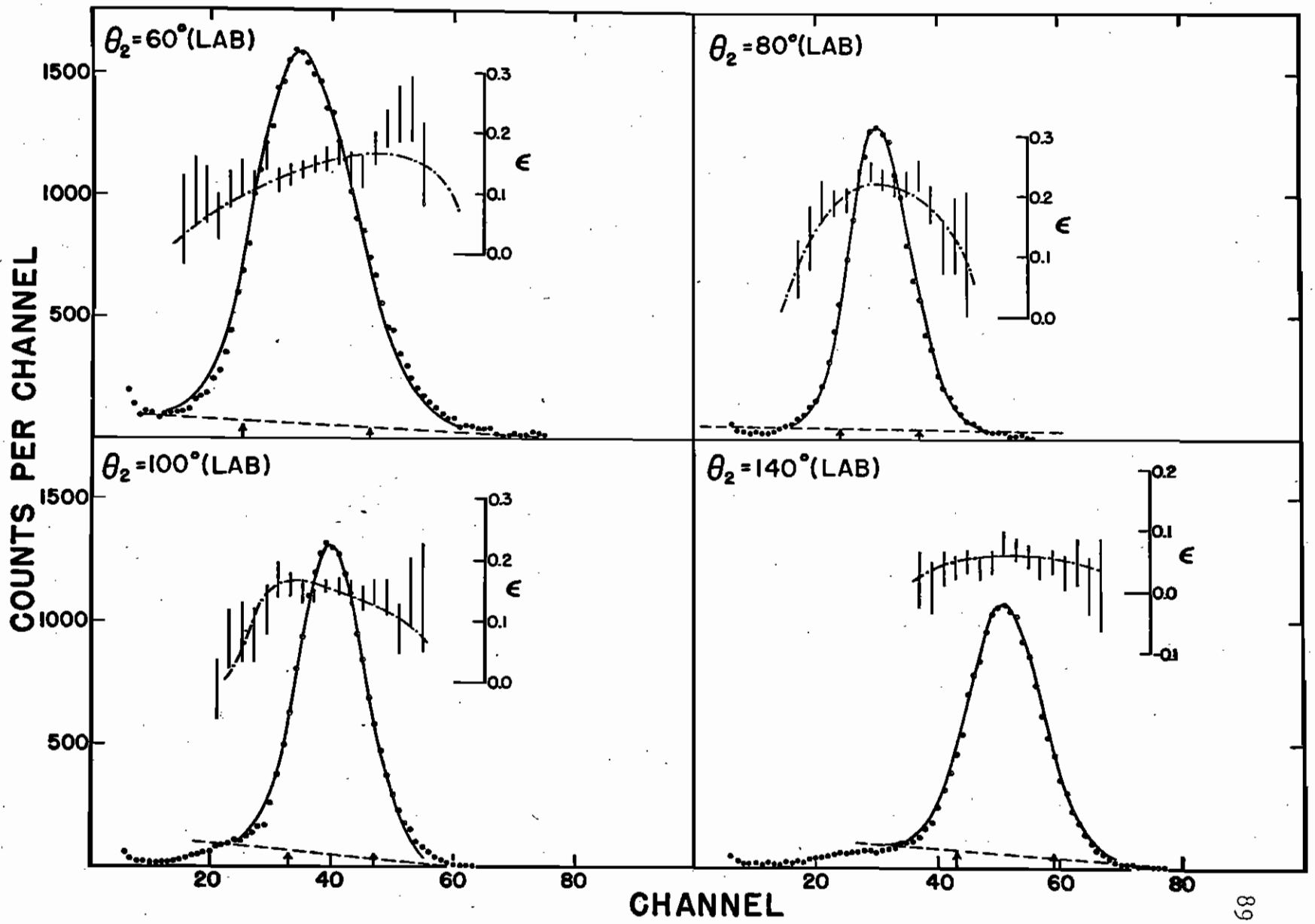
θ2=60°(LAB)
θ2=80°(LAB)
θ2=100°(LAB)
θ2=140°(LAB)
COUNTS PER CHANNEL
CHANNEL
ε
1500
1000
500
20
40
60
80
0.3
0.2
0.1
0.0
-0.1

Fig. 19. Typical 2.4 MeV Coincidence Spectra and Channel-by-Channel Asymmetry

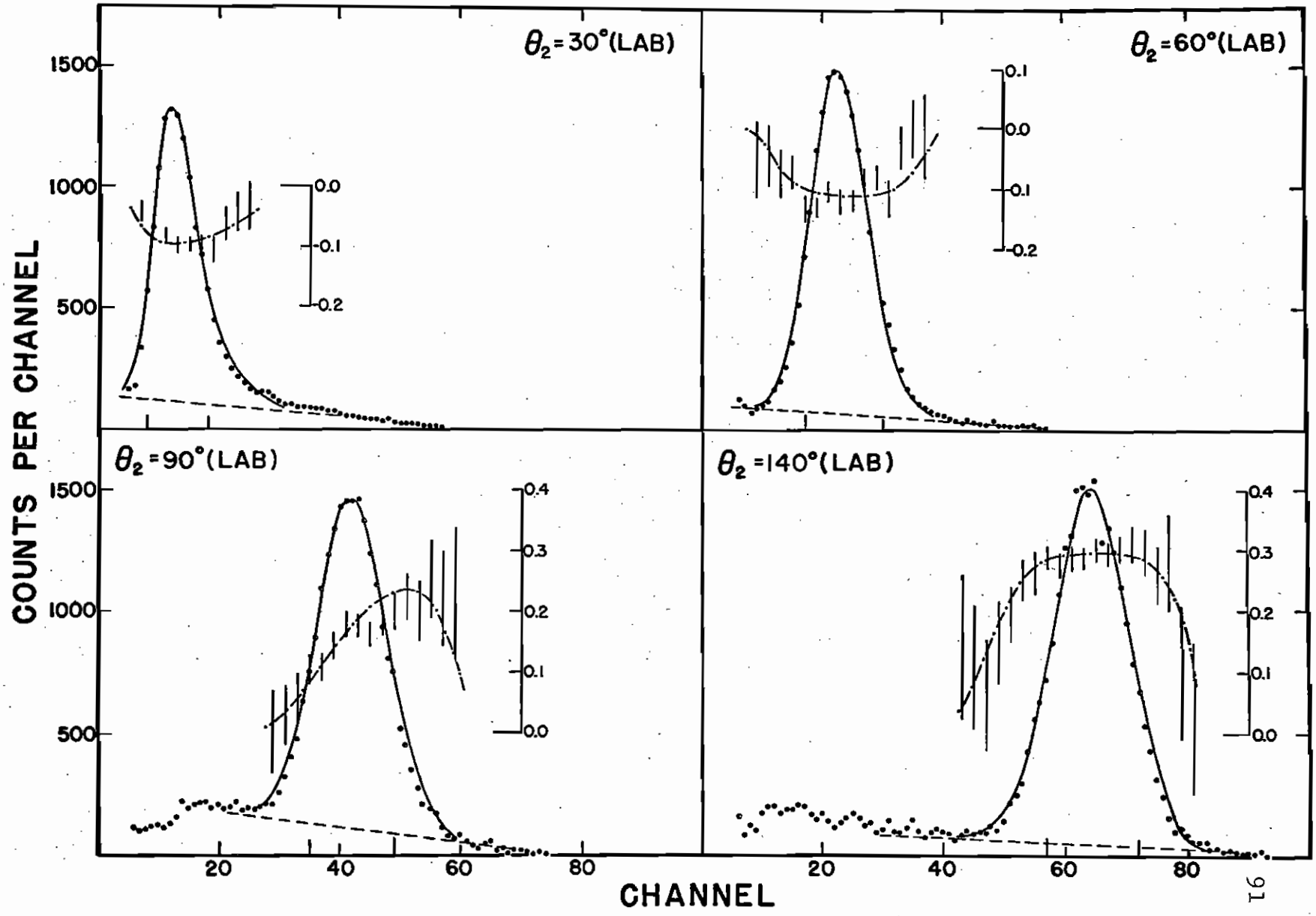
θ2 = 30°(LAB)
θ2 = 60°(LAB)
θ2 = 90°(LAB)
θ2 = 140°(LAB)
COUNTS PER CHANNEL
CHANNEL
1500
1000
500
20
40
60
80
0.0
-0.1
-0.2
0.1
0.4
0.3
0.2

this assumption does not introduce difficulties, the calculated coincidence peak shape was subtracted from the experimental coincidence peak. To within the statistical accuracy of the points, a straight line was obtained. After proper normalization of the calculated curve, our best estimate of the value of the non-subtracting background was then added to the calculated peak shape. The solid curves in Figures 18 and 19 are the results. As can be seen excellent agreement was obtained. Slight deviations of the coincidence spectra from the prediction were tolerated because it was felt that it was not worthwhile to use additional computer time to improve the fit. Furthermore, the MOCCASINS program had assumed a spherical shape for the sensitive helium volume which was not the case. Small deviations from sphericity are expected to slightly increase the size of the tails of the calculated distributions.

As can be seen in Figures 18 and 19, surprisingly satisfying representations of the experimental channel-by-channel asymmetries were obtained using the assumed linear non-subtracting backgrounds together with the smeared histograms. For those analyzing angles where the value of P_2 was changing rapidly with angle, it was necessary to make allowance for the angular dependence of both P_2 and the helium differential cross section in order to obtain a reasonable prediction of the channel-by-channel asymmetry. Allowance for the angular effect was necessary as a result of the relatively large angle subtended by the plastic detector. The relative size of the non-subtracting background was generally about 5% of the integrated peak area at 2.4 MeV but took on slightly higher percentages in the neighborhood of 90° (lab). If the absolute value of the non-subtracting background for a given charge accumulation is plotted as a function of angle, a uniform increase in background is seen as the scattering angle is decreased. At 1.0 MeV the non-subtracting background amounted to approximately 2.5% of the total peak area; the amount of non-subtracting back-

Fig. 20. Angular Dependence of Chance and Room Backgrounds

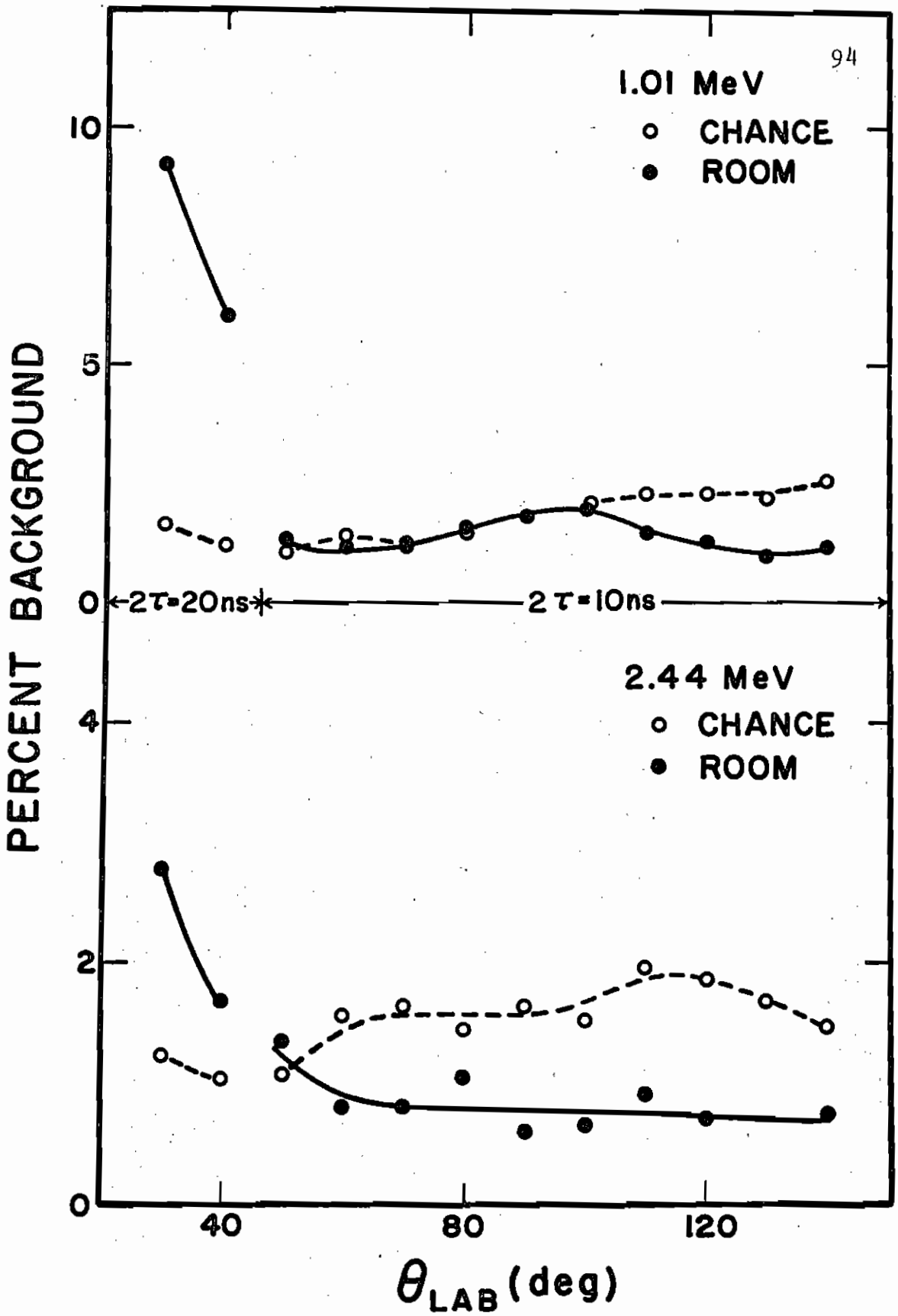
1.01 MeV
CHANCE
ROOM
2.44 MeV
CHANCE
ROOM
PERCENT BACKGROUND
10
5
0
4
2
0
←2τ=20ns→
2τ=10ns
40
80
120
θLAB (deg)

ground tended to be larger at the back angles. The uncertainty associated with this background was estimated to amount to $\pm$ 25% of the necessary correction.

The chance background and room background, which had previously been subtracted, are not shown in Figures 18 and 19. The chance background had been obtained by inserting a delay in the helium cell output so that the coincidence system was not in proper timing. The room background was obtained with the solenoid plugged. Figure 20 shows the angular dependence of the chance and room backgrounds as a percentage of the total peak area. Counts arising from chance coincidences amounted to less than 2.5% of the peak area and were relatively constant in number with respect to angle. The counts arising from room neutrons showed a marked angular dependence being most prominent at the forward angles. The increase at 30° and 40° arose mainly because of the longer pulses used in the coincidence circuitry. In Figure 20, forward angles where a 10 ns clipping stub was used are marked by 2τ = 20 ns. Normally a 5 ns stub was used. Generally the room background contributed less than 2% of the peak area but this value rose to about 9% for 30° at 1.0 MeV. In the final analysis, the counts from both of these sources of background were assumed to be unpolarized which is what one logically expects for the experimental conditions involved.

The values of the experimental asymmetries, the corrected asymmetries, the polarizations using the best estimate of P_1 and the values of all corrections are given in Tables 2 and 3 for 1.0 and 2.4 MeV, respectively. The uncertainties include the uncertainties associated with the corrections as well as with the counting statistics.

Table 2. Asymmetries, Polarizations and Corrections for $E_N = 1.014$ MeV.

θ_{lab}	Exp ε	ROOM	Non-Subtract BKGD	M.S.	P_2	$\Delta P_2(\bar{E})$
30	0.0246	0.0025	0.0016		0.0016	0.0006
40	0.0480	0.0031	0.0013	0.0001	0.0022	0.0007
50	0.0934	0.0012	0.0012	0.0002	0.0046	0.0010
60	0.1453	0.0018	0.0048	0.0005	0.0079	0.0016
70	0.2033	0.0025	0.0073	0.0011	0.0097	0.0022
80	0.2214	0.0038	0.0044	0.0014	0.0058	0.0009
90	0.1910	0.0037	0.0038	0.0010	-0.0002	
100	0.1625	0.0031	0.0032	0.0005	-0.0023	
110	0.1258	0.0019	0.0040	0.0004	-0.0026	-0.0007
120	0.0995	0.0014	0.0023	0.0002	-0.0025	-0.0012
130	0.0732	0.0007	0.0029	0.0002	-0.0022	-0.0005
140	0.0554	0.0007	0.0021	0.0001	-0.0016	-0.0004

Table 2. Asymmetries, Polarizations and Corrections for E_N = 1.014 MeV (continued)

Corrected ε	$\Delta\varepsilon$	θ_{lab}	P_2	ΔP_2
0.0309	0.0050	30	0.1016	0.0163
0.0553	0.0042	40	0.1819	0.0139
0.1019	0.0031	50	0.3352	0.0103
0.1619	0.0040	60	0.5326	0.0131
0.2258	0.0043	70	0.7428	0.0142
0.2377	0.0045	80	0.7819	0.0149
0.1993	0.0043	90	0.6556	0.0141
0.1671	0.0040	100	0.5497	0.0131
0.1288	0.0045	110	0.4237	0.0147
0.0997	0.0039	120	0.3280	0.0129
0.0743	0.0035	130	0.2444	0.0115
0.0563	0.0037	140	0.1852	0.0120

Table 3. Asymmetries, Polarizations and Corrections for E_N = 2.435 MeV.

θ_{lab}	Exp $-\varepsilon$	Non-Subtract BKGD	M.S.	P_2	Corrected $-\varepsilon$	$\Delta\varepsilon$	P_2	ΔP_2
30	-0.0900	-0.0129		-0.0027	-0.1057	0.0039	-0.2308	0.0086
40	-0.1067	-0.0156	-0.0001	-0.0033	-0.1258	0.0051	-0.2747	0.0111
50	-0.1261	-0.0123	-0.0001	-0.0035	-0.1420	0.0044	-0.3100	0.0095
60	-0.1080	-0.0081	-0.0001	-0.0029	-0.1191	0.0045	-0.2600	0.0099
70	-0.0587	-0.0055	-0.0001		-0.0643	0.0042	-0.1404	0.0092
80	0.0364	0.0035		0.0043	0.0442	0.0056	0.0965	0.0122
90	0.1593	0.0163	0.0007	0.0118	0.1881	0.0055	0.4107	0.0121
100	0.2905	0.0227	0.0022	0.0136	0.3290	0.0068	0.7183	0.0149
110	0.3570	0.0268	0.0031	0.0101	0.3969	0.0076	0.8666	0.0167
120	0.3765	0.0217	0.0036	0.0056	0.4075	0.0070	0.8897	0.0153
130	0.3431	0.0164	0.0029	0.0025	0.3649	0.0064	0.7967	0.0139
140	0.2854	0.0121	0.0021	-0.0015	0.2981	0.0057	0.6509	0.0124

C. Measurement of the Analyzing Angle

The accuracy of the determination of the angle θ_2 is crucial to the present experiment. This is quite obvious particularly at 2.44 MeV, since in the region of the cross over a small error in the angle would have a marked effect on the X^2 for that point. The phase shifts of course would be correspondingly affected. Therefore to insure ultimate accuracy in the measurement of this angle, the detector shields were removed and a fine nylon line was drawn from the center of the plastic scintillator to the center of the helium cell. A horizontal line passing through the center of the target spot and the center of the helium cell was also erected. Since it would be very difficult to read accurately the angle between these lines with a protractor, the intersecting lines were photographed on transparent film. This process was repeated for both detectors for all values of θ_2. Care was exercised in placing the center of the lens of the camera on the axis which is perpendicular to the analyzing plane and passes through the center of the helium cell. To prevent distortion due to warping, the developed film was clamped between two sheets of glass. By projecting the image to about three times actual size, extremely accurate measurements of the angle could be made.

As extreme care had been taken in the construction of these lines, it was estimated that the maximum error would be on the order of one line width at each point determining a line. This would result in a maximum error of about 0.15° in the measurement of θ_2 relative to the zero line of the polarimeter. The total uncertainty in θ_2 was estimated to be 0.20°. The measured mean value of θ_2 was 0.10° or less from the stated value for all angles. The maximum alteration in the value of P_2 was 0.003 and this occured at $\theta_2 = 90^\circ$ for 2.4 MeV where the error in θ_2 was 0.10°. At this energy and angle the analyzing power is changing

more rapidly with angle than in any other angular region. In fact, since all the deviations from the predetermined angles were consistent with zero and since the maximum change in P_2 associated with the discrepancy in the measured value of θ_2 and its stated value was small, no correction to the value of the analyzing angle was made.

D. Possible False Asymmetries

In a polarization experiment of high accuracy, care must be taken so that either all false asymmetries are corrected for or that it is certain that they do not exist to an extent that would affect the data. The major contributions to instrumental asymmetries can be eliminated through the use of a spin-precession solenoid and two detectors. In this case the right-left ratio in eq. (7) of Chapter II may be written as

$$r = \sqrt{\frac{I_{1,0} \cdot \eta_{1,0}}{I_{1,\pi} \cdot \eta_{1,\pi}} \cdot \frac{I_{2,\pi} \cdot \eta_{2,\pi}}{I_{2,0} \cdot \eta_{2,0}}} \qquad (3)$$

where $I_{1,0}$ is the number of neutrons striking the detector 1 with spin precession angle 0. The plastic detector efficiency associated with this case in $\eta_{1,0}$. The product $I_{1,0} \cdot \eta_{1,0}$ is the number of neutrons detected. An obvious extension of this notation is used for the second detector and for spin precession angle of π. Since the spin precession process does not alter the energy of the neutron, $\eta_{1,0} = \eta_{1,\pi}$ and similarly for the second detector. Thus, eq. (3) may be rewritten as

$$r = \sqrt{\frac{I_{1,0}}{I_{1,\pi}} \cdot \frac{I_{2,\pi}}{I_{2,0}}}\ , \qquad (4)$$

which is identical to eq. (1). If the detector efficiencies cancel in this manner and if the helium cell phototube gain is constant, no false asymmetries can be introduced by counting longer with the neutron spins precessed through one angle than through the opposite angle.

Alteration of the direction of the fringe field could have a marked effect on the gain of the phototubes had precautions not been taken to eliminate this effect. In order that the cancelation mentioned above would be as nearly complete as possible, the photomultipliers and solenoid were magnetically shielded (Chapter III, Sec. C). To determine to what extent the fringe field could affect the asymmetry in the present experiment, the gain of the plastic detector photomultipliers was measured for both magnitudes of solenoid current used and for several settings of θ_2. The Compton edge for Cs^{137} γ-rays was observed in a multichannel analyzer. To enhance any possible effects, the base line on the multichannel analyzer was set above zero so that only the higher energy portion of the γ-ray detection curve was observed. The counting asymmetry in the region of the sharply sloping Compton edge was calculated. In every case the asymmetry was less than $2.0 \pm 1.1 \times 10^{-3}$. From this asymmetry it was calculated that the maximum effect observed over the θ_2 range would cause an asymmetry of 0.0005 ± 0.0003 when the scintillators were biased to count 50% of the recoil protons. In the majority of cases a considerably higher percentage of the recoils were observed. Since the bias level on the plastic scintillators ranged from 200 to 250 keV in this experiment, this false asymmetry was negligible everywhere but at the largest scattering angles for the 1.0 MeV measurement. Here the scattered neutron energy was four hundred keV, the bias level 200 keV. In this worst case the field effect could have been 0.0005 which was ultimately neglected since the error assigned at this angle was eight times this amount.

Solenoid effects on the gain of the helium cell photomultiplier were not expected to affect the data. If in eq. (3) one assumes that all the

η's are equal and if one further assumes the counting times are equal, then

$$\begin{aligned} I_{1,0} \cdot \eta_{1,0} &= I_{2,\pi} \cdot \eta_{2,\pi} \\ N_{1,0} &= N_{2,\pi} \\ I_{1,\pi} \cdot \eta_{1,\pi} &= I_{2,0} \cdot \eta_{2,0} \\ N_{1,\pi} &= N_{2,0} \end{aligned} \tag{5}$$

where $N_{1,0}$ is the number of counts detected by the first detector with the spin precession angle 0 and an obvious extension of this notation is employed for the other three numbers. Now suppose a magnetic gain effect did exist so that the coincidence pulses observed when the precession angle $\emptyset = \pi$ appear at a higher voltage than the voltage where coincidence pulses appear with spin precession angle $\emptyset = 0$. In a polarization experiment performed with a single detector, one would compare the number of coincidences ($N_{1,0}$ or $N_{2,0}$) in a given pulse height range observed for $\emptyset = 0$ with those ($N_{1,\pi}$ or $N_{2,\pi}$) for $\emptyset = \pi$. If the pulse height for opposite precession angles were different, a quite erroneous asymmetry could be obtained if the entire recoil peak were not included in the range of peak integration as was the case in the present experiment. However, eq. (5) will permit comparison of accumulated coincidences between different detectors. That is if eq. (5) applies, the gain effect, should it exist, will completely cancel. In the present experiment the counting times have been demonstrated to be the same (Chapter III, Sec. C) and the efficiencies were about equal. Actually the ratio of detector efficiences was 0.9.

Even though the foregoing discussion concerning the solenoid effect on the helium cell phototube gain would indicate that any gain effect, should it exist, would have a small effect on the experimental asymmetry,

it was felt some experimental measurement must be obtained in order to demonstrate that this effect would be negligible. Therefore the pulse height of recoils in coincidence with plastic detector scintillations was examined to determine if any change in pulse height existed. To within the accuracy of the measurement, no effect was detected though it was felt that a change as small as 1 part in 200 would have been observed. Since the detector efficiencies were almost equal and the counting times were equal, no appreciable effect was introduced in the experimental asymmetry due to possible gain changes in helium cell photo tube.

A final possible source of false asymmetries could be neutron scattering from the Pb γ-ray shields surrounding the plastic detectors. The principal effect caused by the shield would be to widen the effective analyzing angle subtended by the detector. The reader will remember that the γ-ray shields were in the form of five sided boxes covering the plastic scintillators on every face except the face abutting the light pipe. The scintillators measured 5.1 x 2.5 x 5.1 cm^3 and the Pb layer was 0.5 cm thick. The scintillators were oriented so that they were 5.1 cm deep measured from the side toward the helium cell to the side furthest from it, 5.1 cm high as measured in the $\emptyset$ plane, and 2.5 cm in width as measured in the θ_2 plane. An estimate indicated that less than 3.5% of the coincidence neutrons arise from He-Pb-plastic events ignoring those neutrons which scatter from the Pb covering the side of the plastic detector facing the He cell. It is a valid assumption to ignore these neutrons because they will either scatter away from the plastic scintillator and fail to be detected or if they do scatter into the plastic detector they will have lost very little energy and hence cannot be distinguished from the desired neutrons. About 2.1% of the Pb scattered neutrons come from the Pb that appears to widen the subtended angle measured in the θ_2 plane. The remainder arise from the Pb on the detector top and bottom, i.e. the

Pb that appears to increase the height of the detector. Neutrons arising from the latter source would have a polarization reduced from the mean polarization by a factor of cos $\emptyset$, where $\emptyset$ is the projection of the scattering angle measured in the plane perpendicular to the θ_2 plane. Corrections to the data, which were calculated with the Monte Carlo code, have included the effect of a finite value for $\emptyset$. The Pb on the detector top and bottom would tend to increase the amount of $\emptyset$ correction required. But since in every case cos $\emptyset$ is very close to one and since these neutrons amount to only 1.4% of the observed coincidence neutrons, the change in the asymmetry would be extremely small. Therefore, the effect of Pb scattering from the top and bottom of the γ-ray shield was ignored. We must now consider the neutrons scattering into the plastic from the sides of the Pb shield. About 1% of the total coincidence flux detected by the plastic scintillators will be scattered in from each side. These neutrons will have experienced different polarizations and cross sections in the helium cell. A rough calculation of the effect of the Pb on the detector sides was carried out at both energies and all angles. The calculation was done in such a manner that it could be considered as an upper bound on the magnitude of the effect. The maximum change in the observed polarization was 0.002 and typically the change was much less. Due to the small value of the correction, no alteration to the data was made.

In summary, no false asymmetries existed to an extent that the data could be affected.

Chapter VIII.

RESULTS

A. Present Phase Shift Results

As is mentioned in Chapter VI, the phase shift fit program is designed to search the multi-dimensional surface in X^2 determined by the scattering phase shifts and the incident polarization. The X^2 contour maps for 1.0 and 2.4 MeV plotted against P_1 and δ_o^+ allowing the p-wave phase shifts to take on optimum values, are shown in Figures 21 and 22 respectively. In the usual case one would expect the program to search for a minimal X^2 and spiral down into a "conical" valley in the X^2-δ_o^+-P_1 surface. Such was indeed the case for the 2.4-MeV data. A well-defined valley was found at $P_1 = -0.458$ and $\delta_o^+ = -37.9^o$. However this was found not to be the case at the lower energy. For the 1.0-MeV distribution the expected valley degenerated into a long narrow trough. From the 1-MeV contour map, one can easily see that equally good fits can be obtained for values of P_1 ranging from 0.25 to 0.36 and for values of δ_o^+ ranging from -20^o to -35^o. Even over this broad range there is no appreciable narrowing of the valley. For this reason it was obvious that some other criterion must be placed on either the value of δ_o^+ or P_1 in order that a unique set of phase shifts might be obtained.

Since no sufficiently accurate values of P_1 are available it was required that δ_o^+ must be set. This can be accomplished by one of two

Fig. 21. χ^2 Contour Map for 1.0 MeV

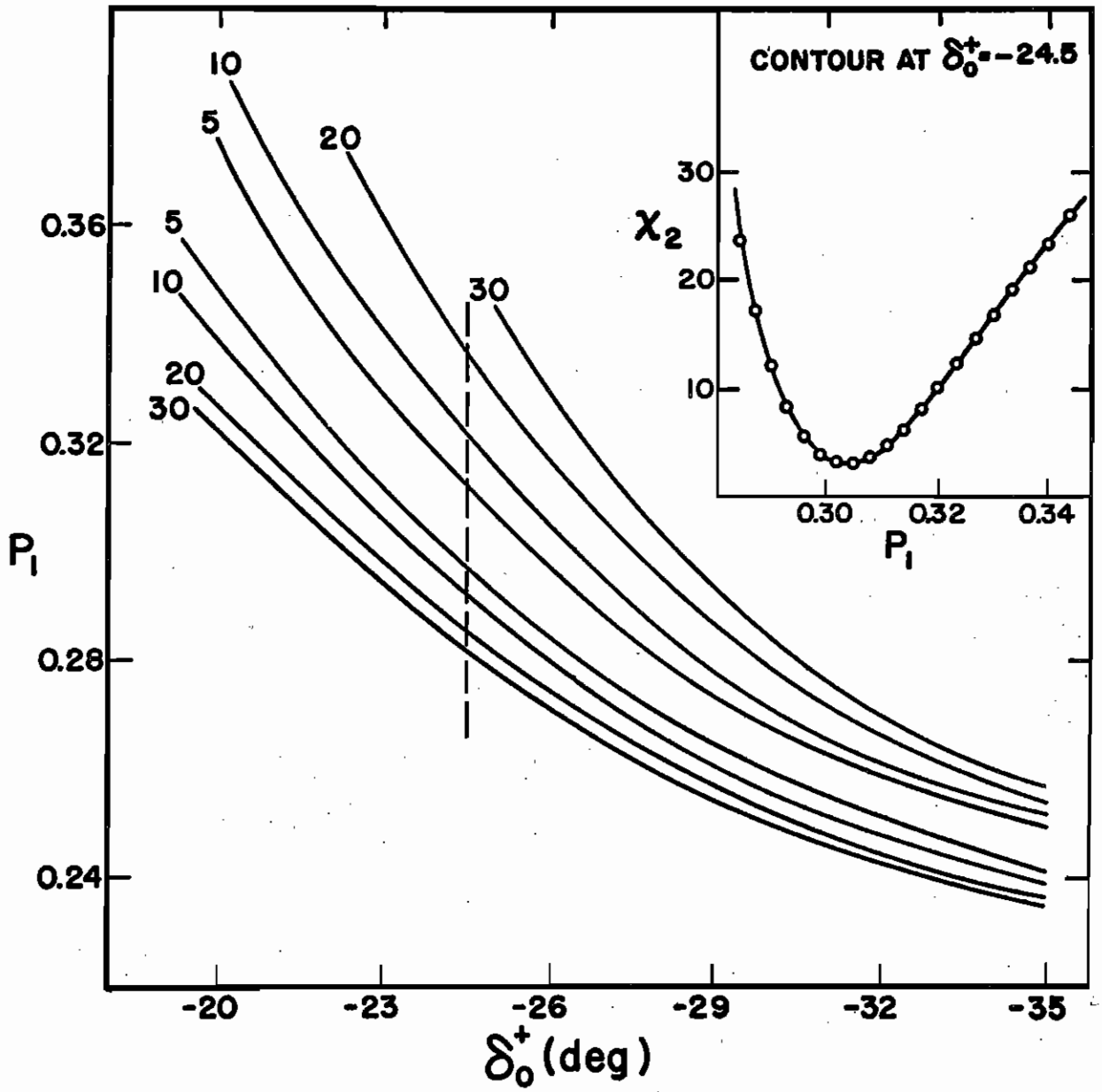
CONTOUR AT $\delta_0^+ = -24.5$
χ_2
30
20
10
0.30
0.32
0.34
P_1
10
5
20
5
10
20
30
30
0.36
0.32
0.28
0.24
P_1
-20
-23
-26
-29
-32
-35
δ_0^+ (deg)

Fig. 22. X^2 Contour Map for 2.4 MeV

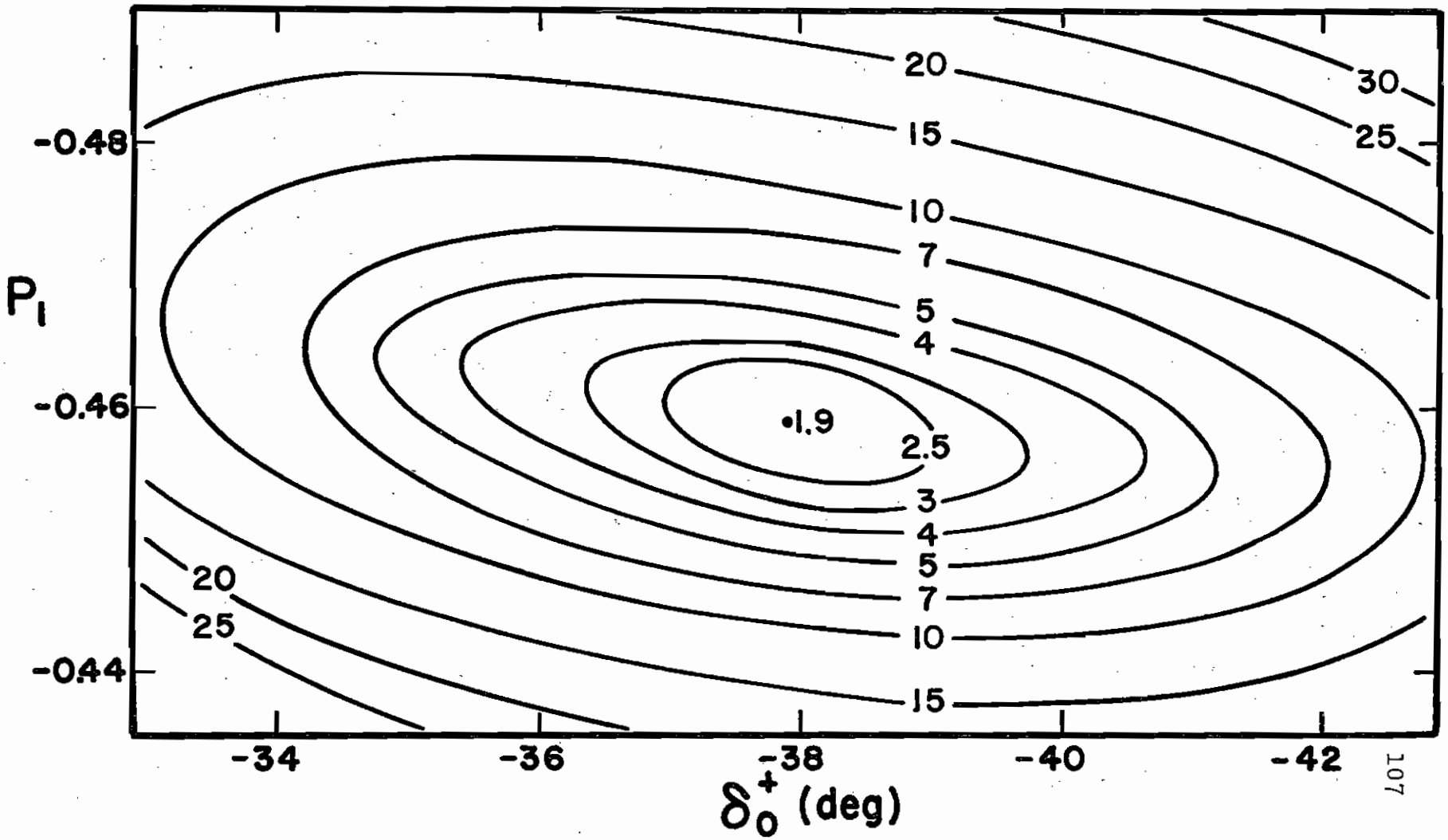
20
30
25
15
10
7
5
4
1.9
2.5
3
4
5
7
10
15
20
25
-0.48
-0.46
-0.44
P_1
-34
-36
-38
-40
-42
δ_0^+ (deg)
107

methods. First the s-wave phase shift may be fixed by requiring the total cross section calculated from the extracted phase shifts to match the experimental value of 6.9 $\pm$ 0.15 b reported by Vaughn et al. (1960). This gives a value of $-25^{o} \pm 3^{o}$ for the s-wave phase shift. The large uncertainty is somewhat inadequate for the present case. Alternatively either the hard sphere or effective range approximations might be used to calculate this phase shift. Though Pisent and Villi (1959) found reasonable linearity below 7 MeV in the product $k \cdot \cot \delta_{o}^{+}$ as would be required if the effective range approximation applied, it was felt that this approximation should not be trusted across a resonance. Lane and Thomas (1958) point out that the effective range expansion fails to be applicable when the R-matrix is rapidly varying. Thus one would certainly not expect effective range formalism to hold across a resonance where there is an infinity of the R-matrix.

On the other hand, an estimate of δ_{o}^{+} may be obtained from the familiar hard sphere relation $\emptyset = kR_{o}$ where R_{o} is the channel radius for s-wave interaction, k is the wave number and $-\emptyset$ is the s-wave hard sphere scattering phase shift. The hard sphere approximation has been discussed by many authors including Lane and Thomas. Assuming the results of the present analysis at 2.44 MeV are correct, we arrive at a value for R_{o} of 2.42 $\pm$ 0.13 fm. The uncertainty in the hard sphere scattering radius arises because the polarization angular distribution is not as sensitive to the s-wave phase shift as it is to the p-wave phase shifts. The lack of sensitivity to the s-wave phase shift can be seen graphically from the 2.4 MeV X^{2} contour plot (Figure 22). A fit of acceptable quality is obtained for values of δ_{o}^{+} which range 2^{o} on either side of the X^{2} minimum. The present value of the hard sphere radius is compared with that employed by other authors in Table 4. As can be seen the present value is in agreement with the more recently employed radii.

Table 4. Hard Sphere Scattering Radii

Author (s)	Reaction	Radius
Critchfield and Dodder (1949)	p-α	2.9 fm
Adair (1952)	n-α	2.9
Dodder-Gammel-Seagrave (1952-3)	n-α	2.9
Gammel and Thaler (1958)	p-α	2.6
Pisent and Villi (1959)	n-α	2.65
Pisent and Saruis (1963)	n-α	2.43
Brown et al. (1966)	p-α	2.48
Present Data	n-α	2.42

The hard sphere phase shift was calculated for 1.0 MeV using $R_o = 2.42$ fm. The resulting $\delta_o^+ = -24.5 \pm 1.5^o$ was taken to be the best estimate of this phase shift and was subsequently used in all calculations. The dashed vertical line at $\delta_o^+ = -24.5^o$ in Figure 21 indicates the s-wave phase shift employed in the present analysis of the 1 MeV data. A slice through the X^2 valley was taken and the valley contour for the chosen δ_o^+ is shown in the inset.

Since a sizeable uncertainty exists concerning the value of δ_o^+ near 1.0 MeV, the optimum p-wave phase shifts and the predicted total cross section have been plotted in Figure 23 as a function of δ_o^+. The uncertainties in the p-wave phase shifts and the σ_T resulting from uncertainties in δ_o^+ are indicated by the braces. Thus if future experiments allow the s-wave phase shift to be more accurately determined, the p-wave phase shifts for best fit to the present data are readily available. The data points are the phase shifts and the σ_T for minimal X^2 obtained holding δ_o^+ at the specified value. The horizontal lines labeled DGS represent the DGS values for the p-wave phase shifts and the predicted σ_T obtained using DGS. The solid vertical lines at $\delta_o^+ = -25.1^o$ mark the DGS s-wave phase shift while the dashed vertical line indicates where the s-wave phase shift was fixed in the present experiment.

Attention should be drawn to the fact that the starting points in the phase shifts search, with the exception of the 1.0-MeV δ_o^+, were the DGS values. This choice probably omitted the possibility of obtaining other solutions should they exist. However in a similar analysis related to the charge symmetric p-α reaction Brown et al. (1966) laid a grid across the $X^2 - \delta - P_1$ surface allowing the δ's to take on every combination of values from 0^o to 180^o in 5^o increments. Their results show only one solution consistent with their polarization data. Similar behavior is expected in the present reaction. The d-wave phase shifts were

Fig. 23. 1.0 MeV P-wave Phase Shifts and Total Cross Section for S-wave Phase Shifts Values from -20^{o} to -35^{o}

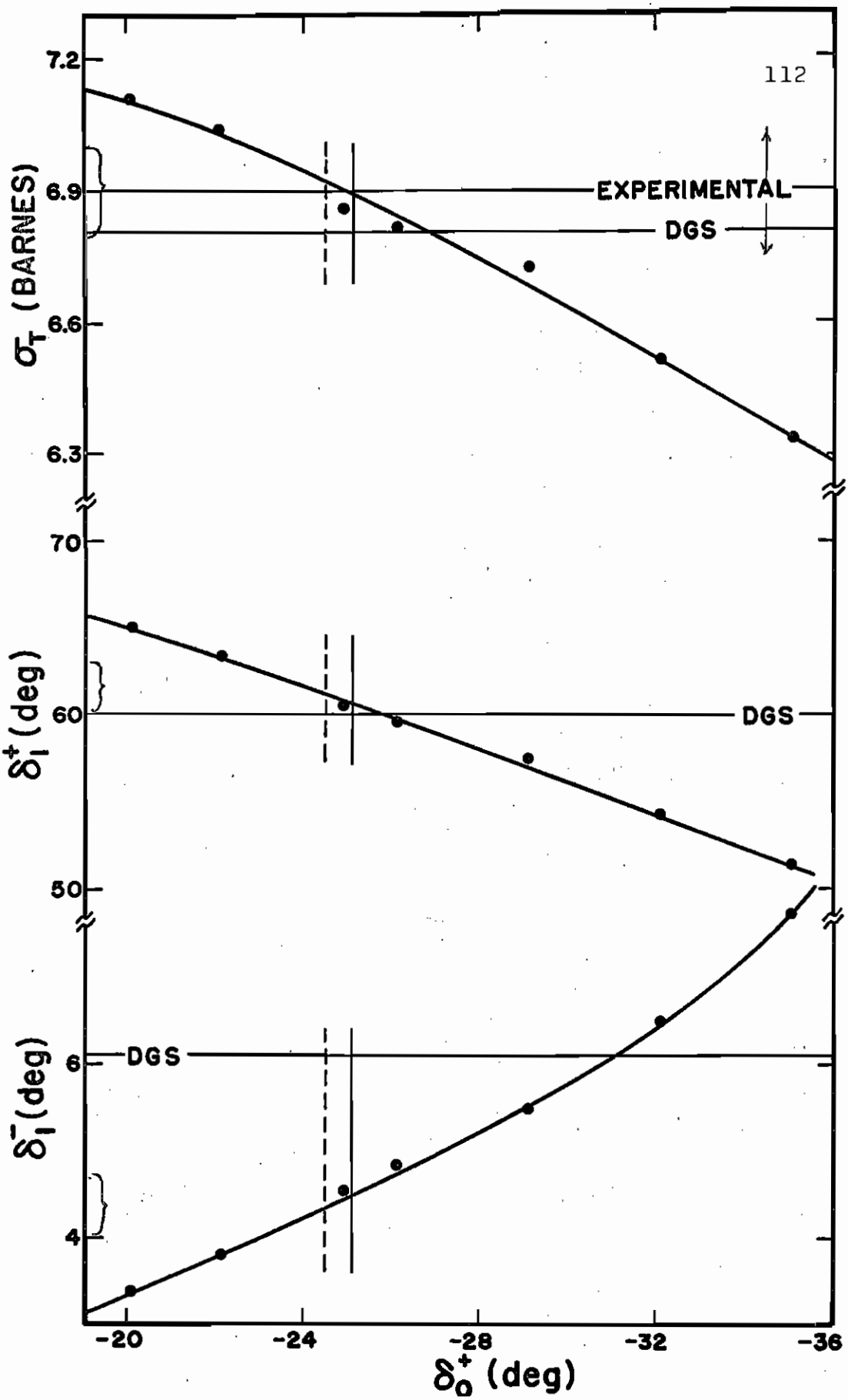
7.2
6.9
6.6
6.3
σ_T (BARNES)
EXPERIMENTAL
DGS
70
60
50
δ_1^+ (deg)
DGS
6
4
δ_1^- (deg)
DGS
-20
-24
-28
-32
-36
δ_0^+ (deg)

required to be zero since hard sphere calculations had indicated that their absolute value should be less than 0.2° at the present energies. Furthermore, the data could be fit satisfactorily without resorting to them. With both d-wave phase shifts restricted to -0.5°, a X^2 search of the data was made and a significantly poorer fit to the data was obtained.

The resulting phase shifts from the above analysis are shown in Table 5, where they are compared with DGS and HB (Hoop and Barschall, 1965) values. The tabulated values for 1.0 MeV assume the hard sphere approximation discussed above. At 2.44 MeV excellent agreement of the present phase shifts with DGS was obtained. The s-wave phase shift differed by 0.8° which was not felt to be a serious discrepancy as the DGS values were quoted by the authors to only the nearest degree. The phase shifts were not felt to be more accurate than a few degrees though little is known as to exactly how accurately they are known (Haeberli, 1963). In addition, at 1.0 MeV the lack of agreement between DGS and the present work is not particularly significant as $d\delta_o^+/dE = 0.15^{\circ}/\text{keV}$. To within the accuracy of the present energy measurement ($\pm$ 7 keV absolute), no disagreement can be established. However, it should be noted that the δ_1^- is about 2.44 MeV and 1.6° smaller at 1.0 MeV. This is a significant difference as δ_1^- is changing only slowly with energy. To determine if this difference in δ_1^- could be accounted for by an error associated with the non-subtracting background calculation, the 2.44 MeV phase shifts were recalculated omitting completely any correction for non-subtracting background, an obviously extreme restriction. The second set of phase shifts labeled present data in Table 5 are the results. As can be seen at 2.44 MeV, a fit of quality equal to the original fit was obtained with δ_1^- 1.8° above DGS though a slightly different s-wave phase shift was required. The calculation at 1.01 MeV yielded δ_1^- differing from the previous one by only 0.1° while the other p-wave phase shift remained almost constant.

Table 5. Phase Shifts

Energy	δ_0^+	δ_1^-	δ_1^+	X^2_{min}	Author (s)
1.01 MeV	-25.1°	6.1°	60.0°	22.5	DGS
	-24.3°	6.1°	61.0°	33.1	HB
	-24.5°	4.4°	61.2°	3.1	Present Data
	-24.5°	4.3°	61.4°	2.2	Present Data*
2.00 MeV	-35.0°	14.0°	117.0°		DGS
	-34.0°	15.0°	118.0°		HB
	-34.2°	15.4°	119.0°	6.5	Present Fit to Data of May et.al.
2.44 MeV	-38.7°	18.4°	121.4°	84.8	DGS
	-37.5°	19.2°	120.8°	112.0	HB
	-37.9°	21.2°	121.6°	1.9	Present Data
	-39.4°	20.2°	121.2°	3.7	Present Data*

* Non-subtracting background omitted.

Thus it can be stated that the present data require δ_1^- to be shifted from the DGS in the direction shown and by approximately the amount indicated. In addition δ_1^+ is shown to be essentially independent of the non-subtracting background.

To compare the present phase shifts to DGS and HB in ability to fit the present data, X^2 was calculated as a function of P_1, holding all phase shifts constant. A plot of X^2 vs. P_1 is shown in Figure 24 for both energies. The presently obtained values give a dramatically better fit to the data at the higher energy. For the lower energy the effects of the long trough may be seen in that even though both DGS and HB yield results in disagreement with the present experimental distribution, the discrepancies are not as pronounced as at 2.44 MeV.

Values of $P_2(\theta_2)$ determined in the present experiment, assuming P_1 for optimum fit, are shown in Figures 25 and 26. Solid lines represent the predicted values of P_2 calculated from the phase shifts in Table 5. Dashed lines are used to represent the values predicted by DGS. The lower portion of each figure shows the data with P_1 adjusted for optimem fit to DGS. Present phase shifts provide a much more satisfactory fit to the data than DGS. For both energies the HB predictiion provided a fit of poorer quality. At 1.0 MeV, there exists a shift of the polarization peak toward forward angles relative to the distribution obtained by using the DGS phase shifts. The opposite tendency was observed above the resonance at 2.44 MeV.

The low value of the X^2 obtained for best fits indicate that the data points agree with the curve considerably better than one would expect from a purely statistical standpoint. In other words, the deviations of the points from the calculated curves are relatively small. The uncertainties in the data points include a large contribution from the non-subtracting background; this was particularly true at 2.4 MeV. In some

Fig. 24. Chi-Square for the DGS, HB, and the Present Phase Shifts in the Region of Optimum P_1

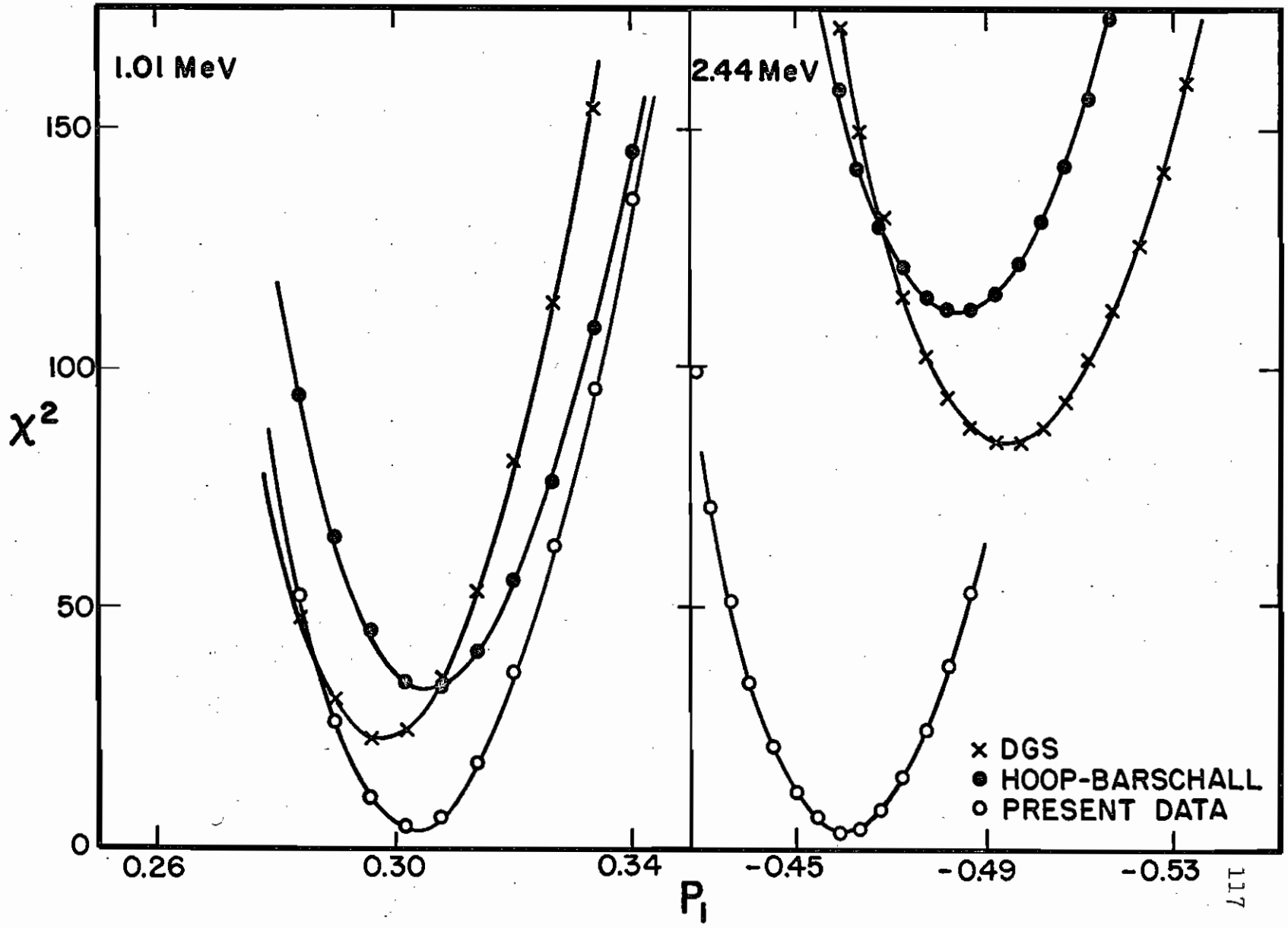
1.01 MeV
2.44 MeV
150
100
50
0
χ^2
0.26
0.30
0.34
-0.45
-0.49
-0.53
P_1
× DGS
● HOOP-BARSCHALL
○ PRESENT DATA

Fig. 25. Comparison of DGS and Present Calculated P_2 Distributions at 1.0 MeV

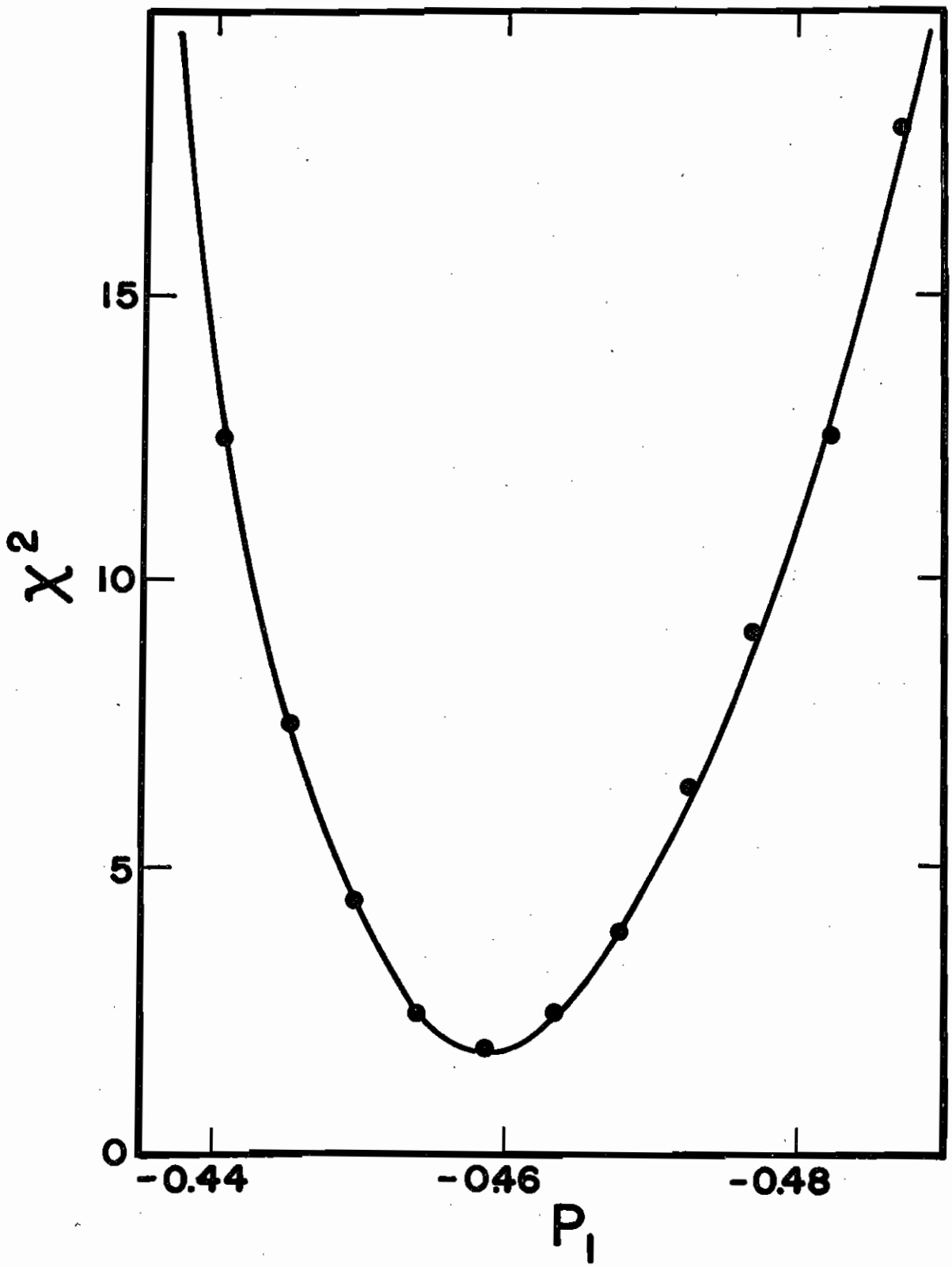
15
10
5
0
χ^2
-0.44
-0.46
-0.48
P_1

Fig. 26. Comparison of DGS and Present Calculated P_2 Distributions at 2.4 MeV

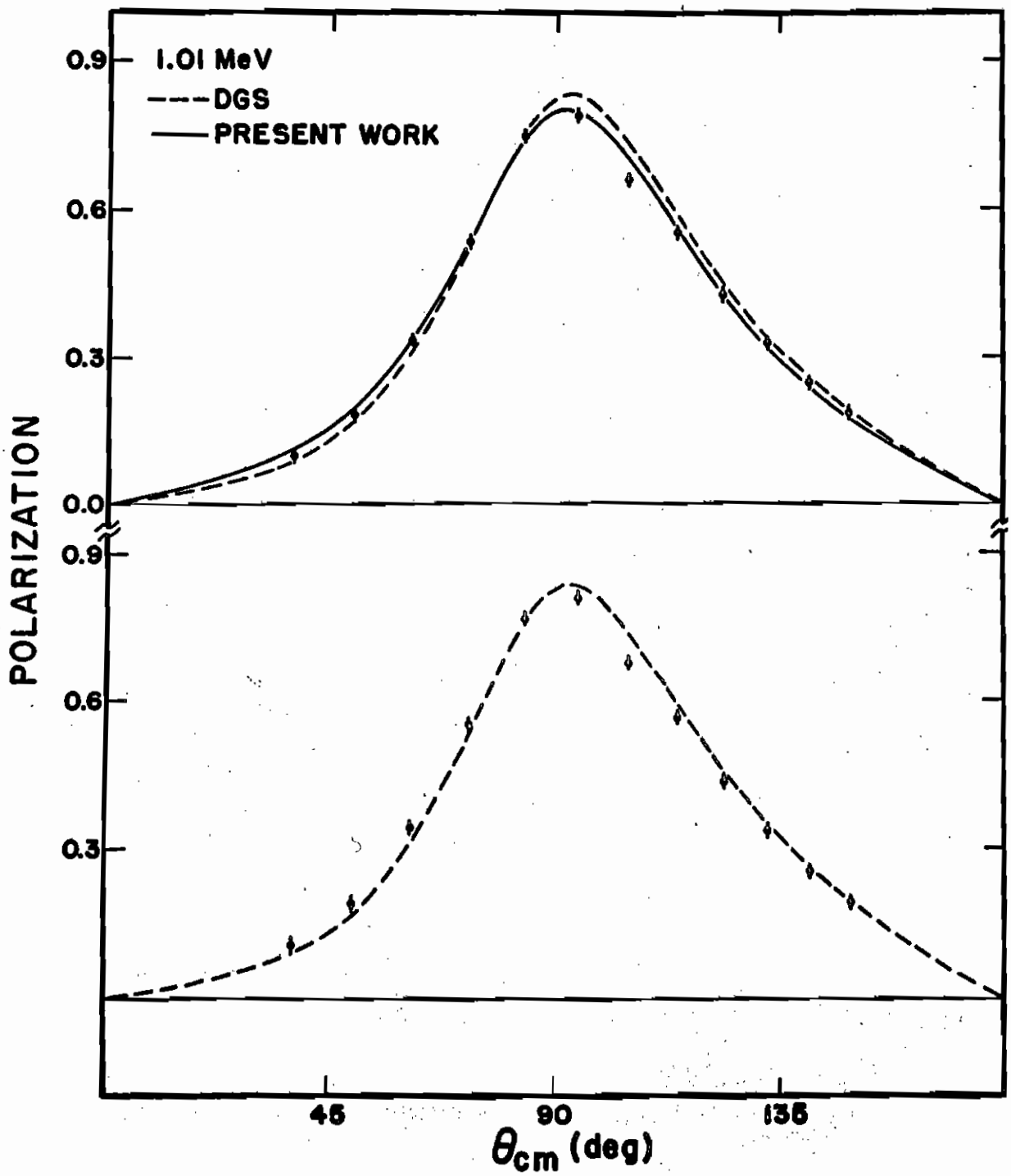
1.01 MeV
DGS
PRESENT WORK
POLARIZATION
0.9
0.6
0.3
0.0
0.9
0.6
0.3
45
90
135
θcm (deg)

cases as much as one half of the total uncertainty is due to the error assigned to the non-subtracting background. Since the correction for this background varies smoothly from point to point, the effect of the uncertainty associated with the non-subtracting background simply increases the uncertainties in the P_2 (θ_2) distribution. As the non-subtracting background enters systematically and increases the error bars, it may explain the small values of X^2 for the final fits to the data.

The $\theta_2 = 114^{\circ}$ (cm) point at 1.0 MeV was omitted from the fit by statistical requirements. It was noticed in fitting the 1.0 MeV data that the polarization at this angle could not be satisfactorily fitted. Since this point was more than three standard deviations from the predicted value obtained using the other points along, Chauvenet's criterion* justifies the omission of this point from consideration in determining the final fit. On the other hand, the 1.0 MeV data show a systematic variation from the calculated curve. At back angles the observed polarization is larger than the P_2 values predicted for corresponding angles while at the forward angles the opposite is true. Even though this tendency is present, the points employed in the final analysis are always within their stated uncertainty from the calculated curve.

---

* See for example, Yardley Beers, Introduction to the Theory of Error, Addison-Wesley Publishing Co., Cambridge, Massachusetts.

B. Incident Polarization and the Effect of Magnetic Depolarization

The present experiment, in addition to determining the phase shifts, provided a highly accurate method of determining the polarization of the incident neutron beam. X^2 as a function of P_1 was calculated allowing all phase shifts to vary with the exception of the δ_o^+ at 1.01 MeV. The resulting curves are shown in Figure 27 for 2.44 MeV and in the upper-right corner of Figure 21 for 1.01 MeV. Minimum X^2 on these graphs marks the optimum incident polarization. For a mean deuteron beam energy of 2.82 MeV incident on a 175-keV thick carbon target, the experimentally observed polarization at 25^o (lab) is -0.458 ± 0.006. Similarly with a 46-keV lithium target at 2.91 MeV incident proton energy, the observed polarization is 0.304 ± 0.008. These values are compared with previous polarization results in Figures 9 and 12 respectively. Slight variations from the general trend can be attributed to the slightly different analyzing power used. Previous results had used the analyzing power predicted by DGS. It should be remembered that the present values include all experimental uncertainties, with the exception of magnetic depolarization, of sufficient magnitude to effect the stated value. The method employed is independent of any set of phase shifts with the exception of the s-wave phase shift requirement at 1.01 MeV.

As has been previously mentioned (Chapter III, Sec. C.) the observed value of P_1 is affected by the depolarization of the beam as it passes through the solenoid. Though this has no effect on the phase shift analysis, it is desirable to know the magnitude of the contribution since the present work represents the most accurate experimental determination of the degree of polarization from a reaction producing fast neutrons. Accurate knowledge of the neutron polarization will be helpful to future workers in this field.

Fig. 27. Chi-Square for the 2.4 MeV Polarization Distribution in the Region of Optimum P_1

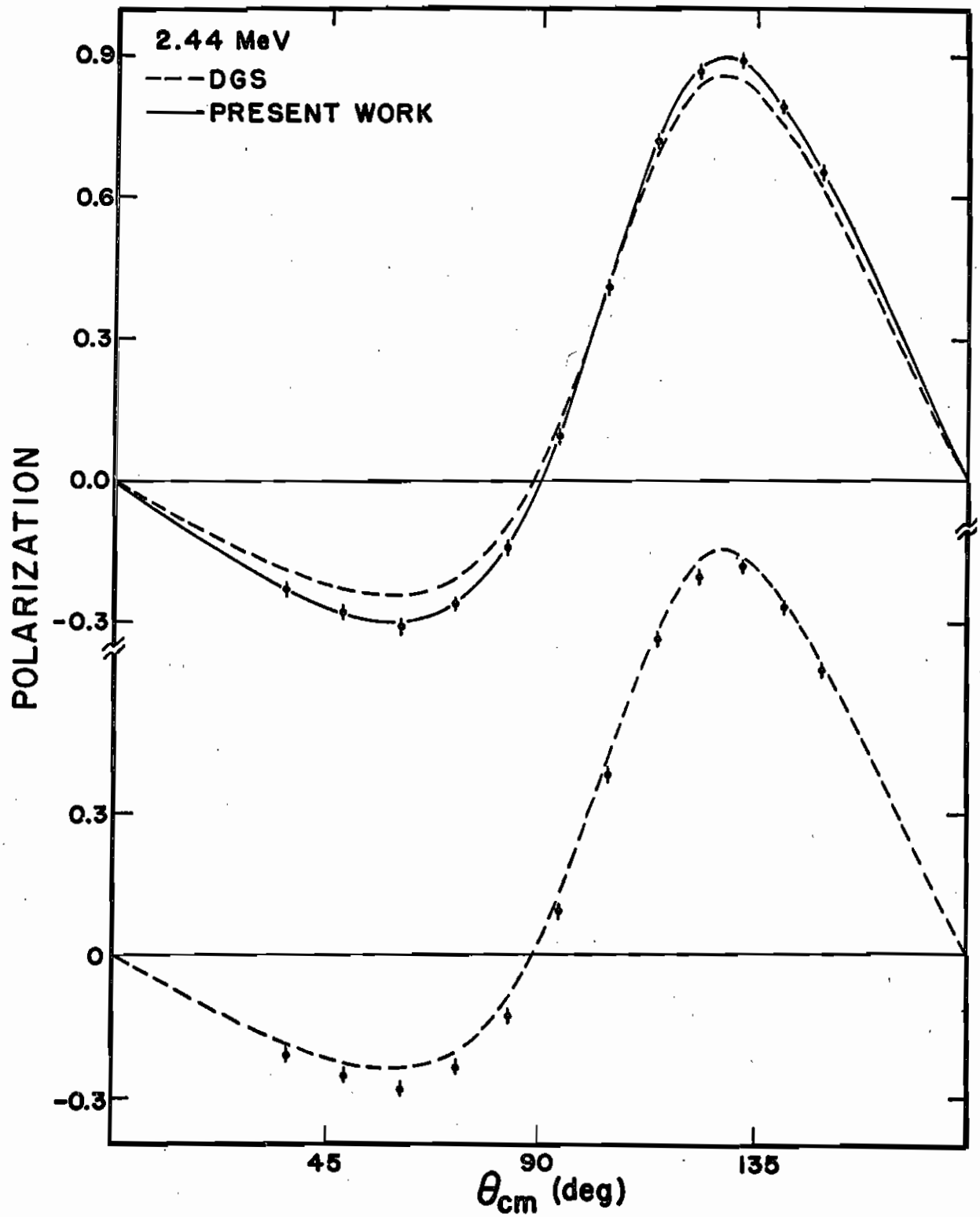
2.44 MeV
---DGS
——PRESENT WORK
0.9
0.6
0.3
0.0
-0.3
0.3
0
-0.3
POLARIZATION
45
90
135
θcm (deg)

Atkinson and Sherwood (1965) calculated the amount of depolarization that a polarized neutron beam experiences in passing through an air core solenoid. It turns out that the amount of depolarization is dependent on the ratio L/a where L is the length of the solenoid and a is the radius of the beam. It is assumed that the beam is cylindrical and that the solenoid consists of a single layer having many turns. For the present case where sharp collimation was used the L/a value was 36. This value is based on the assumption that the a value for a cylindrical beam corresponds to the a value for a conical beam at the center of the solenoid. It was also assumed that the length of the present solenoid was the length of the surrounding Armco box as the box tended to keep the field near the solenoid axis and therefore increased the effective length of the solenoid. Atkinson and Sherwood limit their discussion to $L/a \leq 20$ and furthermore have limited the accuracy of their calculations by the accuracy with which they calculated the magnetic field -- about 1%. They felt this was necessary to conserve computer time. At any rate they show a fractional depolarization of about 1.1% for $L/a = 10$. Extrapolation of their results gave an expected value of the fractional depolarization of 0.30% for the present case. This would result in an increase in P_1 for carbon neutrons of 0.0014 and about 0.0009 for lithium neutrons. Also they mention that the use of two or more coils to approximate a solenoid, as was done in the present experiment, reduces the amount of depolarization. This is attributed to the fact that the direction of precession between the solenoid sections is in the opposite direction from that observed inside a coil. However, they failed to investigate this effect further. The values listed above should therefore be considered as upper bounds. The P_1 values given in this work have not been corrected for depolarization due to the small size of the correction to the uncertainty in its value. However, the direction of the change is known and the L/a ratio is given so that correction can be made as further calculations become available.

C. Previous Experiments

The most accurate previous polarization angular distribution in the present energy range is that of May et al. (1963). An experimental arrangement similar to the present one was used. Since no multiple scattering of P_2 corrections were made by the authors, the necessary changes were calculated at this laboratory through the use of MOCCASINS and applied to the May asymmetries. Two minor problems were encountered: May et al. did not give the experimental energy resolution of their helium cell and the source to helium cell distance was not available. The resolution was obtained by looking at the paper by Walter et al. (1962) which gave a resolution of 10% for Po-α pulses. Assuming energy dependence of the resolution similar to that observed at Duke, this would mean that the resolution at 2 MeV incident neutron energy was about 23%. The helium cell to source distance was taken to be 1 m which was in agreement with the angular spread subtended by the helium cell given in the May paper. These values were typical of the Wisconsin polarimeter (Walter, 1966). The asymmetries, corrections and uncertainties are listed in Table 6 together with the polarization P_2 for optimum fit.

The phase shift fit program was used to search the corrected May data for minimum X^2. These data by themselves exhibited such large uncertainties that no unique fit could be defined. So in order to sharpen the valley, the hard sphere value for δ_0^+ was used. In addition the total cross section was required to be consistent with the value of 4.0 ± 0.1 b as reported by Vaughn et al. This permitted the determination of the p-wave phase shifts. The use of d-waves was ruled out since they did not appear necessary at 2.44 MeV. The phase shifts obtained are listed in Table 5 where they are compared with DGS and HB. The δ_1^+ phase shift appeared 2° above DGS. The value of the δ_1^-, which is changing slowly

Table 6. E_N = 2.00 MeV. Polarization Data of May, Walter and Barschall

θ_{lab}	ε	$\Delta\varepsilon$	P_2	M.S.	Corrected ε	P_2	ΔP_2
30	-0.030	0.011	-0.0017		-0.0317	-0.141	0.050
40	-0.034	0.011	-0.0019		-0.0359	-0.159	0.050
50	-0.018	0.012	-0.0013	-0.0001	-0.0194	-0.086	0.055
60	-0.016	0.011	-0.0021		-0.0181	-0.081	0.050
70	0.003	0.011	0.0001		0.0031	0.014	0.050
80	0.057	0.013	0.0018	0.0003	0.0591	0.262	0.059
90	0.122	0.013	0.0054	0.0007	0.1281	0.568	0.059
100	0.146	0.014	0.0058	0.0013	0.1531	0.679	0.064
110	0.182	0.014	0.0049	0.0017	0.1886	0.836	0.064
120	0.182	0.015	0.0033	0.0015	0.1868	0.828	0.068

with energy, is 1.4° larger than DGS. Assuming the present variations from DGS discussed earlier are correct and using linear interpolation, the predicted value of δ_1^- at 2.0 MeV would be 1.5° above DGS. Over the small energy range involved, δ_1^- is a linear function of energy to within about $1/2^{\circ}$. Thus the May data tend to favor the present value of the δ_1^- phase shift over DGS even though the data is not sufficiently accurate to allow an independent determination of the phase shifts.

Figure 28 is a plot of the predicted $P_2(\theta_2)$ using the phase shifts obtained in the present work. Comparison is made with the DGS predictions and it can be seen that the preferred phase shifts force the polarization peak toward back angles as was observed in the present experiment at 2.44 MeV.

Experimental values of neutron-helium scattering phase shifts below 3 MeV are shown in Figure 29. Clementel and Villi (1955) using graphical methods have obtained phase shifts over the whole energy range of the present experiment from the $d\sigma/d\Omega$ data of Adair (1952). There is also the early experimental determination by Seagrave (1953) at 2.6 MeV which exhibited the low value of δ_1^-. At 2.0 MeV there is the work of Austin et al. (1962). All of these experimental phase shifts were obtained from the analysis of differential cross section data. Phase shifts obtained by these workers were not felt to be of sufficient accuracy to warrant critical comparison with the present values. The value of these cross section analyses consisted in demonstrating that the DGS phase shifts closely approximated the true situation. Also shown at 2.0 MeV are the phase shifts presently obtained from the polarization data of May et al. (1963) in addition to the new values presently obtained at 1.0 and 2.4 MeV.

Fig. 28. Comparison of DGS and Present Calculated P_2 Distributions with the Data of May, Walter and Barschall at 2.0 MeV.

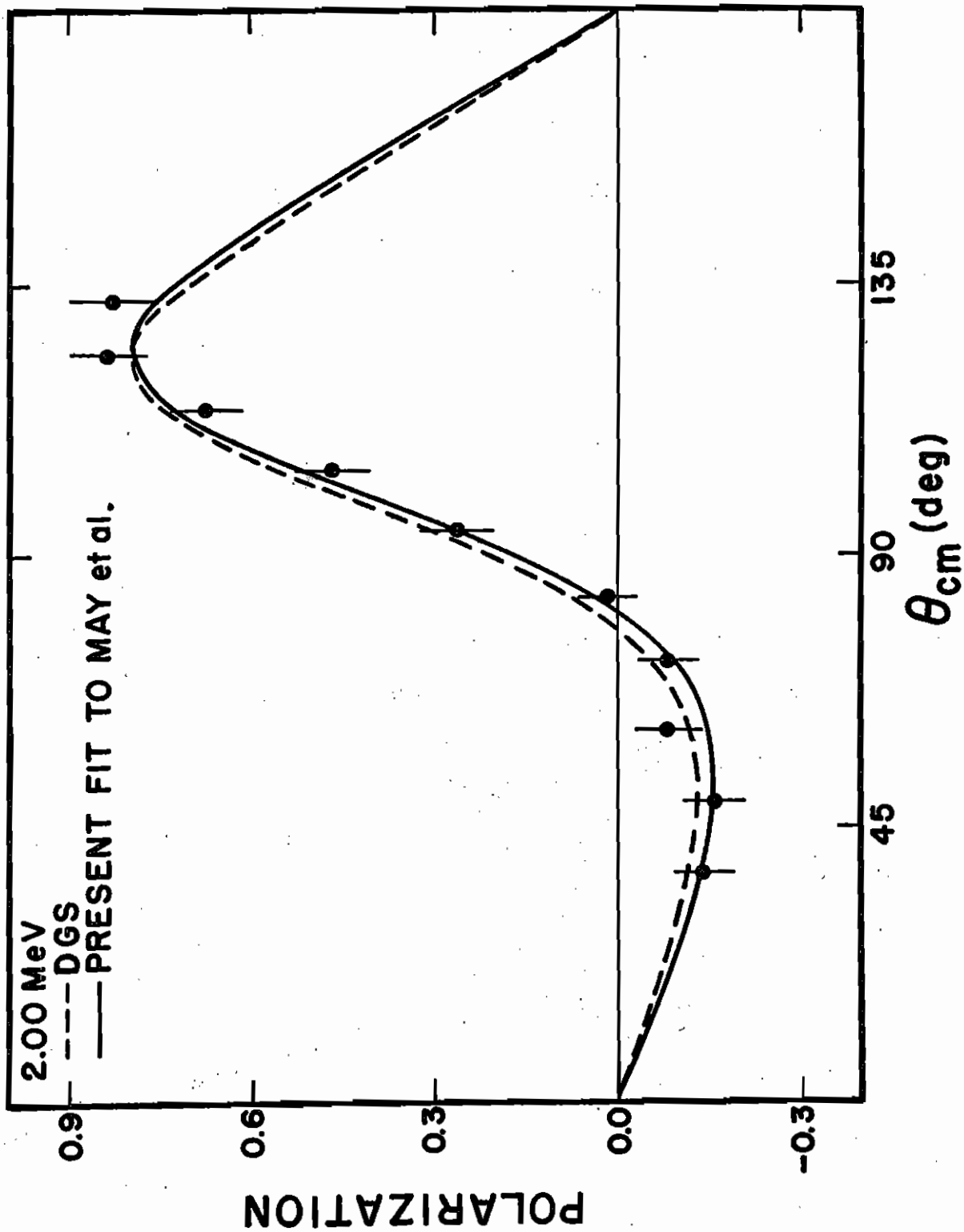
2.00 MeV
---DGS
——PRESENT FIT TO MAY et al.
POLARIZATION
0.9
0.6
0.3
0.0
-0.3
45
90
135
θ_{cm} (deg)

Fig. 29. Scattering Phase Shifts Below 3.0 MeV

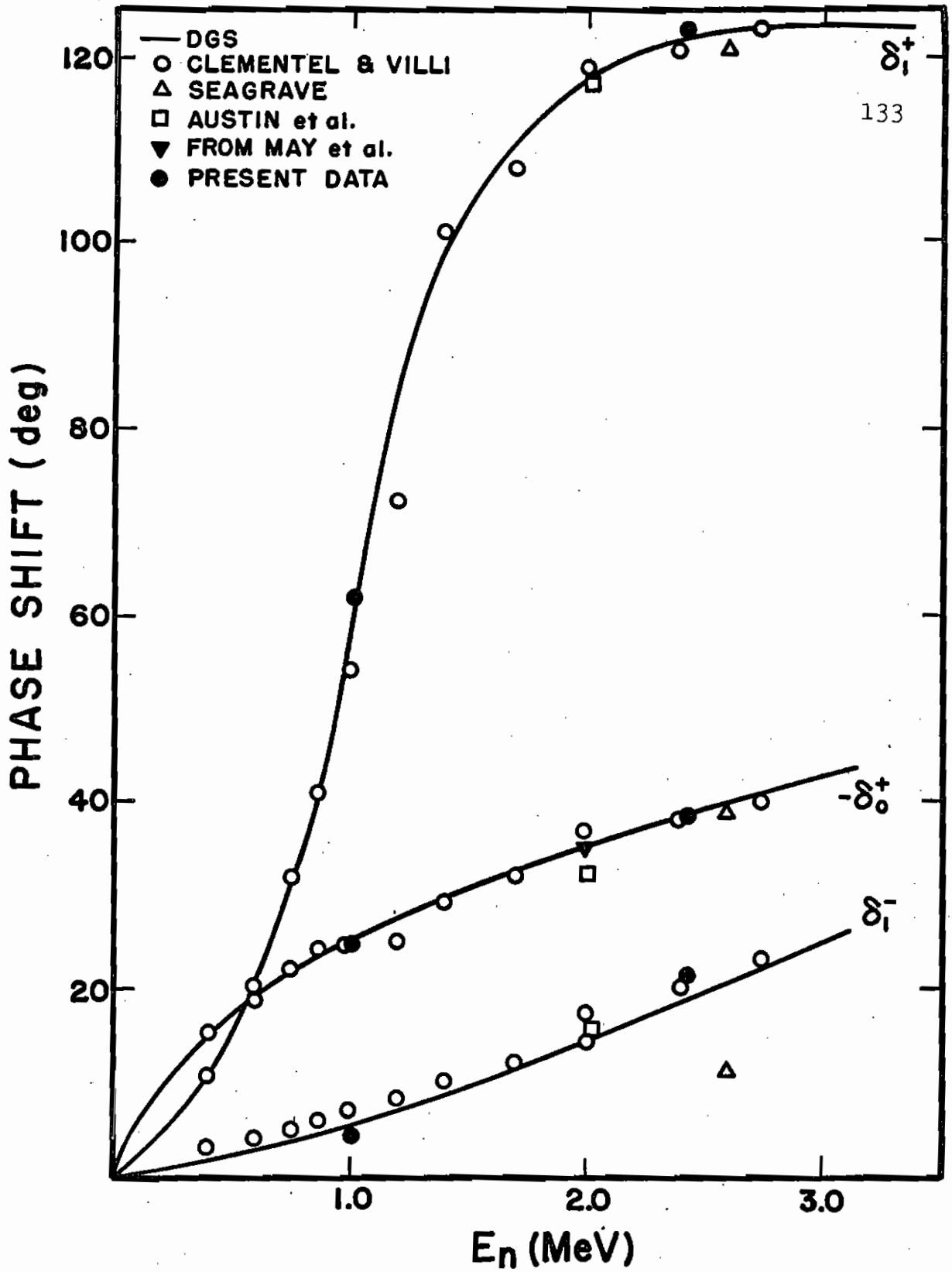
DGS
CLEMENTEL & VILLI
SEAGRAVE
AUSTIN et al.
FROM MAY et al.
PRESENT DATA
δ_1^+
$-\delta_0^+$
δ_1^-
PHASE SHIFT (deg)
120
100
80
60
40
20
1.0
2.0
3.0
E_n (MeV)

D. Conclusion

As a result of the complex manner by which the phase shifts determine the polarization, it is somewhat difficult to estimate the experimental uncertainty in the determined δ's (Haeberli, 1963). The method used in the present experiment was to observe how far from the optimum value the phase shift had moved when the X^2 reached twice its minimum value. In this manner we estimate the uncertainty in the values of the scattering phase shifts at 2.44 MeV to be ± 2.4, ± 0.5, and ± 0.5 for $\delta_0^+ = -37.9$, $\delta_1^- = 21.2$, and $\delta_1^+ = 121.6^\circ$ respectively. Both the δ_0^1 and the δ_1^+ phase shifts are in agreement with the ones quoted by DGS. The δ_1^- was found to be 2.8° higher than DGS.

In view of the failure to find a valley in the X^2 surface in the present experiment at 1.01 MeV, the hard sphere approximation had to be used to fix the s-wave phase shift, where the calculation was based on the value of the hard sphere radius determined at 2.44 MeV. Using this restriction the phase shifts were determined to be $\delta_0^+ = -24.5 \pm 1.5^\circ$, $\delta_1^- = 4.4 \pm 1.0^\circ$, and $\delta_1^+ = 61.2 \pm 4.5^\circ$. The uncertainty in the s-wave phase shift arises from the uncertainty in the calculated hard sphere radius. The $\pm$ 7 keV uncertainty in the neutron energy has contributed negligibly to the uncertainty of the phase shifts with the exception of the δ_1^+ which is changing rapidly with energy ($d\delta_1^+/dE = 0.15^\circ$ / keV). However, the major contributor to the uncertainty in this phase shift and the others is the lack of sufficient sensitivity of the X^2 search to the phase shifts. The phase shifts at 1.0 MeV are in agreement with DGS with the exception of δ_1^- which is 1.6° below DGS. It is hoped that the work of Morgan et al. discussed below will considerably reduce this source of uncertainty.

The difference between the presently obtained values of δ_1^- and the DGS values is significant in calculations of the helium analyzing power.

(However, since the DGS δ's were only expected to be good to about 3°, one must qualify the disagreement.) The high value of δ_1^- at 2.44 MeV is not consistent with the low experimental result of Seagrave (1953) at 2.6 MeV but is in agreement with the general trend calculated by Clementel and Villi (1955) from Adair's data. At 1.0 MeV the present δ_1^- is in disagreement with higher values of Clementel and Villi as well as the quoted values of DGS.

Quite recent experiments at Duke by Morgan et al. (1966) have yielded precision angular distributions of $d\sigma/d\Omega$ for n-He^4 scattering. Unfortunately analysis of the data is not yet complete though preliminary results should be available shortly. Because cross section angular distribution data can be accumulated quickly in comparison with polarization angular distributions, the data of Morgan et al. was obtained at many energies in addition to the two energies studied in the present work. It is doubtful that the cross section data can lead to a sensitive determination of the phase shifts, but when the cross section data is fit along with the present polarization data to the single level resonance formula, hopefully the n-He δ's will be fixed accurately enough that helium can be very reliably used as an analyzer of polarized neutron beams.

The present experiment also provides the most accurate determination of the polarization of two frequently used neutron sources, the $Li^7(p,n)Be^7$ and the $C^{12}(d,n)N^{13}$ reactions. By searching the δ's and P_1, it was found that one can limit the value of P_1 to -0.458 ± 0.006 for the reaction $C^{12}(d,n)N^{13}$ for an incident deuteron energy of 2.82 MeV when the neutrons are observed at 25° (lab). A similar determination of the incident polarization in the reaction $Li^7(p,n)Be^7$ can be obtained when the s-wave phase shift is restricted to the hard sphere value. For an incident proton energy of 2.92 MeV and at a laboratory angle of 50° the neutron polarization was observed to be 0.304 ± 0.008.

APPENDIXES

Appendix I.

A. Production of the Lithium Metal Targets

Lithium metal targets were used to produce 1.0 MeV polarized neutrons. The targets were made of lithium metal evaporated onto a 10 mil tantalum backing. The following discussion describes the techniques employed in the production of these targets. Elaborate precautions were taken to prevent oxidation of the highly active lithium metal.

First the tantalum backing was scoured and placed inside a carriage vessel which was then mounted in the evaporator. The carriage vessel was a small aluminum canister fitted with spring clips to hold the tantalum backing disk. A small piece of lithium (about 3 mm in diameter) was placed in an out-gassed tantalum "boat". After evacuating the evaporator chamber, the lithium was heated and allowed to outgas. During this process a shield placed immediately over the "boat" prevented the outgassing products from reaching the clean target backing. The shield was removed from the beam path and the lithium was then evaporated onto the tantalum backing through a beam-defining aperature which prevented lithium buildup on the O-ring surface.

At the completion of the evaporation process, the carriage vessel was closed under vacuum and then the evaporator was let up to slightly above atomospheric pressure with helium. The seal on the carriage vessel was not airtight and permitted helium to seep into the

vessel. After removal from the evaporator, the carriage vessel was inserted into a polyethylene bag inflated with helium. With the beam tube also filled with helium, the polyethylene bag was slipped over the beam tube opening. Still within the inert atmosphere, the carriage vessel was opened and the lithium metal target installed on the beam tube. After evacuating the beam tube, the target was ready for use.

The total time lapse from the completion of the evaporation process until the installation of the beam tube was typically less than ten minutes and the target was never allowed to come in contact with oxygen in the atmosphere. The viewing port on the beam tube (Figure 4) permitted visual examination of the target. No discernable difference in the appearance of the target while in the evaporator and its appearance on the beam tube was noted. This was taken as evidence that no significant oxidation of the lithium surface had occurred.

B. Production of Thin Carbon Foils

Nuclear experiments often require the use of thin foils for employment as targets. In the present experiment, a thin foil was used as a standard whose neutron yield was compared with other thicker targets to obtain the latter's thicknesses. The following discussion is included in order that the procedures employed might be documented. We shall describe the production techniques required to produce the 5- to 30- keV thick carbon foils. The thickness shall be interpreted as meaning the thickness to protons of lithium threshold energy. The discussion that follows is completely general and therefore includes some methods not required for the present work.

To start with, one should take a clean microscope slide and dip it into a solution of detergent and water; the detergent and water solution

should be only slightly cloudy. Using a lint-free tissue, the microscope slide should be wiped almost clean, i.e. until very little detergent remains on the slide. (It is almost impossible to wipe off too much detergent.) After allowing this to dry a few minutes, the slide should be dipped in an alcohol solution of colloidal graphite* the requisite number of times. Only brief drying periods are necessary between dips. During the drying process the slides should be allowed to stand propped almost vertically with their lower ends resting on a lint-free tissue to promote drainage of the excess. As soon as is practical, the foil should be removed from the slide as allowing it to remain in place a lengthier amount of time may render it more difficult to remove. To remove the foil from the slide, scrape the edges of the microscope slide clean with a sharp razor blade. Then place the slide in a smooth-bottomed, shallow pan resting at a slight angle with the horizontal and filled to a maximum depth of about 0.5 cm with distilled water. The slide should be placed in the water at the shallow end and carefully pushed toward the deeper end in such a manner as to force the surface tension to "lift" the foil from the slide.

At this point in the procedure one of two approaches may be taken. First, the foil may be lifted directly from the water surface with another slide. It should be allowed to dry with the pick-up slide in a horizontal position and the foil hanging vertically downward from it. This method is most suitable for the thicker foils. After drying the foil may be glued to the foil-holding ring with a small amount of Eastman 910 † contact

---

* Dag Dispersion No. 154, available from Acheson Colloids Co., Port Huron, Michigan. The solution should be diluted with alcohol about 5 or 6 to 1 to give a target thickness of about 40 keV per dip.

† Available from Eastman Chemical Products, Inc., Kingsport, Tennessee.

adhesive. One need only use sufficient adhesive to barely moisten the surface of the foil holder. Care should be taken to prevent the adhesive from being in a position where it could be exposed to the beam. The holder is then lowered onto the foil which sould now be resting horizontally on a cushioned layer of lint-free tissues. After the adhesive sets, the holder may be picked up and a sharp razor blade may be used to trim the excess foil.

The second method is more suitable for the thinner foils. While the foil is still floating on the surface of the water in the removal tray, the foil holder should be prepared with contact adhesive and then carefully lowered onto the foil. On contact the adhesive begins setting. The foil-foil holder combination may now be moved to the shallowest part of the tray taking care not to allow the foil to break contact with the surface of the water. At this point the foil holder is allowed to rest, pressing the foil against the bottom of the tray. Using a sharp knife the excess foil may be cut away. If the foil is relatively thick it may be picked up directly and after drying will be ready for use. However, with the thin foils this will not be possible as the surface tension will destroy the foil during removal. To avoid this difficulty, one may place a drop of the detergent-water solution in the neighborhood of the foil to reduce surface tension of the water. In this manner foils as thin as 5 keV may be successfully lifted off the water surface. Unfortunately, if allowed to dry in this form, the foil will not be suitable for use as a target as a layer of detergent will remain on it. Using a wash bottle filled with distilled water, the foil can be washed free of this contaminant. The nozzle of the wash bottle should be held over the foil support ring allowing the water to flow across the foil itself. Care should be taken not to allow the jet of water to burst the foil.

Some contaminating detergent will remain in all foils due to pick up from the slide, but the majority of this may be "baked-out" by allowing the foil to experience a beam for 10 - 20 minutes. Oxygen is the primary contaminant introduced from the detergent.

C. Carbon Target Thickness Measuring Techniques

The mean energy at which a nuclear reaction takes place can be calculated only if the target thickness is known. Therefore target thickness measuring techniques become a prime consideration. The following is a description of the procedures used in determining the thickness of the carbon targets used in the present experiment.

A long counter and a relatively thin (5- to 20- keV) LiF target were used to make a threshold determination. This also served as a calibration of the machine energy. The carbon foil whose thickness was desired was introduced into the beam path and again the Li^7 (p, n) Be^7 threshold was determined. The difference in machine energy between these two threshold determinations was taken as the foil thickness to protons of lithium threshold energy. Then using standard tables the thickness was converted to the thickness for deuterons at the desired energy.

For thicker targets, the above described method was not applicable due to the large amount of energy straggling inherent with a thick target. To find the thickness of these targets, the accelerator ion source was switched to deuterons. Comparison of the yield of $C^{12}(d, n)N^{13}$ neutrons from the thicker target with the yield of a standard target whose thickness had been previously determined in the above manner allowed the thickness of the former target to be determined. A blank tantalum beam catcher was installed and the background determined so that the measurement could be accurately corrected for its contribution.

Appendix II.

HELIUM CELL COATING

In the present experiment, helium gas contained in a high pressure scintillation cell served as the polarization analyzer and detector for the recoiling α-particles. The interior of the cell was treated to insure optimum light output in the sensitive range of the photomultiplier. The following discussion covers the coating techniques. A similar procedure was employed by Shamu (1961) and shown by him and more recently by Morgan (1965) to provide linear energy response and reasonable energy resolution.

The interior of the cell, which was highly polished during manufacture, was cleaned and the cell was mounted in the evaporator. About 20 mg of fine aluminum wire was wrapped around a tungsten filament. The filament was centered on the axis of the cell 1 cm inside the plane of the cell's rim. Current was applied and the aluminum melted, then evaporated. The resulting layer of aluminum had a thickness of about 100 $\mu g/cm^2$.

After removing the cell from the evaporator and clamping it in a vise with the opening down, a strip of metallic magnesium was burned at the mouth of the cell until a layer of MgO about 1.5 mm thick covered the interior of the cell. The excess MgO covering the lip and O-ring seat was removed with a tightly wrapped cotton swab. The cell was re-installed in the evaporator above a circular tantalum boat 1.6 cm in diameter. Long

current leads were provided so that it could be positioned well inside the cell. The boat and cell were coaxial. In an effort to allow uniform pulse height regardless of the position of a recoil in the cell, a non-uniform layer of diphenyl stilbene was used. The use of a thicker layer of wavelength shifter toward the rear of the cell had first been proved effective by Shamu (1961). Two evaporations were used, the first with the boat 4.0 cm from the rear of the cell and the second with a distance of 7.1 cm. The amounts of diphenyl stilbene used were 4.6 and 4.3 mg respectively resulting in a coating about 110 $\mu g/cm^2$ thick at the rear of the cell and about 80 $\mu g/cm^2$ thick on the walls near the glass window. Since the diphenyl stilbene evaporates quite rapidly on reaching its sublimation temperature, care was taken so that no rapid change in temperature was experienced. The typical evaporation time was about 20 minutes. By approaching the temperature slowly loss of the evaporant by vaporization-induced spilling was avoided. Evaporation of the wave-length shifter completed the coating of the cell proper.

The window was coated with a layer of wavelength shifter 30 $\mu g/cm^2$ thick. With the boat 7.6 cm away, 12.2 mg of diphenyl stilbene was evaporated. The bracket holding the glass disk prevented buildup of the wavelength shifter on the O-ring surface. The cell was assembled and after pumping for several days was filled with the scintillation gas. The filling was done slowly so that turbulence was held to a minimum to prevent destruction of the coating layers.

LIST OF REFERENCES

LIST OF REFERENCES

Robert K. Adair, Phys. Rev. 86, 155 (1952).

W. D. Andress, Jr., F. O. Purser, J. R. Sawers, Jr., and R. L. Walter, Nuclear Phys. 70, 313 (1965).

J. Atkinson and J. E. Sherwood, Nucl. Instr. Methods 34, 137 (1965).

S. M. Austin, S. E. Darden, A. Okzaki, and Z. Wilhelmi, Nuclear Phys. 22, 451 (1961).

S. M. Austin, H. H. Barschall, and R. E. Shamu, Phys. Rev. 126, 1532 (1962).

J. A. Baicker and K. W. Jones, Nuclear Phys. 17, 424 (1960).

H. H. Barschall, Helv. Phys. Acta 29, 145 (1956).

"Basel Convention", Helv. Phys. Act. Supplementum VI, 1961.

P. R. Bevington, W. W. Rolland and H. W. Lewis, Phys. Rev. 121, 871 (1961).

R. J. Blin-Stoyle, Proc. Phys. Soc. (London) 65A, 452 (1952).

H. J. Boersma, Thesis, Free University, Amsterdam (1963).

Louis Brown, W. Haeberli, and Walter Trachslin, Private Communications to R. L. Walter, (1966).

E. Clementel and C. Villi, Nuovo Cimento 2, 1121 (1955).

C. L. Critchfield and D. C. Dodder, Phys. Rev. 76, 602 (1949).

F. Demanins, G. Pisent, G. Poiani and C. Villi, Phys. Rev. 125, 318 (1962).

D. C. Dodder and J. L. Gammel, Phys. Rev. 88, 520 (1952).

A. J. Elwyn and R. O. Lane, Nuclear Phys. 31, 78 (1962).

James H. Foote, Owen Chamberlain, Ernest H. Rogers, and Herbert M. Steiner, Phys. Rev. 122, 959 (1961).

J. L. Gammel and R. M. Thaler, Phys. Rev. 109, 2041 (1958).

W. Haeberli, Fast Neutron Physics, ed. by J. L. Fowler and J. B. Marion (Interscience Publishers, New York, 1963) Part II, Chap. V.G.

A. O. Hanson and J. L. McKibben, Phys. Rev. 72, 673 (1947).

P. Hillman, G. H. Stafford, and C. Whitehead, Nuovo Cimento 4, 67 (1956).

C. E. Hollandsworth, S. G. Buccino, and P. R. Bevington, Nucl. Instru. Methods 28, 353 (1964).

B. Hoop, Jr., A. H. Bond, Jr., and R. H. Stuewer, Bull. Am. Phys. Soc. 10, 423 (1965).

B. Hoop, Jr., and H. H. Barschall, Private Communication to R. L. Walter (1965).

P. Huber and E. Baldinger, Helv. Phys. Act. 30, 436 (1952).

R. W. Jewell, W. John, J. E. Sherwood and D. H. White, Phys. Rev. 142, 3-687 (1966).

L. Koch, Thesis, Centre d'Etudes Nucleaires de Saclay, Paris, 1960.

A. M. Lane and R. G. Thomas, Rev. Mod. Phys. 30, 257 (1958).

J. V. Lepore, Phys. Rev. 79, 137 (1950).

I. I. Levintov, A. V. Miller, and V. N. Shamshev, Nuclear Phys. 3, 221 (1957), J. Exptl. Theoret. Phys. (U.S.S.R.) 32, 274 (1957), and Soviet Physics -- JETP 5, 258 (1957).

T. H. May, R. L. Walter, and H. H. Barschall, Nuclear Phys. 45, 17 (1963).

M. M. Meier, L. A. Schaller and R. L. Walter (to be published).

G. L. Morgan, C. E. Hollandsworth, and R. L. Walter, Bull. Am. Phys. Soc. 10, 440 (1965).

G. L. Morgan, Private Communication, 1965.

G. L. Morgan and L. A. Schaller, Private Communication, 1966.

S. J. Moss and W. Haeberli, Nuclear Phys. 72, 417 (1965).

R. B. Perkins and C. Glashausser, Nuclear Phys. 60, 433 (1964).

G. Pisent and C. Villi, Nuovo Cimento 11, 300 (1959).

G. Pisent and A. M. Saruis, Nuovo Cimento 28, 600 (1963).

F. O. Purser, Private Communication, (1965).

F. O. Purser, Private Communication, 1966.

F. O. Purser, Thesis, Duke University, 1966.

L. David Roper, Private Communication, 1965 and Bull Am. Phys. Soc. 10, 155 (1965).

J. R. Sawers, Jr., F. O. Purser, Jr., and R. L. Walter, Phys. Rev. 141, No. 3, 825 (1966).

J. Schwinger, Phys. Rev. 69, 681 (1946).

J. Schwinger, Phys. Rev. 73, 407 (1948).

John D. Seagrave, Phys. Rev. 92, 1222 (1953).

R. E. Shamu, Nucl. Instr. Methods, 14, 297 (1962).

R. E. Shamu and J. G. Jenkin, Phys. Rev. 135, B99 (1964).

H. R. Striebel and P. Huber, Helv. Phys. Act. 30, 67 (1957).

H. R. Striebel, S. E. Darden, and W. Haeberli, Nuclear Phys. 6, 188 (1958).

S. Suwa and A. Yokosawa,, Phys. Letters 5, 351 (1963).

F. J. Vaughn, W. L. Imhof, R. G. Johnson and M. Walt, Phys. Rev. 118, 683 (1960).

R. L. Walter, W. Benenson, P. S. Dubbeldam, and T. H. May, Nuclear Phys. 30, 292 (1962).

R. L. Walter, Private Communication, 1966.

W. G. Weitkamp, Bull. Am. Phys. Soc. 8, 537 (1963).

T. A. Welton, Fast Neutron Physics, ed. by J. L. Fowler and J. B. Marion (Interscience Publishers, New York, 1963) Part II, Chap. V. F.

L. Wolfenstein, Phys. Rev. 75, 1664 (1949).

L. Wolfenstein and J. Ashkin, Phys. Rev. 85, 947 (1952).

L. Wolfenstein, Phys. Rev. 96, 1654 (1954).

L. Wolfenstein, Ann. Rev. Nuclear Sci. 6, 43 (1956).

P. E. Hodgson, Phil. Mag. Supplement 7, 1 (1958).

BIOGRAPHY

James Richard Sawers, Jr.

Born: February 4, 1940
Memphis, Tennessee

Education: B. S. Duke University, 1962
Research Assistant, 1961-1962
National Science Foundation Fellow, 1962-1965
Research Assistant, 1965-1966

Societies: Sigma Xi
American Physical Society

Publications:

Proton- Angular Correlations in the $C^{12}(d,p)C^{13}$ Reaction at Low Energies (with Katman, Tilley, Williamson, Gerke, and Lacambra), Bull. Am. Phys. Soc. 8, 11 (1963).

Polarization of Neutrons from the $D(d,n)He^3$ Reaction at 3.2 MeV (with Purser and Walter), Bull. Am. Phys. Soc. 8, 320 (1963).

Measurement of Neutron Polarizations and Cross Sections from the $C^{12}(d,n)N^{13}$ Reaction from 2.8 to 4.2 MeV (with Walter and AND Purser), Proceedings of the Conference on Nuclear Spectroscopy with Direct Reactions, ANL-6848 (1964).

Polarization of Neutrons from the $D(d,n)\ He^3$ Reaction between 1.9 and 3.7 MeV. (with Purser and Walter), Bull. Am. Phys. Soc. 9, 33 (1964).

Polarization of 2.4-MeV Neutrons Inelastically Scattered from Iron (with Purser and Walter), Bull. Am. Phys. Soc. 9, 445 (1964).

Scattering of 2.4- and 2.7-MeV Polarized Neutrons from Carbon (with Purser, Morgan and Walter), Bull Am. Phys. Soc. 9, 445 (1964).

Depolarization in n-p Scattering at 2.5 MeV (with Walter and Purser), Bull Am. Phys. Soc. 9, 446 (1964).

Measurement of the Neutron Polarization and Cross Sections for the $^{12}C(d,n)^{13}N$ Reaction between 2.8 and 4 MeV (with Walter and Purser), Bull. Am. Phys. Soc. 9, 675 (1964).

Polarization of Neutrons from the $^{7}Li(p,n)^{7}Be$ Reaction for 3 to 4 MeV Protons (with Andress, Purser, and Walter) Nuclear Phys. 70, 313 (1965).

Polarization of Neutrons from the $D(d,n)\,He^{3}$ Reaction (with Purser and Walter) Phys. Rev. 140, B870 (1965).

Measurement of the Polarization of $C^{12}(d,n)N^{13}$ Neutrons from 1.8 to 2.8 MeV Incident Deuteron Energy (with Purser and Walter), Bull. Am. Phys. Soc. 10, 440 (1965).

The $C^{12}(d,n)N^{13}$ Reaction Near the Resonance at $E_d = 4.0$ MeV (with C. E. Hollandsworth, Purser and Walter) Bull. Am. Phys. Soc. 10, 440 (1965).

Polarization of Neutrons from the $Li^{7}(p,n)\,Be^{7}$ (GS) Reaction for 3.0 to 4.0 MeV Protons (with Andress, Walter and Purser), Bull. Am. Phys. Soc. 10, 440 (1965).

Cross-Section and Polarization Determinations for the $C^{12}(d,n)\,N^{13}$ Reaction from 2.8 to 4.2 MeV (with Purser and Walter) Phys. Rev. 141, No. 3, 825 (1966).

A Measurement of the Depolarization Parameter in n-p Scattering at 2.6 MeV (with Purser and Walter) Proceedings of the International Conference on Polarization Phenomena of Nucleons, Karlsruhe, 1965 (to be published).

Polarization of Neutrons from the $C^{12}(d,n)N^{13}$ Reaction for 1.8 to 4.0 MeV Deuterons (with Purser and Walter), Proceedings of the international Conference on Polarization Phenomena of Nucleons, Karlsruhe, 1965 (to be published).

Phase Shifts for n-α Scattering at 1.01 MeV and 2.44 MeV (with Walter, Morgan and Schaller) Bull. Am. Phys. Soc. 11, 304 (1966).

Cross-Section Measurements for Neutrons from the $C^{12}(d,n)N^{13}$ Reactions for Energies from 3.8 to 5.0 MeV. (with Hollandsworth, Purser and Walter), to be published.